A Theoretical and Experimental Study of Modal Interactions in Metallic and Laminated Composite Plates

by

Kyoyul Oh

Dissertation submitted to the faculty of the
Virginia Polytechnic Institute and State University
in partial fulfillment of the requirements for the degree of

DOCTOR OF PHILOSOPHY

in

Engineering Mechanics

APPROVED:

Ali H. Nayfeh, Chairman

Dean T. Mook

Michael W. Hyer

Scott L. Hendricks

John A. Burns

December, 1994

Blacksburg, Virginia

A Theoretical and Experimental Study of Modal Interactions in Metallic and Laminated Composite Plates

by

Kyoyul Oh

Committee Chairman: Ali H. Nayfeh

Department of Engineering Science and Mechanics

(ABSTRACT)

This dissertation focuses on nonlinear modal interactions in plates. Our first investigation involved the activation of a two-to-one internal resonance in the response of a metallic cantilever plate. Although the plate was excited around the frequency of its second bending mode, its response contained a contribution from its first torsional mode. The frequency ratio between the bending and torsional modes was nearly two-to-one.

Next, we investigated the energy transfer from high-frequency to low-frequency modes in a cantilever graphite-epoxy composite plate $(90/30/-30/-30/30/90)_s$. The plate was excited around the natural frequency of its seventh (third torsional) mode. For some excitation amplitudes and frequencies, we observed the activation of a low-frequency (first bending) mode accompanied by an amplitude and phase modulation of the seventh mode.

We studied combination resonances in the responses of cantilever composite plates with the layups $(90/30/-30/-30/30/90)_s$ and $(-75/75/75/-75/75/-75)_s$ to harmonic base excitations. We activated the combination resonance $f_e \approx \omega_2 + \omega_7$ in the $(90/30/-30/-30/30/90)_s$ plate, where the ω_i are the natural frequencies of the plate and f_e is the excitation frequency. In the $(-75/75/75/-75/75/-75)_s$ plate, we activated the external combination resonance $f_e \approx \frac{1}{2}(\omega_2 + \omega_5)$ and the combination internal resonance $f_e \approx \frac{1}{2}(\omega_2 + \omega_{13}) \approx \omega_8$.

We carried out an experimental-modal analysis (EMA) of a nonclassically supported plate with and without a constrained-layer damping (CLD) patch attached on its upper left-hand side surface. The natural frequencies and mode shapes were used to ascertain the effect of the CLD patch.

ACKNOWLEDGEMENTS

I would like to express my sincere appreciation to my advisor, Dr. Nayfeh, for his guidance, encouragement, and patience throughout my residency in Virginia Tech. I am grateful for Dr. Nayfeh's enthusiasm in exploring new areas of research and investigation. Also, I would like to thank my committee members Drs Mook, Hyer, Hendricks, and Burns for guiding me through the various course works, ideas, discussions, and encouragements throughout the PhD program.

Special thanks are due to Sally Shrader for her support, friendship, and assistance. I am thankful for the seniors of the Nonlinear Vibrations Group: Drs B. Balachandran, M. Bikdash, J. Masad, I. Oh, and F. Pai for setting the standards of excellence within the group. I greatly value the friendships and cooperations with Tony Anderson, Samir Nayfeh, Mahmood Tabaddor, Tariq Nayfeh, Wayne Kreider, and Jon Pratt.

I am indebted to the faculty of Worcester Polytechnic Institute, Worcester, Massachusetts, especially Drs Boyd, Grandin, Noori, and Pryputniewicz for encouraging me to pursue the PhD program. I am most indebted to my parents who have given me the love, guidance, support, and trust throughout my life and especially during the graduate studies. Special thanks are also due to my brother and parents-in-law for their love and support.

I dedicate this work to my wife, Petrina Lynn, and daughter, Alythea Hyun-Sook Oh. Without their understanding, support, and love, this work would not have been possible.

This work was supported by the United States Air Force Office of Scientific Research under Grant No. F49620-92-J-0197. Portion of this work was partially supported by the Ford Motor Company Research gifts.

TABLE OF CONTENTS

LIST OF FIGURES

LIST OF TABLES

Chapter 1

INTRODUCTION

At the current state of technology, a structure is expected to be lighter and more efficient. This trend has forced the engineer to evaluate existing materials and consider alternate materials that are lighter and have higher strength-to-mass ratios. This trend has pushed the advancement of fiberous composite structures and hastened the introduction of advanced materials into consumer products, such as tennis rackets, golf clubs, bicycle frames, boats, automobiles, and airplanes.

Often, the material requirements have led to the design of flexible structures. The flexibility of structures and material types have produced many complicated nonlinear phenomena in their dynamics. Flexibility results in large curvatures, nonlinear deformations through the thickness, and midplane stretching. Building a structure with fiberous composites adds many complications to the equations of motion. The directionality properties of each layer of the fiberous composite structure result in bending-twisting and bending-stretching coupling effects. These coupling effects result in five highly coupled partial differential equations.

1.1 *Literature Review*

The nonlinear dynamics of plates can be very complicated (Nayfeh and Mook, 1979; Chia, 1980). Nayfeh and Mook (1979) described a wide variety of systems exhibiting nonlinear modal interactions. Nayfeh and Balachandran (1989) surveyed theoretical and experimental studies of the influence of modal interactions on the nonlinear response of harmonically excited structural and dynamical systems. Leissa (1981) surveyed the literature on

the vibration and buckling of composite plates. Bert (1985) reviewed the dynamic response of laminated composites. Reddy (1984a,1985) reviewed the application of the finite-element method to plate vibrations. Next, pertinent works on the nonlinear vibrations of plates and other structures are reviewed.

1.1.1 Nonlinear vibrations of plates

Yang and Sethna (1992) analytically investigated nonlinear phenomena in the forced vibrations of a nearly square isotropic plate. They concentrated on the antisymmetric modes of vibration of a simply supported plate. The physical phenomena studied are due to a one-to-one autoparametric resonance of two antisymmetric modes. The results show that the response can be a single-mode or two-mode motion and it can also be in the form of traveling waves or *pseudo-standing* waves. The *pseudo-standing* waves are traveling waves with jerky motions. Yang and Sethna concluded that the presence of a Hopf bifurcation in the evolution equations leads to amplitude-modulated traveling waves as well as to a sequence of period-doubling bifurcations, culminating in chaos. Their analysis was based on the dynamic analog of the von Kármán plate equations. They considered a case of low damping and a single source of excitation.

Chang et al. (1993) analytically investigated the nonlinear vibrations of a rectangular plate with a one-to-one autoparametric resonance. They found that for low damping levels, the presence of Hopf bifurcations in the mixed-mode response leads to complicated amplitude- and phase-modulated responses, period-doubling bifurcations, chaos, and coexistence of multiple chaotic motions. The analysis was based on the von Kármán plate equations and considered a single source of excitation.

Yamaki and Chiba (1983) and Yamaki, Otomo, and Chiba (1983) investigated theoretically and experimentally the nonlinear vibrations of a clamped rectangular plate with an initial deflection and an initial edge displacement. The analysis assumed that damping is negligible and considered a single excitation source. They found that for steady-state symmetric periodic responses, the theoretical results match well with the experimental re-

sults; however, there are quantitative discrepancies for large-amplitude vibrations. They also found a variety of nonsymmetric and nonperiodic responses that are not predicted by the theory, such as internal resonances, combination resonances, and dynamic snap-through phenomena.

Cole (1990) conducted an experimental investigation into the effectiveness of spoiler surfaces in suppressing the onset of flutter for a low-aspect-ratio, rectangular wing. He found that above a certain spoiler size, the wing underwent a torsional instability at dynamic pressures that are well below the expected flutter conditions. Inspection of the natural frequencies of the wing reveals that the frequency of the second bending mode is approximately twice the frequency of the first torsional mode. Hence, it is possible that modal interactions between these modes were responsible for the observed torsional instability.

In the study of laminated composite plate vibrations, shear deformation is very important because the ratio of the in-plane Young's moduli to the transverse shear moduli is very large compared to those of isotropic materials. Therefore, an adequate theory is needed to account for the distribution of transverse shear stresses. There are many theories that were developed to account for shear deformations. Reddy (1984b), Bhimaraddi and Stevens (1984), and Librescu and Reddy (1989) presented third-order shear-deformation theories in which the governing differential equations are derived by using variational principles. These theories account for a cubic variation of the in-plane displacements through the thickness and zero shear stresses on the top and bottom surfaces. Hence, no shear correction-factor is needed. In extending these theories to account for geometric nonlinearities due to moderate rotations of the plate, many researchers use von Kármán strains. Recently, Pai and Nayfeh (1991a) presented a theory that accounts for nonlinear curvatures, mid-plane strains, and third-order shear deformations.

Experimental investigations of laminated composite plate vibrations did not receive the same attention as theoretical ones. Bert and Mayberry (1969) compared experimentally and theoretically obtained natural frequencies and mode shapes of laminated anisotropic plates with clamped edges. They neglected the shear deformations in their theoretical calcula-

tions and used the Rayleigh-Ritz approximation. The difference between the experimental and theoretical results was approximately 10%. Mayberry and Bert (1968) also experimentally and theoretically investigated the nonlinear vibrations of composite plates. Their study focused on a glass-epoxy plate clamped on all edges. They observed an increase in the measured natural frequencies as the excitation level was increased; however, they did not find other complicated responses, such as superharmonic and subharmonic resonances. Clary (1972) studied the variation of the natural frequencies of a composite panel with fiber orientation to the boundaries. The difference between their theoretical and experimental results was between 2% and 3% for the beam-type modes and between 2% and 10% for the plate-type modes. Crawley (1979) also experimentally and theoretically investigated the natural frequencies and mode shapes of laminated composite plates and shells. He found the difference between the theoretical and experimental values to be approximately 12%.

Lyons (1975) proposed the use of the statistical energy analysis (SEA) as an alternative for the analysis of the response of dynamical systems. The SEA method reduces the response into a spatially averaged square-velocity value, yielding a simple and compact linear approximation to the structural response. However, the SEA method breaks down if there are nonlinear modal interactions between/among modes. Crandall (1977), Crandall and Kulvets (1977), and Crandall and Zhu (1983) concentrated on the aspects of structural responses to wideband random excitations where the usual SEA does not hold. They performed both experimental and theoretical work. Crandall (1977) experimentally and theoretically identified the interesting phenomenon of "intensification zones." These zones are created when the structure is forced at a point with wideband random signals. In the intensification zones, the local response is higher (or lower) than the nearly uniform response of the rest of the structure. Studying the asymptotic behavior of classical modal analysis for a general, linear structural system, Dowell and Kubota (1985) arrived at the same result as the SEA. Kubota and Dowell (1986) later verified experimentally the asymptotic modal analysis approach. They reported that the deviation of the experimental results from the analytical results when the point force is placed near the edge of the plate is larger than

those when the point force is located at the center of the plate.

Recently, there has been much effort at Ford Motor Company to utilize the SEA technique in conjunction with experimental techniques, such as Computer Aided Holometry (CAH), to investigate sound pressure distributions inside a car body. Brown et al. (1992a,1992b) reported on the use of the vibration amplitude and phase obtained from the CAH measurements of a sample corrugated plate as input boundary conditions to calculate the sound pressure distributions on the surface of the structure. They concluded that the measured and computed sound pressure values were in good agreement, thereby supporting the contention that the CAH measured shape, vibration amplitude, and phase values are essential for computing the sound pressure values. However, this approach does not provide any information regarding the distribution of the vibrating modes. Information about the dynamic content of the participating modes can be very useful in the design of a particular part and in the placement of damping materials.

1.1.2 Nonlinear vibrations of other structures

Balachandran and Nayfeh (1990) and Nayfeh and Balachandran (1990) experimentally and theoretically investigated the response of a two-degrees-of-freedom structure with quadratic nonlinearities and a two-to-one internal resonance to an external harmonic excitation. They studied metallic as well as composite structures. They observed periodic, quasi-periodic, and chaotic responses for both configurations.

Pai and Nayfeh (1990) analytically investigated the nonplanar response of a cantilever beam to a lateral harmonic base excitation. They found steady whirling motions, whirling motions of the beating type, and chaotic motions. They also investigated the response of a cantilever composite beam to lateral harmonic base excitations (Pai and Nayfeh, 1991b; Pai and Nayfeh, 1991c) when the frequency of the first in-plane flexural (chordwise) mode is approximately twice the frequency of the first out-of-plane flexural-torsional mode.

Anderson, Balachandran, and Nayfeh (1992) observed nonlinear interactions in the response of a flexible cantilever beam to a parametric excitation. Under certain combinations

of the excitation amplitude and frequency, they experimentally found chaotically modulated motions. They also reported an energy transfer from the high-frequency excited modes to the low-frequency first mode accompanied by amplitude and phase modulations of the high-frequency modes.

Nayfeh (1984) applied nonlinear modal interactions to quench a primary resonance by a combination resonance. Similarly, Tuer et al. (1991) showed an example of regulating vibrations of flexible structures via internal resonance. Balachandran et al. (1992) discussed the consequences of using a linear modal identification package, such as ERA (Eigensystem Realization Algorithm), on the identification of structures that exhibit modal interactions. They found the identified damping coefficient to be oscillatory and to assume negative values.

1.1.3 Damping

Damping is one of the most important parameters in the dynamics of a structure. The strength and type of damping mechanisms determine the rate of decay of transient motions and the stability domains of structural elements. Although damping may dissipate the energy of a system, it may induce very complex motions, including chaos, and even instabilities under certain conditions. Despite the importance of damping, a general theory for it is not available. This is because there is a large number of possibilities. Hence, experimental data are typically used to determine the damping coefficients of assumed models. The most widely used damping model is a linear viscous damping model because this is the easiest and most convenient model. Bert (1973) reviewed several damping models and damping coefficient measurement techniques. In particular, he compared the energy loss per cycle of the models and discussed their shortcomings. Crandall (1970) discussed damping mechanisms and indicated that damping depends on the amplitude and frequency of the cyclic motion. He discussed examples where damping affects the stability of the dynamic system. Banks and Inman (1991) investigated a spatial hysteresis model with a linear viscous air damping as a possible damping mechanism. They found that this model

gives the best quantitative agreement with experimental time histories.

1.2 *Objectives*

The main objective of this research was to investigate the mechanisms that produce nonlinear modal interactions in isotropic and laminated composite plates. The focus was on the effect of the geometric nonlinearities on the vibrations of plates. Composite plates have an added complication due to the directionality property of each layer of the laminate. Hence, plate responses are highly coupled. In addition, we also focused on the effect of a damping material on the modal parameters of a nonclassically supported isotropic plate. The study was broken into three investigations:

1. An investigation of a forced cantilever metallic plate,
2. An investigation of a forced cantilever laminated composite plate,
3. Modal analyses of a nonclassically supported metallic plate with and without a constrained-layer damping (CLD) patch.

The first two experimental studies started with a modal analysis of each plate configurations to obtain information about the natural frequencies, mode shapes, and damping coefficients. A computer-aided test system and the modal-plus software were utilized for acquiring the data, estimating the natural frequencies and mode shapes, and estimating the damping factors. The mode shapes of the forced cantilever metallic plate were compared with those obtained with the time-average hologram interferometry or holometry technique.

Next, sine-sweep and sine-dwell techniques were used to capture the nonlinear dynamics of the plates. The data was captured by dwelling at specific frequencies. We present results showing the activation of a two-to-one internal resonance in the response of the metallic plate to a harmonic excitations. In the second investigation, we discuss modal interactions in the response of $(90/30/-30/-30/30/90)_s$ and $(-75/75/75/-75/75/-75)_s$ laminated composite plates to harmonic excitations. The data are presented in the form of power

spectra, force-response curves, frequency-response curves, Poincaré sections, and pseudo-state planes. These data are used to distinguish among periodic, quasi-periodic, and chaotic motions. Time-average holometry images are available only for the forced metallic plate. These images confirm the mode shapes obtained from the experimental-modal and finite-element analyses.

The third study concentrated on the effect of a constrained layer patch on the the modal parameters of a square plate. The modal analysis of a nonclassically supported plate show the difference between the normal and complex mode shapes.

Chapter 2

TWO-TO-ONE INTERNAL RESONANCE

2.1 *Introduction*

The nonlinear dynamics of plates can be very complicated (Nayfeh and Mook, 1979; Chia, 1980). Nayfeh and Mook described variety of systems exhibiting nonlinear modal interactions. Nayfeh and Balachandran (1989) surveyed theoretical and experimental studies of the influence of modal interactions on the nonlinear response of harmonically excited structural and dynamical systems. Yang and Sethna (1992) and Chang et al. (1993) analytically investigated the nonlinear dynamics of plates with one-to-one autoparametric resonances. Yamaki and Chiba (1983) and Yamaki, Otomo, and Chiba (1983) investigated theoretically and experimentally the nonlinear vibrations of a clamped rectangular plate with an initial deflection and an initial edge displacement.

Cole (1990) conducted an experimental investigation into the effectiveness of spoiler surfaces in suppressing the onset of flutter for a low-aspect-ratio, rectangular wing in a wind-tunnel test. He found that above a certain spoiler size, the wing underwent torsional instability at dynamic pressures well below the expected flutter conditions. Inspection of the natural frequencies of the wing revealed that the frequency of the second bending mode is approximately twice the frequency of the first torsional mode. Hence, it is possible that modal interactions between these modes were responsible for the observed torsional instability.

In this study, a cantilever aluminum plate was excited using a 2000-lb table shaker. We observed that by sweeping the excitation frequency or amplitude upward near the resonance of the second bending mode, we were able to excite the first torsional mode of the plate. This

phenomenon was identified by time histories, power spectra, and pseudo-state plots and was further characterized by force-response curves. The indirect excitation of the torsional mode is similar to that observed by Cole. A detailed description of the experimental methodology is given in the next section, and the results are discussed in the following section.

2.2 *Methodology*

The physical dimensions and material properties of the plate are listed in Table 2.1. We used two different experimental setups in this study. The first setup, displayed in Fig. 2.1(a), was used for the experimental modal analysis (EMA). This figure displays the spatial discretization of the plate surface used in the EMA. We limited our identification of the linear natural frequencies and mode shapes to the first 12 modes. Therefore, using the results from the finite-element analysis (FEA) and computer-aided time-average holometry (CAH) mode shapes, we used a 7×5 grid discretization of the plate surface. We obtained the experimental natural frequencies, mode shapes, and modal damping factors from this setup. The details of the EMA, FEA, and CAH are given in the next three sections. The results from the EMA, FEA, and CAH are compared and discussed in the following section.

The second setup, displayed in Fig. 2.1(b), was used for the force-response measurements. We identified the modal interactions between the second bending and first torsional modes from this setup. To test the quality of the shaker and the attachment condition from the base clamp to a 2000-lb shaker table, we fixed the base clamp without the plate on top of the shaker table. We attached two accelerometers to monitor the clamp-shaker dynamics. One accelerometer was attached at the center of the clamp where it was also used to monitor the input excitation condition during the force-response measurements. The other accelerometer was attached at the edge of the base shaker table. The base clamp was then forced with a random function having a frequency bandwidth ranging from 20 to 2020 Hz. The two accelerometer locations are ideal for observing if there are any noticeable shaker-armature motions other than the prescribed one. We used a spectral analyzer to compute

Table 2.1: Physical dimensions and material properties of the cantilever plate.

Properties	Aluminum Plate
Thickness (h)	0.250 in.
Width (a)	20.00 in.
Length (b)	30.00 in.
Modulus, E	10.60×10^6 psi
Density, ρ	$0.101\,\mathrm{lb/in^3}$
Poisson's ratio, ν	0.33

the frequency-response functions (FRFs) of the accelerometer output signals and the input signals from the random-waveform generator. Each data set was passed through Hanning window and each of the FRFs was averaged 50 times. Figures 2.2(a) and (b) show the Bode plot of the center- and edge-accelerometer signals, respectively. We note that for the frequency bandwidth ranging from 20 to 620 Hz, the two Bode plots appear to be similar in shape and magnitude to the FRFs ($\approx$ 1.6dB). There are some activity between 620 to 820 Hz and at the higher frequencies. The higher frequency peaks represent the shaker-armature resonance conditions. These activities are more apparent in the edge-accelerometer Bode plot shown in Fig. 2.2(b). We conclude from this test that within the frequency range of interest, from 20 to 620 Hz bandwidth, there seems to be no shaker-armature motion due to the addition of the base clamp on the shaker table.

2.2.1 Experimental-modal analysis

The natural frequencies and mode shapes were experimentally obtained by exciting the plate at the grid point 30Z, see Fig. 2.1(a). The responses were measured at the marked grid-point locations on the plate using a set of 7 small accelerometers each weighing approximately 2.20 grams. Therefore, the total mass of the accelerometers is 15.4 grams whereas the mass of the plate is 6.60 kilograms. Thus the added mass ratio is approximately 0.2%, and hence it has an insignificant effect on the natural frequencies and mode shapes of the cantilever plate (Oh and Pryputniewicz, 1990).

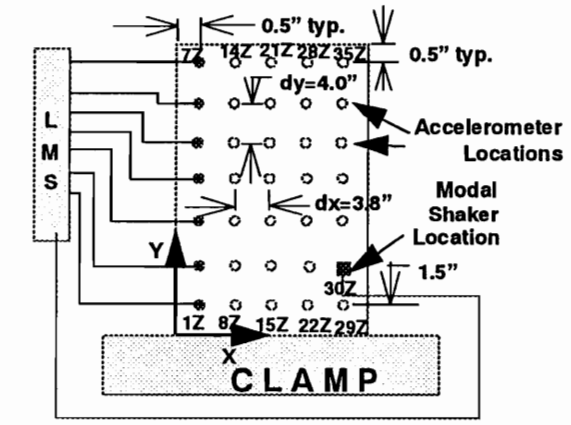

(a)

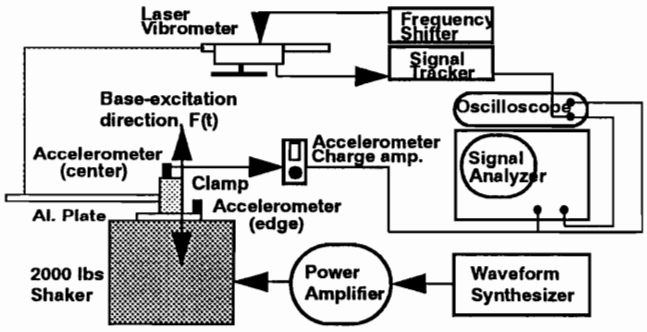

(b)

Figure 2.1: The setup for the cantilever plate: (a) experimental modal analysis (EMA) and (b) amplitude-sweep technique.

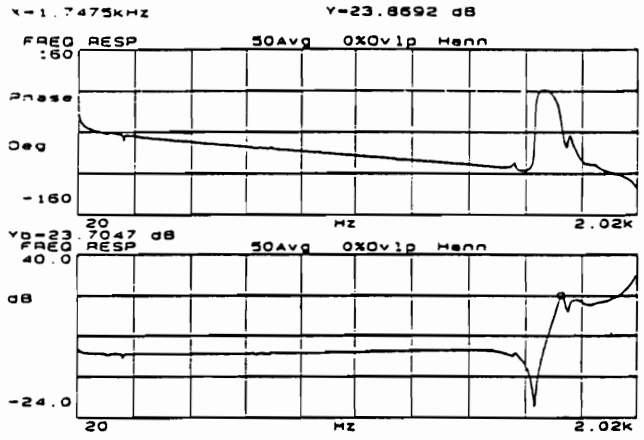

(a)

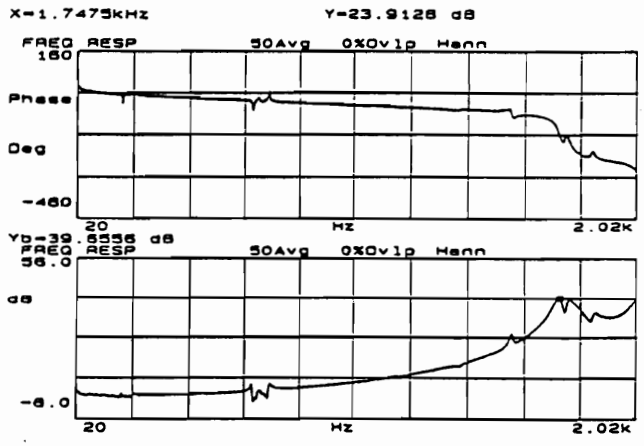

(b)

Figure 2.2: The signature of the 2000-lb table shaker with the base clamp attached: (a) Bode plot of the center-accelerometer signal and (b) Bode plot of the edge-accelerometer signal. [see Fig. 2.1(b)]

Measurements were made from the 7 × 5 grid points outlined on the plate surface as displayed in Fig. 2.1(a). The grid spacing in the x-direction is 3.8 inches and the y-direction is 4.0 inches. The grid points start from the lower-left coordinate at (0.5,1.5) in. and the upper-right coordinate at (19.5,29.5) in. with the axes origin at the lower-left corner of the plate surface. We assumed a two-dimensional model in the EMA. The driving-point frequency-response curve is shown in Fig. 2.3. The plate was excited using a 10-lb modal shaker that produced a 512 Hz bandwidth burst-random signal.

The data from five sequential measurements of 7 vertically aligned accelerometer signals were used to calculate the frequency-response functions (FRFs). These FRFs, totaling 35, were calculated and stored using an LMS Cada Version 2.7 modal analysis test system. The LMS system used is at the Alpha Body Engineering Methodology Laboratory, Alpha Simultaneous Engineering, Ford Motor Company, Dearborn, MI. A uniform windowing method was used for both the input and the response, and a total of 100 averages were taken for each FRF. With 4096 lines of resolution for the bandwidth of 512 Hz, the frequency resolution was 0.125 Hz per line. The natural frequencies, mode shapes, and damping coefficients were calculated from the collected FRFs by using the direct parameter method provided in the LMS Cada software. The direct parameter estimate technique is a multi-degree-of-freedom frequency-domain curve-fitting technique. The first twelve experimentally obtained natural frequencies along with the ones obtained from the finite-element analysis (FEA) are listed in Table 2.2. The first four corresponding mode shapes are shown in Fig. 2.4. These mode shapes are also compared with the ones obtained with the computer-aided time-average holometry technique and they are displayed in Fig. 2.4.

2.2.2 Finite-element analysis

The natural frequencies and mode shapes were approximated using the commercially available finite-element software ABAQUS. The aluminum plate was subdivided into 20 by 30 elements in the width and length directions, respectively. We used the eight noded quadrilateral thick shell element S8R and utilized the reduced integration scheme. This

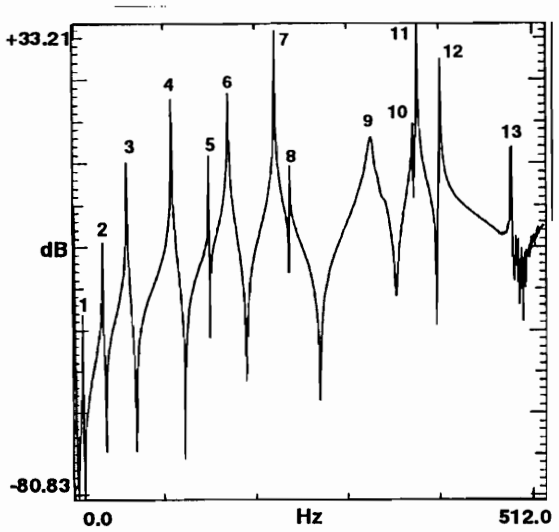

Figure 2.3: The driving-point frequency-response curve from LMS Cada modal analysis test system.

element was also chosen because it approximates the Mindlin-type element. It takes into account the first-order shear deformation through the thickness of the element and rotary inertia effects. The twelve converged eigenvalues are listed in Table 2.2, and the corresponding first four mode shapes are shown in Fig. 2.4.

2.2.3 Time-average holometry

Hologram interferometry or holometry involves the recording of multiple object positions onto the same medium. The diffraction patterns created by the interference of the reconstruction of these multiple exposures of the object produce fringe patterns on the reconstructed surface, which indicate the movement of the object during the test period. In time-average holometry, a single exposure of an object going through cyclic vibrations is made. The exposure time is normally much longer than the period of the vibration cycle.

A schematic of the holographic setup is shown in Fig. 2.5. We used the holographic

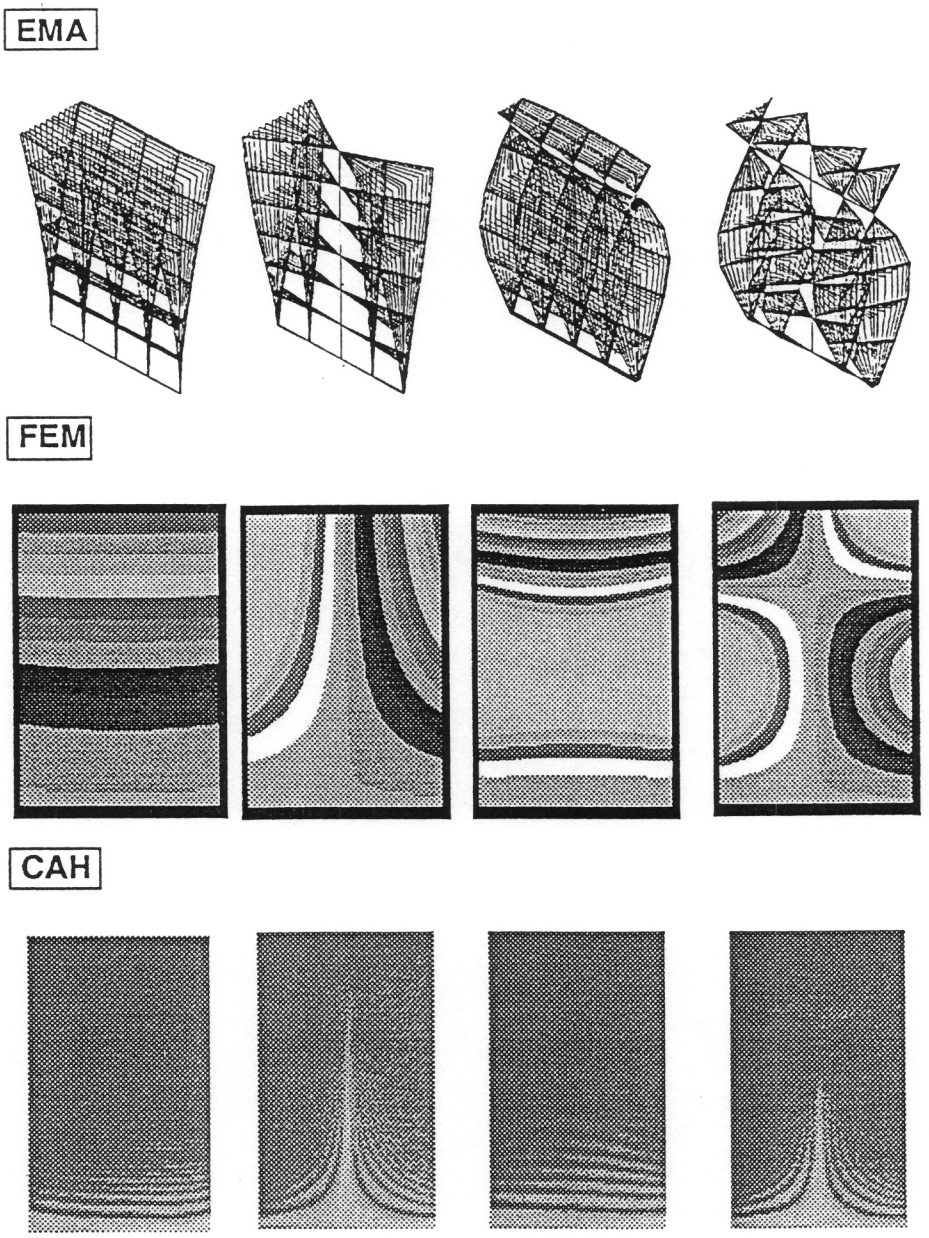

Figure 2.4: The first 4 mode shapes obtained with the experimental modal analysis (EMA), finite-element analysis (FEA), and computer-aided time-average holometry (CAH).

setup located at the Computer Aided Holometry (CAH) Laboratory, Manufacturing Systems Department, Materials Research Laboratory, Ford Research Laboratory, Ford Motor Company, Dearborn, MI. The laser is a continuous-wave (CW) 25 watt argon laser operating at 3 watts and a wavelength of 514.5 nm. The laser beam is divided into two beams by using a beam splitter. One beam, referred to as the object beam, illuminates the aluminum plate under study, and the other, referred to as the reference beam, illuminates the holographic plate; the interference between these two beams creates a time-averaged hologram. This hologram illuminated with a reconstruction reference beam creates a fringe pattern, in this case a Bessel function of order zero on the reconstructed surface. The fringe pattern on the reconstructed surface is referred to as a time-averaged (TA) holometry image. These images were "grabbed" using a video CCD camera, mounted behind the hologram position and interfaced with the computer. The aluminum plate was acoustically excited using natural frequencies obtained from the modal analysis. The first four mode shapes obtained with the time-averaged holometry technique are displayed in Fig. 2.4. Details of the time-averaged holographic interferometry technique can be found in Vest (1979) and Pryputniewicz (1985).

2.2.4 Nonlinear force-response measurements

The nonlinearity in the plate vibration can be revealed through slow amplitude or frequency sweeps near the resonance frequency of the mode of interest. In applying the amplitude-sweep technique, one needs to keep the frequency of excitation constant. Conversely, in the frequency-sweep technique, one needs to keep the amplitude of excitation constant. However, it was difficult to keep the excitation amplitude constant during the frequency sweep near a resonance because we did not have a closed-loop vibration monitor system available with the 2000-lb shaker. We found that keeping the excitation frequency constant while varying the excitation amplitude was easier without the closed-loop vibration monitor system. Therefore, we present only the results from the amplitude-sweep technique.

To capture the nonlinear modal interactions between the bending and torsional modes,

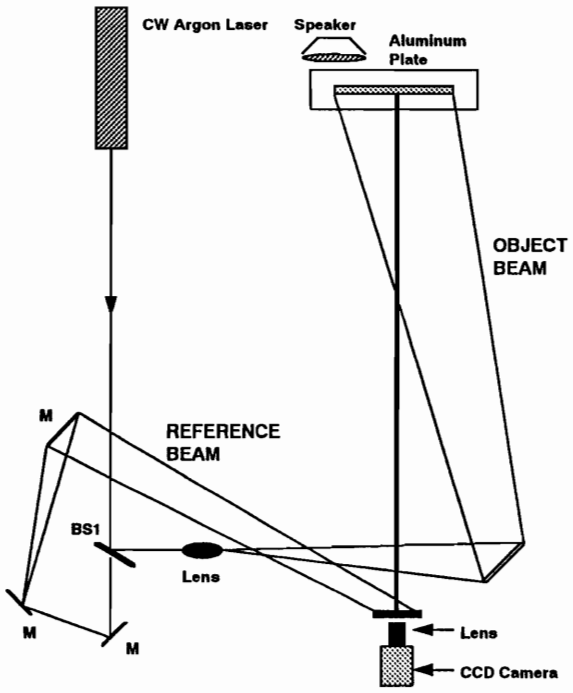

Figure 2.5: A schematic of the time-averaged holometry.

we mounted the plate horizontally on the shaker and excited the plate near the second bending frequency while incrementally increasing the amplitude of excitation. This configuration is displayed in Fig. 2.1(b). We monitored the input excitation using an accelerometer mounted on the base of the clamp and the plate response using a laser vibrometer. The accelerometer signal was fed to a charge amplifier, the vibrometer signal was fed to a signal tracker, and then they were used in the spectrum analyzer. In this way, we always monitored the frequency contents of the input and output during the amplitude sweep. At each increment of the excitation amplitude, we waited until the transients had settled down by observing the input and output signals on an oscilloscope and a spectral analyzer. The analyzer was set to display the dynamic range of 60 dB from the highest signal level. We assumed that any signals below the 60 dB range were insignificant. After the transients had settled down, we obtained the autospectra of the input and output signals using the analyzer. We used 50 averages for each measurement. The input acceleration level was then obtained from the autospectrum of the accelerometer signal. Similarly, the response of the plate was obtained from the autospectrum of the vibrometer signal. The responses of the directly excited, second bending mode, and the indirectly excited, first torsional mode, were determined from the corresponding frequency peaks in the autospectrum plots. A Macintosh II FX computer with an A/D card was also used to acquire time-domain data for additional spectral analysis and data presentations.

2.3 *Results*

2.3.1 Linear natural frequencies and mode shapes

The natural frequencies and mode shapes obtained with the FEA, EMA, and CAH are listed in Table 2.2 and Fig. 2.4. The agreement among them is good with the discrepancies being within 3% for the first 12 modes. We suspect that the discrepancies are largely due to the misalignment between the modal shaker, which was suspended in the air, and the cantilever plate, which was fixed on the floor. Therefore, the dynamics of the plate during

Table 2.2: Natural frequencies obtained with the experimental-modal analysis (EMA) and finite-element analysis (FEA).

Mode No.	Experimental modal (Hz)	Finite element (Hz)
1	9.50	9.46
2	31.75	31.29
3	59.07	58.62
4	108.74	105.96
5	148.50	145.46
6	170.19	169.07
7	221.25	217.12
8	237.60	230.89
9	327.04	327.22
10	371.78	362.02
11	377.00	370.38
12	402.22	393.70

the modal test also included the dynamics of the stinger attached between the modal shaker and the cantilever plate.

2.3.2 Nonlinear plate vibrations

We captured the nonlinear behavior of the plate by harmonically exciting the plate at a frequency near that of the second bending mode. The excitation to the plate was arranged, shown in Fig. 2.1(b), such that only bending modes or symmetric modes were directly excited. Hence, any significant responses detected by the instrumentation at the torsional mode or antisymmetric mode frequencies are assumed to be the result of their being indirectly excited via nonlinear modal interactions.

Our focus was to excite the first torsional mode through a two-to-one internal-resonance mechanism. Hence, we excited the cantilever plate near the frequency of the second bending mode. The variable parameters that were used to activate the internal resonance were the excitation frequency and amplitude. We fixed the excitation frequency at $f_e = 56.72$ Hz and swept the excitation amplitude, A_e, forward and backward from 0.50 g to 2.00 g.

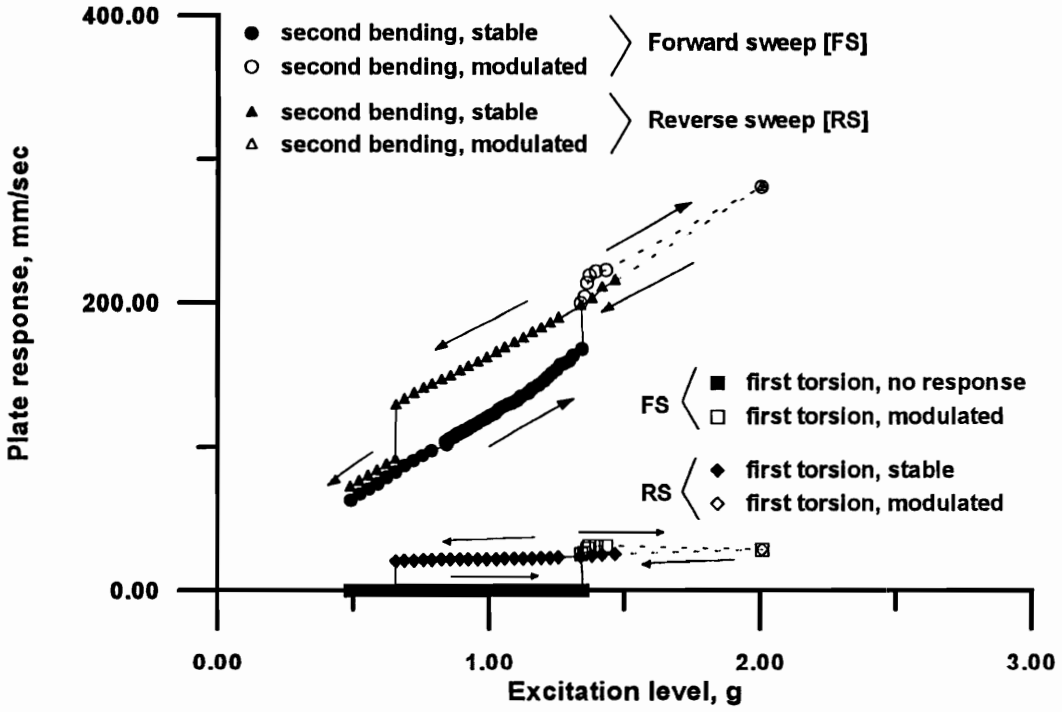

Figure 2.6: Amplitude-response curves for the second bending mode and first torsional mode of the cantilever plate during a sweep-up and sweep-down of the excitation amplitude.

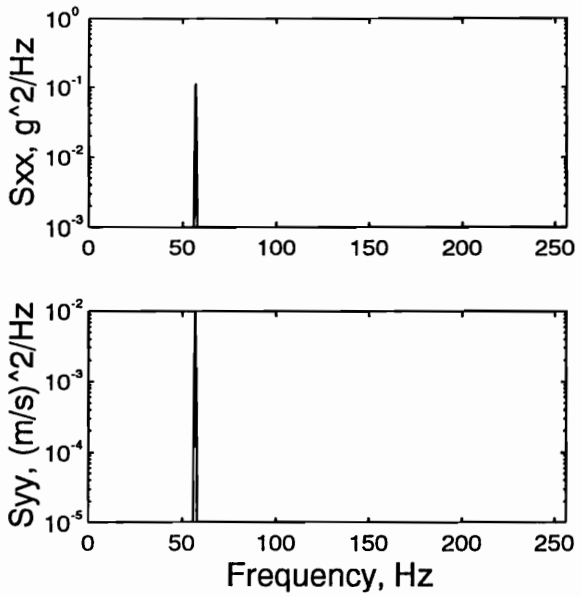

Figure 2.7: The power spectra for the input, S_{xx}, and plate response, S_{yy}, before the activation of the two-to-one internal resonance.

The obtained force-response curves are shown in Fig. 2.6. In forward sweep, the o and □ symbols represent the bending and torsional responses, respectively. The dark symbols indicate stable periodic motions, whereas the hollow symbols indicate modulated motions. Similarly, in the reverse sweep, the △ and ◇ symbols represent the bending and torsional responses, respectively. During the forward sweep, initially, as the excitation amplitude, A_e, was increased, the amplitude of the directly excited bending mode increased, and the torsional mode was not activated. The power spectra for the excitation and plate response before the torsional mode was activated are shown in Fig. 2.7. The power spectra of the input and response signals clearly show that only the directly excited second bending mode at $f_e = 56.72$ Hz was excited.

However, as the excitation amplitude increased beyond approximately 1.33 g, the amplitude of the torsional mode jumped up. Moreover, the amplitude of the bending mode also jumped up to a higher value. In addition, both the torsional and bending mode responses were amplitude and phase modulated. Therefore, data displayed in the amplitude-response

curves beyond $A_e = 1.33\ g$ during the forward sweep, represent the average of the modulated signals. By increasing the excitation amplitude while keeping the excitation frequency constant, we indirectly excited the torsional mode by activating the two-to-one internal resonance. Within the 60 dB dynamic amplitude range, besides f_e, the power spectra S_{xx} and S_{yy}, shown in Fig. 2.8, contain a component at $\frac{1}{2} f_e$. Due to the limitation of the shaker-armature assembly in balancing the eccentric load or external moment when the torsional mode of the plate was excited, there was a little feedback from the plate to the shaker. This is evident from the input spectrum, S_{xx}, shown in Fig. 2.8, where there is a small component at $\frac{1}{2} f_e$. By comparing the magnitudes of the peaks at f_e and $\frac{1}{2} f_e$ in the response power spectrum, S_{yy}, we conclude that the two-to-one internal-resonance phenomenon observed in our experiment is considerably less pronounced than the torsional instability reported by Cole (1990). This is due to the difference between our experimental setup and Cole's wind-tunnel setup. In our setup, the cantilever plate is fixed along the entire edge of the plate. In Cole's setup, the plate is only fixed along a 2.25 inch strip located 4.88 inches down from the leading edge on the shorter dimension of the plate (Cole, 1990). Hence, our plate is much stiffer in torsion than that of Cole.

To verify the activation of the two-to-one internal resonance, we constructed a state-control space using data collected over four seconds at a sampling frequency $f_s = 512.00$ Hz from the accelerometer monitoring the input acceleration and the vibrometer monitoring the plate velocity. The plot displayed in Fig. 2.9 shows a typical plot for a system in which the response period is twice that of the excitation. This agrees with Fig. 2.8 where $\omega_2 \approx \frac{1}{2} f_e$ was indirectly excited by the two-to-one internal resonance when the plate was excited at $f_e = 56.72$ Hz and the excitation amplitude was $A_e \geq 1.33\ g$. In addition, we suspect that the width of the trace in the plot may be an indication of amplitude and phase modulations in the response.

To clarify this, we computed the autocorrelation functions using 35,840 points from a digitized time history sampled at $f_s = 512.00$ Hz over 70 seconds. The autocorrelation

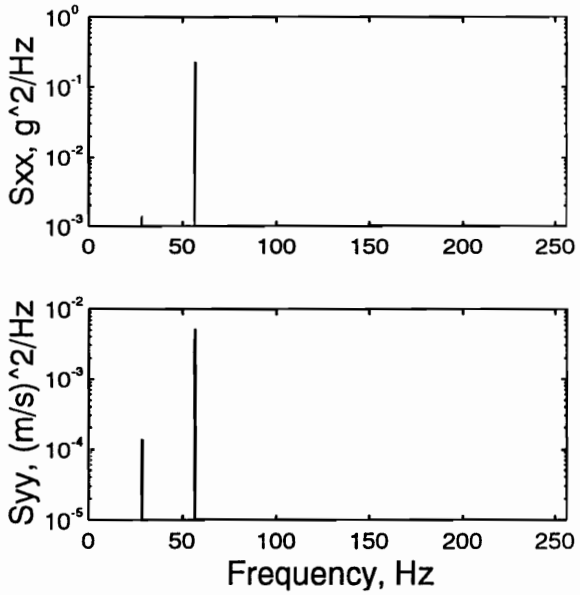

Figure 2.8: The power spectra for the input, S_{xx}, and plate response, S_{yy}, after the activation of the two-to-one internal resonance.

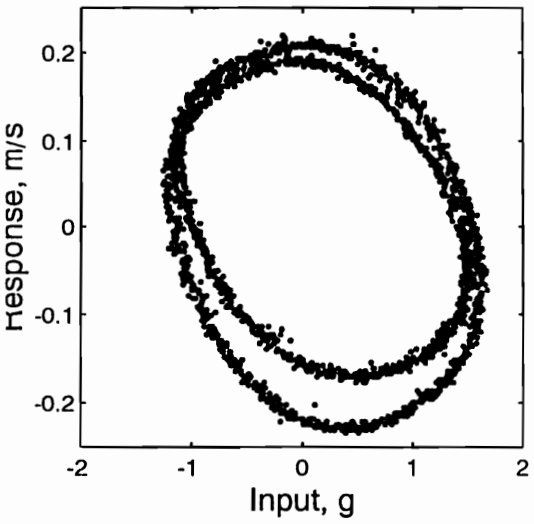

Figure 2.9: A state-control space obtained by plotting the input acceleration against the plate velocity when the two-to-one internal resonance was activated.

function for a given stationary signal $x(t)$ is

$$\hat{R}_{xx}(\tau) = \lim_{T\to\infty} \frac{1}{T} \int_0^T x(t)\, x(t+\tau)\, dt.$$

For a finite discretized N data points, x_n, $n = 1, 2, \ldots, N$, sampled at equal intervals, $\Delta t = 1/f_s$, the autocorrelation function can be estimated from

$$R_{xx}(r\Delta t) = \frac{1}{N-r} \sum_{n=1}^{N-r} x_n x_{n+r}$$

for $r = 0, 1, 2, \ldots, m$, where r denotes the time-delay points and m is the maximum time-delay point ($m < N$) (Bendat and Piersol, 1986). We implemented the latter approach using the MATLAB function XCORR and normalized the sequence so that the estimated autocorrelation function had a value of unity at zero time delay. The autocorrelograms for the input acceleration signal, R_{xx}, and plate velocity, R_{yy} are displayed in Fig. 2.10. By examining the envelope of an autocorrelogram, one can gain insight into the nature of the motion. We note that because of the finite number of data points, the envelope of an autocorrelogram decays linearly to zero as τ becomes large. The details can be found in Bendat and Piersol (1986). Both of the autocorrelograms in Fig. 2.10 show signs of modulated waveform, and after a closer look, we see three basic frequency components: f_e and $\frac{1}{2} f_e$, corresponding to a fast time scale, and f_v, corresponding to a slow time scale. The first two frequencies are already known from examining the power spectra, but f_v is new. With a new lead, we reexamined the power spectra of the input acceleration and plate velocity. We increased the resolution of the power spectra to $\Delta f = 0.10$ Hz by zooming into the frequency bandwidth from 20 – 70 Hz. The zoomed power spectra are presented in Fig. 2.11 and we limit our observation to 60 dB range from the largest peak in the spectrum. However, we do not see any side bands at either of the frequency components that may indicate amplitude or phase modulations of the plate motion. Hence, after reexamining the autocorrelograms and zoomed power spectrum, we conclude that the motion at the slow time scale is insignificant.

As the excitation level was further increased, the average of the modulating bending-mode response continued to increase steadily. However, the average of the modulating

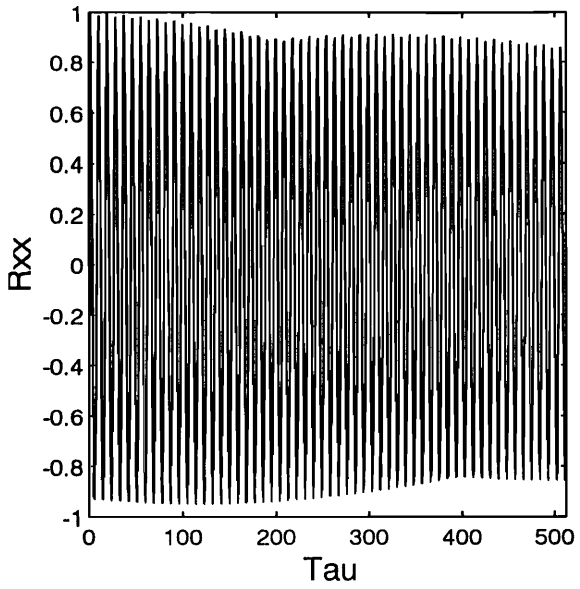

(a)

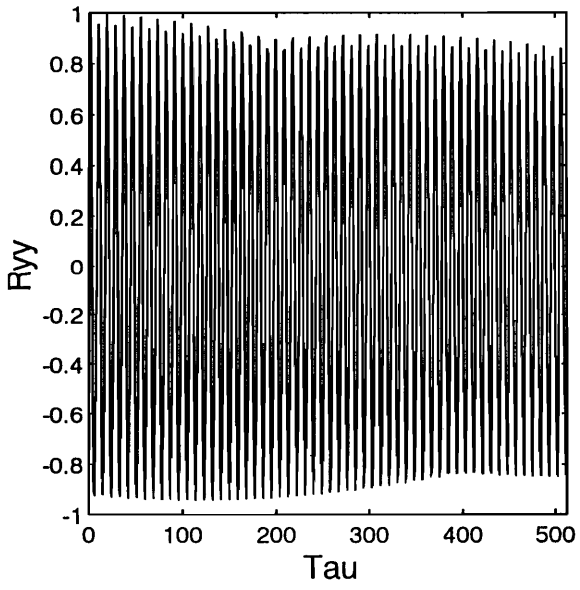

(b)

Figure 2.10: The autocorrelograms obtained from (a) the input acceleration and (b) the plate velocity when the two-to-one internal resonance was activated.

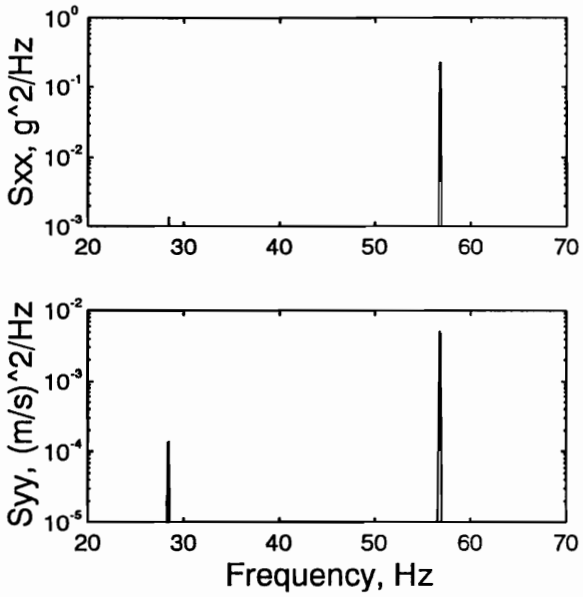

Figure 2.11: The power spectra for the input acceleration, S_{xx}, and plate velocity, S_{yy}: zoom span between 20 – 70 Hz, $\Delta f = 0.10$ Hz.

torsional-mode response remained constant with a slight decrease near $A_e = 2\ g$. We represent the averaged modulating signals for both modes as dashed lines in the amplitude-response curves. At this point, we reversed the sweeping direction.

In the reverse amplitude sweep, starting from $A_e = 2.00\ g$, we found that initially both the bending and torsional responses followed the same curve that they followed during the forward sweep. However, there is a slight difference in the slope of the dashed lines for both the bending and torsional modes shown in the amplitude-response curves. We note that at the starting of the reverse sweep, both the bending and torsional mode responses were modulated. Therefore, the difference in the slopes of the dashed lines can be attributed to the uncertainties in averaging the modulated motions. As we continue to sweep-down in amplitude, at $A_e \approx 1.43\ g$, we observed both signals to be periodic.

The existence of a periodic solution near the modulated-solution branches when the two-to-one internal resonance is active has been investigated by Pai and Nayfeh (1991d)

for three-dimensional vibrations of composite beams. Their analysis focused on the case of primary resonance of the first in-plane flexural mode when its frequency was approximately twice the frequency of the first out-of-plane flexural-torsional mode. In Fig. 2.12, we show the analytically obtained force-response curves by (a) including the cubic and quadratic nonlinearities and (b) keeping the quadratic nonlinearities and neglecting the cubic nonlinearities. Figure 2.12(b) displays a typical force-response curve dominated by quadratic nonlinearities with a slight detuning in the excitation frequency. This figure, shows a possible jump phenomenon at f_2 and f_3 with $f = f_3$ being a subcritical pitchfork bifurcation point. The dynamics is much more complicated in the presence of the cubic nonlinearities, as shown in part (a). Although the plate and beam configurations are different, the study by Pai and Nayfeh (1991d) indicate a possible complication in the dynamics of a system having cubic and quadratic nonlinearities interacting with each other. In our case, the cubic nonlinearities dominate the quadratic nonlinearities.

The periodicity in both signals continued with the amplitude of the bending response continually decreasing and the torsional response maintaining a constant amplitude. At $A_e = 0.65\ g$, the torsional response jumped down to zero, and the bending response jumped down to near its original response amplitude prior to the activation of the two-to-one internal resonance.

2.4 *Closure*

Our experimental results illustrate a possible mechanism for the torsional instability observed in the experiment of Cole (1990) in his wind-tunnel experiments. He found that an added spoiler drastically reduced the flutter boundary on a flat plate and produced a torsional instability.

In our experiment, we excited the second bending mode using a shaker. In Cole's experiment, the second bending mode was most likely excited by pressure fluctuations in the wake of the spoiler. In both cases, it seems that energy was transferred from a high-

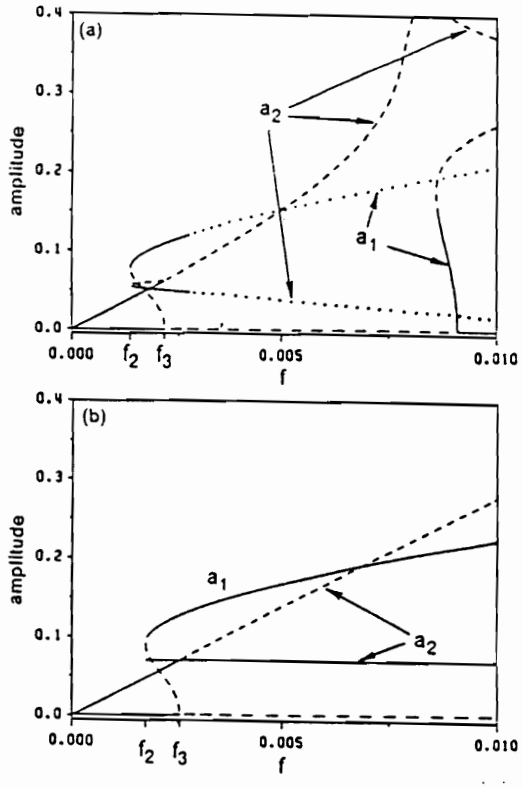

Figure 2.12: Force-response curves obtained by Pai and Nayfeh (1991d) by (a) including the cubic and quadratic nonlinearities and (b) neglecting the cubic but including the quadratic nonlinearities.

frequency mode to a low-frequency mode by means of an internal resonance. Such a transfer is potentially dangerous because, for a given amount of energy, a reduction in frequency must be accompanied by an increase in amplitude.

We performed the experiment by harmonically exciting a cantilever aluminum plate at its base using a shaker, thereby, allowing mostly the bending modes to be excited. By keeping the excitation frequency constant and sweeping the excitation amplitude forward and backward between 0.50 g to 2.00 g, we excited the first torsional mode. An overview of the plate responses for a given excitation frequency is presented in force-response curves. We utilized the time histories, power spectra, and state-control plots to characterize the plate motions. We have shown through an experiment that, if the frequency of a directly excited bending mode is approximately twice the frequency of a torsional mode of a plate, the torsional mode can be indirectly excited through a two-to-one internal-resonance mechanism.

Chapter 3

HIGH- TO LOW-FREQUENCY MODAL INTERACTIONS

3.1 *Introduction*

The complicated dynamic behavior of weakly nonlinear systems has been the focus of recent research efforts. A large number of these investigations involve a special frequency relationship between two or more linear natural frequencies and/or a special relationship between the natural frequencies and the excitation frequencies, where the steady-state response of the system may contain large contributions from several modes. Interaction among the modes (i.e., modal interactions) can lead to surprisingly large-amplitude responses in modes that are predicted by linear analyses to have no response. The possible types of modal interactions depend on the natural frequencies of and the type of nonlinearities present in the system.

Modes with commensurate or nearly commensurate natural frequencies ω_i can interact via internal or autoparametric resonances. In systems having cubic nonlinearities, internal resonances may occur if $\omega_n \approx \omega_m$, $\omega_n \approx 3\omega_m$, $\omega_n \approx |\pm 2\omega_m \pm \omega_k|$, or $\omega_n \approx |\pm\omega_m \pm \omega_k \pm \omega_l|$. In systems with quadratic nonlinearities, additional resonances may occur if $\omega_n \approx 2\omega_m$ and $\omega_n \approx \omega_m + \omega_k$. Analyses of nonlinear oscillators with internal resonances have been successfully investigated using perturbation methods (e.g., Nayfeh, 1973, 1981; Nayfeh and Mook, 1979; Crespo da Silva, 1980; and Bajaj and Johnson, 1990). These analyses have been experimentally validated (e.g., Nayfeh and Balachandran, 1989). The perturbation results are in good agreement with the experimental results. Therefore, the activation of a low-frequency mode with an excitation frequency near that of a high-frequency mode

through an internal resonance is well documented.

Other types of nonlinear modal interactions are possible for a multi-degree-of-freedom system subjected to a single-frequency harmonic excitation. For a system with cubic nonlinearities, if the excitation frequency $f_e \approx 2|\pm\omega_m \pm\omega_k|$, $f_e \approx |\pm 2\omega_m \pm\omega_k|$, $f_e \approx \frac{1}{2}(\omega_m \pm\omega_k)$, or $f_e \approx |\pm\omega_m \pm\omega_k \pm\omega_l|$, then a combination resonance may occur. Additional combination resonances may occur in systems with quadratic nonlinearities if $f_e \approx |\pm\omega_m \pm\omega_k|$. Dugundji and Mukhopadhyay (1973) investigated the response of a cantilever beam to a parametric excitation whose frequency is close to the sum of the first bending and first torsional modes. They observed a large contribution from the low-frequency first bending mode besides the ones at the excitation frequency and from the first torsional mode. Thus, a high-frequency excitation can produce a large-amplitude response in a low-frequency mode. Similar modal interactions were observed for other parametrically excited systems via combination resonance. Interested readers are referred to Nayfeh and Mook (1979) and Schmidt and Tondl (1986) for comprehensive treatments of this class of problems and lists of references.

Haddow and Hasan (1988) observed an indirect excitation of a low-frequency mode when a cantilever beam was parametrically excited near twice the natural frequency of its fourth mode. They observed that, as the planar periodic response of the fourth mode lost stability and produced a nonplanar chaotic response, the energy cascaded down through the modes. As a result, the steady-state response contained a low-frequency component. In a similar experiment, Burton and Kolowith (1988) reported that the chaotic response of the beam contained the lowest seven in-plane bending modes, including the first torsional mode. Cusumano and Moon (1989) observed a cascading of energy to low-frequency components when an externally excited cantilever beam was in transition to chaotic nonplanar motions.

Recent studies have shown that yet another type of modal interaction can couple the high- and low-frequency modes. Anderson, Balachandran, and Nayfeh (1992) found that when a slender cantilever beam was parametrically excited near a high-frequency mode, the beam response contained a large contribution from a low-frequency first bending mode. They found that the excitation of the low-frequency mode was accompanied by slow modu-

lations of the amplitude and phase of the high-frequency mode. The modulation frequency was equal to the frequency of the low-frequency mode. Nayfeh and Nayfeh (1994) also found energy transfer from a high-frequency to a low-frequency mode in an externally excited slender cantilever rod. Their experimental results show that the activation of the low-frequency first mode is accompanied by modulations of the amplitude and phase of the higher-frequency mode. Moreover, they found that the first-mode response was also modulated. Popovic et al. (1994) experimentally characterized the transfer of energy from a low-amplitude, high-frequency excitation to a high-amplitude, low-frequency response in a flexible three-beam-frame structure.

In this chapter, we present an experimental characterization of energy transfer from high-frequency to low-frequency modes in a cantilever graphite-epoxy composite plate. This plate is stiff in contrast with the flexible structures studied by Anderson et al. (1992), Nayfeh and Nayfeh (1994), and Popovic et al. (1994). A 2000-lb table shaker was used to excite a cantilever six-layer laminated graphite-epoxy composite plate having a symmetric stacking ply sequence of $(90/30/-30/-30/30/90)_s$ with a frequency near that of its seventh (third torsional) mode. For some excitation amplitudes and frequencies, we observed the activation of a low-frequency (first bending) mode accompanied by amplitude and phase modulations of the seventh mode. The energy transfer from a high-frequency to a low-frequency mode observed in this experiment is similar to that observed by Anderson et al. (1992), Nayfeh and Nayfeh (1994), and Popovic et al. (1994) in flexible structures. However, due to the two-to-one frequency relations between the third and second torsional modes, we observed that, for some excitation amplitudes and frequencies, the second torsional mode as well as the first bending mode were activated by the high-frequency excitation. Time-history and power-spectra plots are used to characterize the experimental data. Furthermore, the dynamics of the plate is characterized by using force-response curves.

Table 3.1: Physical dimensions and material properties of the plate.

Properties	Mean Value
Thickness (h)	0.138 in.
Width (a)	6.870 in.
Length (b)	11.500 in.
E_{11}	$22.14 \times 10^6\ lbf/in^2$
E_{22}	$1.281 \times 10^6\ lbf/in^2$
E_{33}	$1.165 \times 10^6\ lbf/in^2$
G_{12}	$0.765 \times 10^6\ lbf/in^2$
G_{23}	$0.668 \times 10^6\ lbf/in^2$
G_{13}	$0.765 \times 10^6\ lbf/in^2$
ν_{12}	0.297
ν_{23}	0.485
ν_{13}	0.297
ρ	$1.460 \times 10^{-4}\ lbf\,s^2/in^4$

3.2 *Methodology*

A six-layer symmetric laminated graphite-epoxy composite plate was manufactured at the Virginia Tech, Center for Composite Materials and Structures, Fabrication Laboratory. The stacking sequence for the plate is $(90/30/-30/-30/30/90)_s$. The material properties of the laminated composite plate were experimentally obtained by Anderson (1993) from uniaxial and symmetric cross-ply plates made from the same material and cured by using the same cure cycle as the plate investigated in this chapter. The measured dimensions and material properties are listed in Table 3.1.

As a first part of this study, we compared the natural frequencies and mode shapes of the plate obtained by using a finite-element analysis (FEA) with those obtained by using an experimental modal analysis (EMA). We used a Mindlin-type element in the FEA. A calibrated impact hammer served as an input source and a laser vibrometer measured the plate response for the EMA. The largest difference in the natural frequencies obtained from the two analyses is approximately 6% and the first 9 mode shapes obtained from the two

analyses are in qualitative agreement. The FEA estimated the 10th mode to be a first in-plane stretching mode. This mode could not be identified with the EMA because the excitation did not allow any energy to be input into the in-plane mode of vibration and the vibrometer was not directed to measure in-plane motions. The sequence of the 11th and 12th modes calculated from the FEA is opposite to that obtained with the EMA. These differences are discussed further in the following section.

Next, we investigated the response of the plate to a single-frequency harmonic excitation. The control parameters are the excitation frequency and amplitude. Setting the excitation frequency near that of the 7th mode and varying the excitation amplitude, we observed an energy transfer from this high-frequency mode to a low-frequency mode, namely, the first bending mode. In addition, for some excitation amplitudes and frequencies, we also observed the activation of a two-to-one internal resonance, yielding a response at $\omega_4 \approx \frac{1}{2}\omega_7$. We present force-response curves when (i) high- to low-frequency modal interactions occur and (ii) a two-to-one internal resonance and high- to low-frequency modal interactions are simultaneously activated. For specific excitation amplitudes, time traces and power spectra were used to characterize these modal interactions. We present the details of the finite-element, experimental-modal, and force-response analyses in the subsequent sections.

3.2.1 Finite-element analysis

We used the commercially available finite-element software ABAQUS to compute the natural frequencies and mode shapes of the plate. The dimensions and material properties used in the calculations are listed in Table 3.1. We assumed that each layer is orthotropic and the thickness of each layer is equal to the overall thickness of the plate divided by the number of layers. Therefore, the thickness of each layer is $(0.138/12)\,\text{in.} = 0.012\,\text{in.}$

The plate was subdivided into 30 by 20 elements in the length and width directions, respectively. The eight noded quadrilateral thick shell element (S8R) and reduced integration scheme were used in the analysis. This element approximates the Mindlin-type element that accounts for rotary inertia effects and first-order shear deformations through

the thickness. The first 12 calculated natural frequencies are listed in Table 3.2 along with the ones estimated from the modal analysis. The corresponding mode shapes are displayed in Fig. 3.3.

3.2.2 Experimental-modal analysis

A schematic of the experimental-modal analysis (EMA) is shown in Fig. 3.1. The plate is vertically clamped at the base and fixed to the floor. An instrumented hammer was used as a source of an impulse force and the response of the plate was measured using a laser vibrometer. The surface of the plate was discretized by the 7×5 grid displayed in Fig. 3.1. The grid spacing in the x-direction was $\delta x = 1.5$ inches and in the y-direction was $\delta y = 1.6$ inches. The dimensions were referenced to the lower-left corner of the plate. The bounding grid points for the 7×5 grid discretization were 1Z, 7Z, and 29Z. The coordinates for the three grid points were as follows: $1Z \rightarrow (0.406, 1.613)$ in.. $7Z \rightarrow (0.406, 11.213)$ in., and $29Z \rightarrow (6.406, 1.613)$ in. We chose to fix the measurement point at grid point 5Z and varied the forcing location along the grid points. We note that the use of a nonintrusive sensor, such as a laser vibrometer, is critical for obtaining accurate modal data because the mass of a composite plate, such as the one used in this study, is approximately the same order as the mass of a small (2.5 gram) accelerometer.

The transfer functions were estimated using a computer-aided testing system and the modal analysis was conducted using the modal-plus software from SDRC, a resident program in the computer-aided test system. At each grid point, we averaged 20 individual impulse force-response functions and set the measurement conditions to have a 0.5 Hz resolution. The modal parameters were estimated using the polyreference method, which is a multi-degree-of-freedom complex least-squares method in the time domain (User manual for Modal Analysis 9.0, 1985). The modal parameters are listed in Table 3.2 and the corresponding mode shapes are shown in Fig. 3.4.

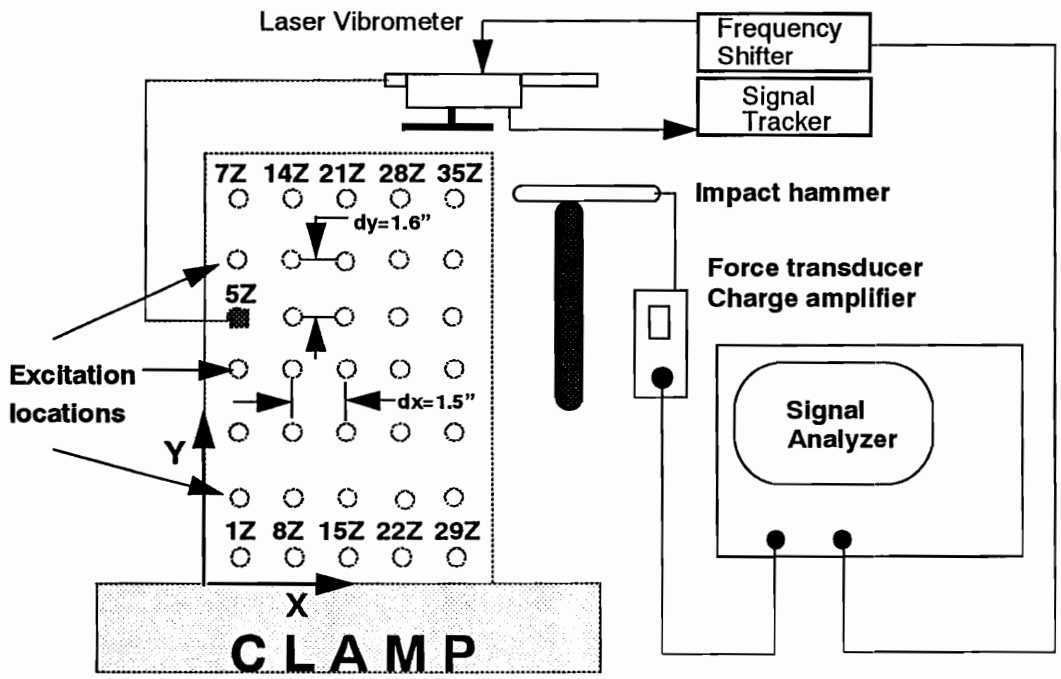

Figure 3.1: A schematic of the experimental-modal analysis (EMA).

3.2.3 Force-response analysis

To produce force-response curves, one keeps the excitation frequency constant and slowly varies the excitation amplitude. On the other hand, to produce frequency-response curves, one keeps the excitation amplitude fixed and slowly varies the excitation frequency. In our setup, it was difficult to keep the excitation amplitude constant during the frequency sweep near a resonance because we did not have a closed-loop vibration monitor system available with the 2000-lb shaker. We found that keeping the excitation frequency constant while varying the excitation amplitude was an easier task without the closed-loop vibration monitor system. Therefore, we present only force-response curves.

To capture the nonlinear interactions between the seventh (third torsional) mode and the first bending mode, we mounted the plate horizontally on the 2000-lb table shaker. A schematic of the test setup is shown in Fig. 3.2. The plate was excited near its seventh natural frequency ω_7 while slowly increasing the excitation amplitude. The procedure for generated force-response curves and the methodology for collecting time and frequency domain data are described in Section 2.2.4.

3.3 *Results*

3.3.1 Linear natural frequencies and mode shapes

The natural frequencies and mode shapes obtained by using the FEA and EMA for the first nine modes are in good agreement. Inspecting the tabulated natural frequencies in Table 3.2, we note that the largest difference appears in the estimated value of the second natural frequency. The largest difference is approximately 6%. The difference in the natural frequencies is within the bounds of the experimental uncertainties and theoretical simplifications in the finite-element method. The 10th mode predicted by the FEA is the first in-plane stretching mode. This mode could not be ascertained with the EMA analysis because the excitation and measurement directions were only capable of exciting and detecting out-of-plane modes. It follows, from Figs 3 and 4 that the order of the 11th

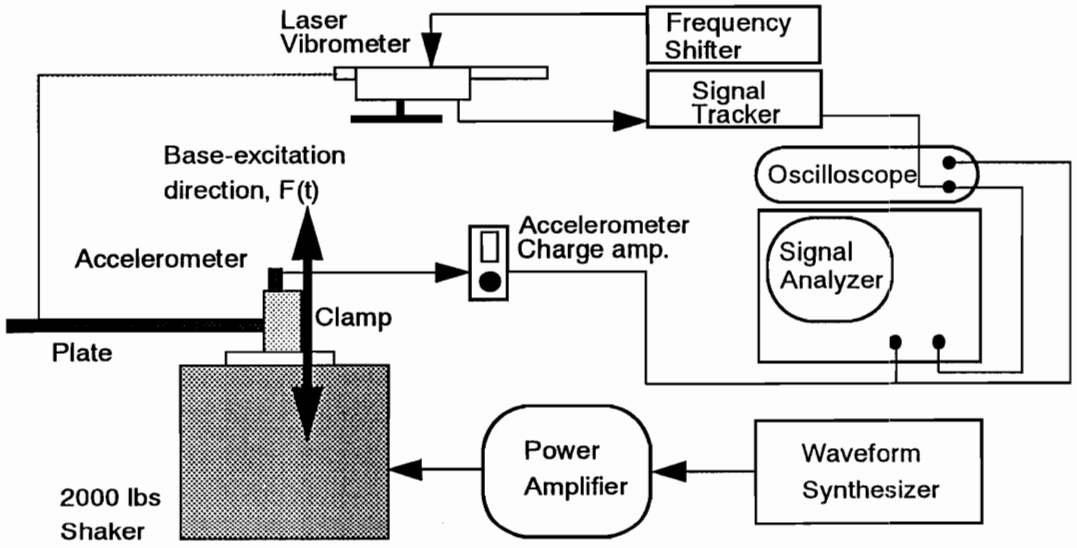

Figure 3.2: A schematic of the force-response measurements.

Table 3.2: Comparison of the natural frequencies obtained with the finite-element analysis (FEA) with those obtained with the experimental modal analysis (EMA).

	Natural frequencies		
Mode number	FEA [Hz]	EMA [Hz]	**Modal damping factor**
1	41.636	42.792	4.90×10^{-2}
2	151.60	145.75	0.17×10^{-2}
3	258.38	275.11	0.49×10^{-2}
4	503.11	489.68	1.10×10^{-2}
5	712.41	734.66	0.42×10^{-2}
6	813.48	798.03	0.27×10^{-2}
7	999.26	1001.4	0.21×10^{-2}
8	1161.5	1110.4	0.35×10^{-2}
9	1426.5	1507.1	0.55×10^{-2}
10	1639.2	N.A.	N.A.
11	1690.6	1679.8	0.44×10^{-2}
12	1745.5	1733.9	0.33×10^{-2}

and 12th mode shapes predicted by the FEA is opposite to that obtained with the EMA. On the other hand, the mode shapes of the first nine modes obtained with the two analyses are well correlated, as clear from Figs 3.3 and 3.4.

To test the accuracy of the mode shapes predicted by EMA using the polyreference method, we took the same set of transfer functions and repeated the parameter estimation procedure using the direct parameter method. The direct parameter estimation technique is a multi-degree-of-freedom frequency-domain curve-fitting technique (User manual for Modal Analysis 9.0, 1985). The largest difference in the estimated natural frequencies is the first bending mode which is approximately 4.2%. The mode shapes estimated with both methods are qualitatively the same. Similarly, to test the consistency of the FEA predicted mode shapes, we perturbed all three dimensions, material properties, and lay-up angles in sequence and in some cases in combination. We did not find any mode switching or skipping. Thus, using a first-order shear-deformation element along with rotary inertia effects and using the material properties measured by Anderson (1993), we conclude that

the order of the mode shapes estimated from this method are robust. The switching in the order of the 11th and 12th modes may be due to neglecting higher-order shear deformations.

In our comparative investigation between the FEA and EMA, we note that, for high-frequency modes, there are cases of mode skipping and switching. This observation is not restricted to the laminated composite plate studied in this chapter, but also applicable to steel and aluminum plates. Oh and Pryputniewicz (1990) observed mode switching and skipping in their study of a square cantilever plate by using the finite-element and holographic interferometry methods. They also used a Mindlin-type element in their finite-element analysis. Hadian and Nayfeh (1993) presented a comparison of the natural frequencies of shear-deformable cross-ply laminated plates obtained by using the classical plate theory and third-order shear-deformation theory. They found that, as the mode number increases, the frequency obtained using the classical plate theory deviates rapidly from that obtained using the higher-order shear-deformation theory. However, they did not compare the corresponding mode shapes. Therefore, we believe that the mode switching observed in the 11th and 12th modes may be due to an inadequate account of the shear deformation through the thickness of the plate.

3.3.2 High- to low-frequency modal interactions

To characterize nonlinear modal interactions, we used the setup in Fig. 3.2. Normally, for a base excited metallic plate with the experimental setup diagramed in Fig. 3.2, only symmetric bending modes can be directly excited. However, for a composite plate, due to the directionality of each layer, there can be an inherent bending-twisting coupling. In order to assess the degree of coupling, we calculated the $[D]$ matrix of the ABD matrix from the classical lamination theory (Whitney, 1987). The result is

$$[D] = \begin{bmatrix} 1.867 & 0.620 & 0.081 \\ 0.620 & 2.503 & 0.029 \\ 0.081 & 0.029 & 0.632 \end{bmatrix} \times 10^{-3}\, lbf\, in.$$

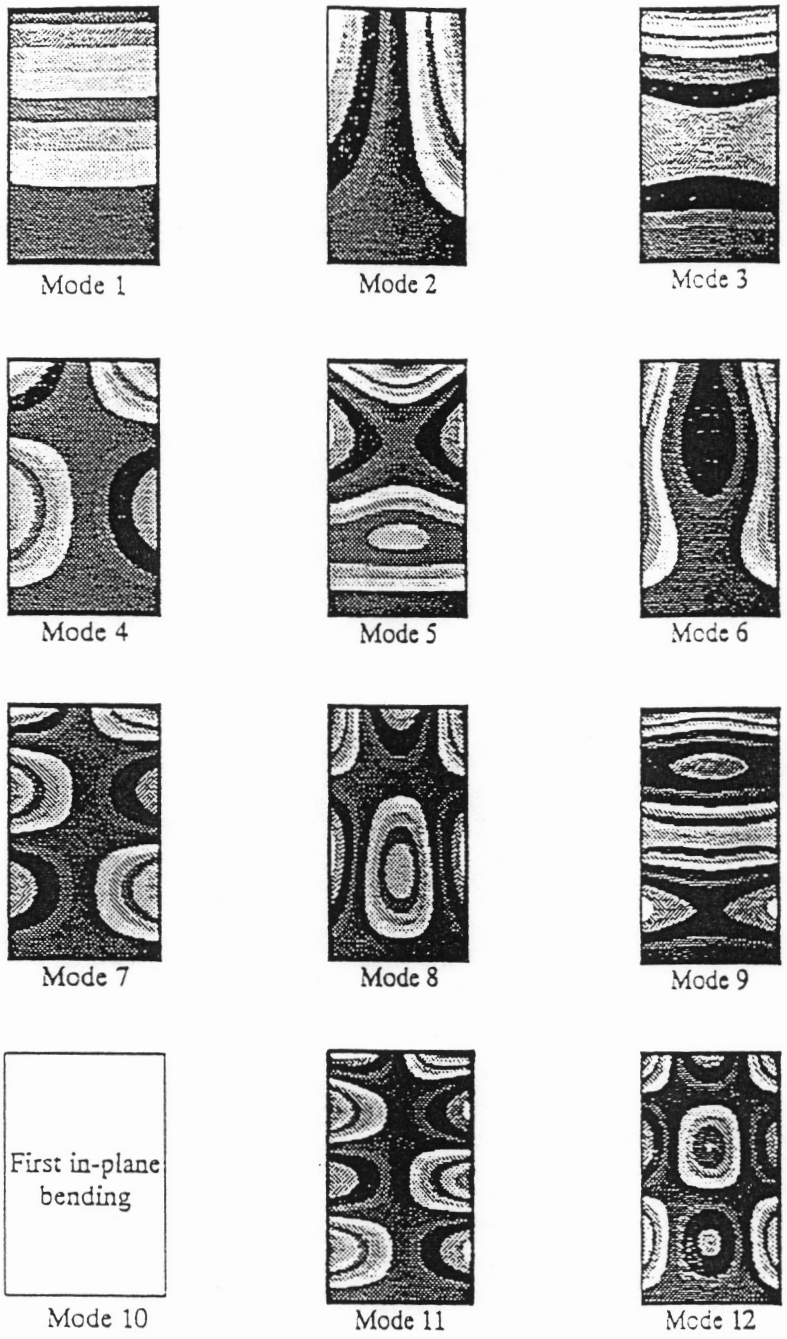

Figure 3.3: The first 12 mode shapes obtained by using the finite-element analysis (FEA).

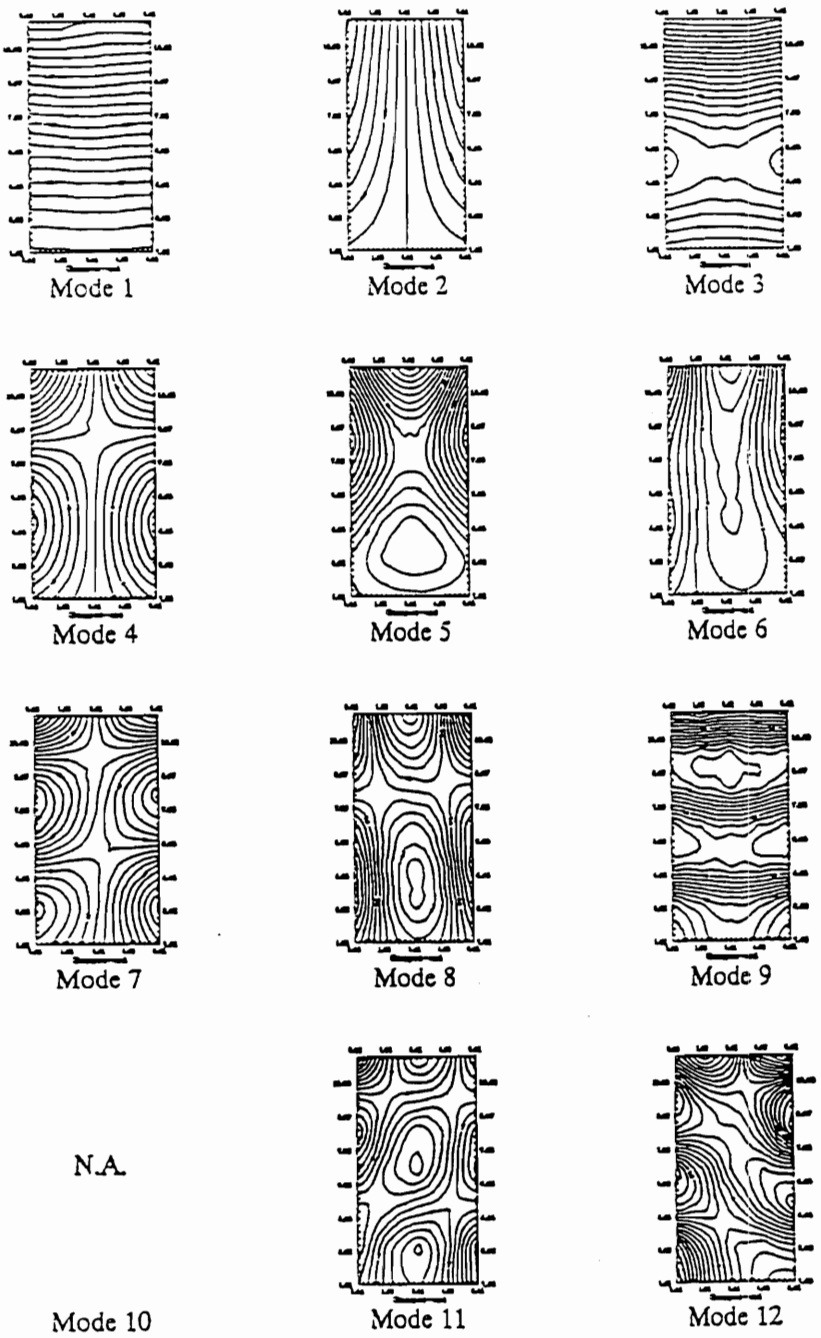

Figure 3.4: The first 12 mode shapes obtained with the experimental modal analysis (EMA).

We note that the terms D_{16} and D_{26} are small but nonzero, and hence there is some bending-twisting coupling inherent in the plate. However, because these terms are small, we expect the torsional modes to be slightly directly excited.

Our initial objective in this investigation was to activate the fourth (second torsional) mode by directly exciting the plate near the frequency of its seventh (third torsional) mode via a two-to-one internal resonance. We assumed this was possible because ω_7 is approximately twice ω_4: $\omega_7 = 1001.4$ Hz and $\omega_4 = 489.68$ Hz, and hence $\omega_7 \approx 2(\omega_4 + \epsilon)$, where $\epsilon \approx 11.02$ Hz is a small detuning parameter. Hence, we set the excitation frequency at $f_e = 1018.33$ Hz and slowly increased the excitation amplitude starting from $A_e = 11.00\ g$. We monitored the excitation conditions using an accelerometer attached on the clamp of the plate and the plate response using a laser vibrometer. A schematic of the experimental setup is shown in Fig. 3.2. Surprisingly, at $A_e = 12.92\ g$, we observed a large contribution to the response from the first mode but no contribution to the response from the fourth mode. Hence, instead of activating a two-to-one internal resonance, we observed an energy transfer from the seventh (high-frequency) mode to the first (low-frequency) mode. To characterize the phenomenon of energy transfer from this high-frequency mode to the low-frequency mode, we repeated the experiment by carefully observing the responses at the excitation frequency $f_e \approx \omega_7$ and the frequencies ω_1 and ω_4. At each increment of the excitation amplitude, we waited for the transients to settle down and collected 4 seconds worth of data at the sampling frequency $f_s = 8192.0$ Hz.

The results obtained in the forward- and reverse-amplitude sweeps are displayed in Figs 3.5(a) and (b), respectively. In these figures, we plot the amplitudes of the modes contributing to the plate response against the input excitation amplitude. The symbol □ marks the response at the excitation frequency ($\approx \omega_7$). o marks the response at the frequency ω_1 of the first bending mode, and △ marks the response at the frequency ω_4 of the fourth (second torsional) mode. The darkened symbols indicate either a periodic motion or no response and the hollow symbols indicate modulated motions.

We characterized the dynamics further at the marked positions in Fig. 3.5(a) by time

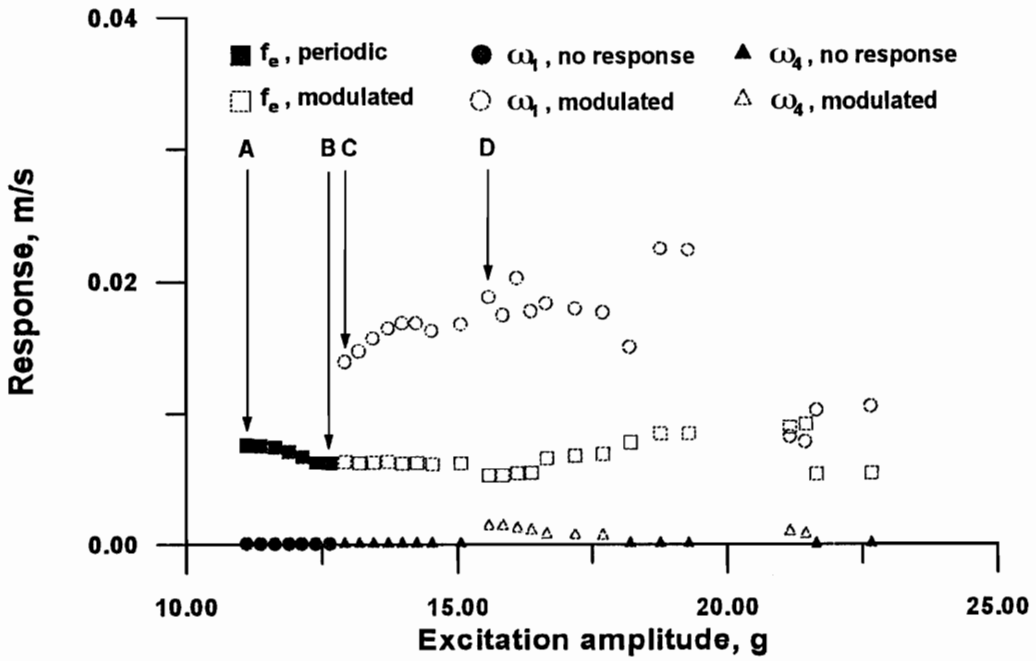

(a)

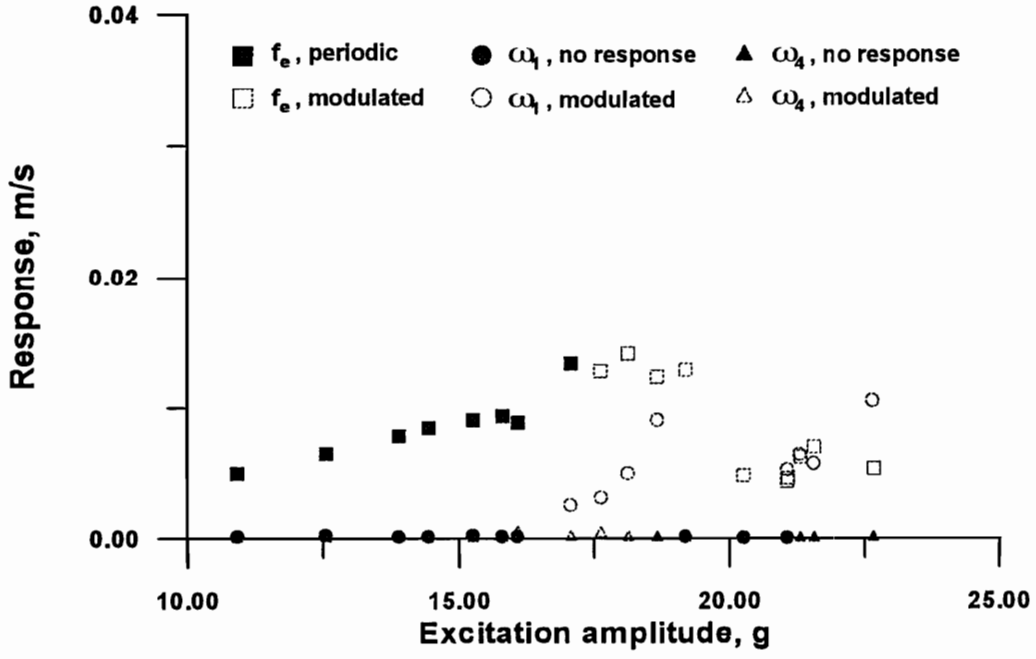

(b)

Figure 3.5: Force-response curves when $f_e = 1018.33$ Hz: (a) forward-amplitude sweep and (b) reverse-amplitude sweep.

histories and power spectra. As a reference, we sampled both the input and response signals at the start of the sweep, marked A in Fig. 3.5(a), they are displayed in Fig. 3.6. The time traces displayed in Fig. 3.6(a) show a periodic excitation and a periodic motion with some degree of noise. The power spectra of both signals in Fig. 3.6(b) show that most of the noise seen in the time traces is insignificant compared to the magnitude of the response at f_e.

Increasing the excitation amplitude past a critical value, we activated the first mode, point B of Fig. 3.5(a). The excitation and response signals at this point are displayed in Fig. 3.7, where part (a) shows the time traces and part (b) shows the power spectra of the signals. The time trace of the response in part (a) indicates a larger distortion than that in the time trace of the response during the initial stage of the amplitude sweep, shown in Fig. 3.6(a). Inspecting the power spectra of the signals in Fig. 3.7(b) shows that the distortion is relatively small compared to the response at f_e.

As we increased the excitation amplitude further to $A_e = 12.92\ g$, marked as location C in Fig. 3.5(a), we observed a significant increase in the first-mode response. This change is displayed in Fig. 3.8(a) and (b) in the time and frequency domains, respectively. The time trace clearly displays the activation of the first mode, where the low-frequency motion dominates the high-frequency motion. This is evident in the power spectrum S_{yy} of the response signal in part (b). The response spectrum also shows the presence of side bands around f_e, which are asymmetric. The spacing between the side bands and f_e is approximately ω_1. Therefore, the amplitude and phase modulations of the directly excited mode accompany the activation of the low-frequency first mode. This modal interaction mechanism is similar to that reported on beams by Anderson et al. (1992) and Nayfeh and Nayfeh (1994) and a flexible frame structure by Popovic et al. (1994). However, we believe that this is the first report of the transfer of energy from a high-frequency to a low-frequency mode in a stiff structure, namely, a composite plate.

To complete the force-response curve, we increased the excitation amplitude further. At $A_e = 15.84\ g$, marked location D in Fig. 3.5, we observed contributions to the response

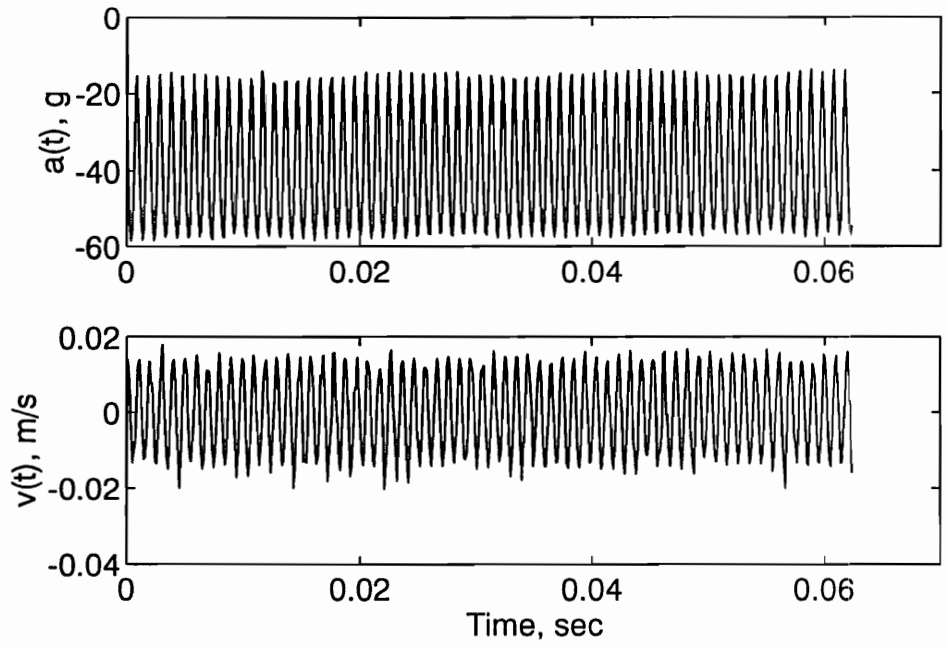

(a)

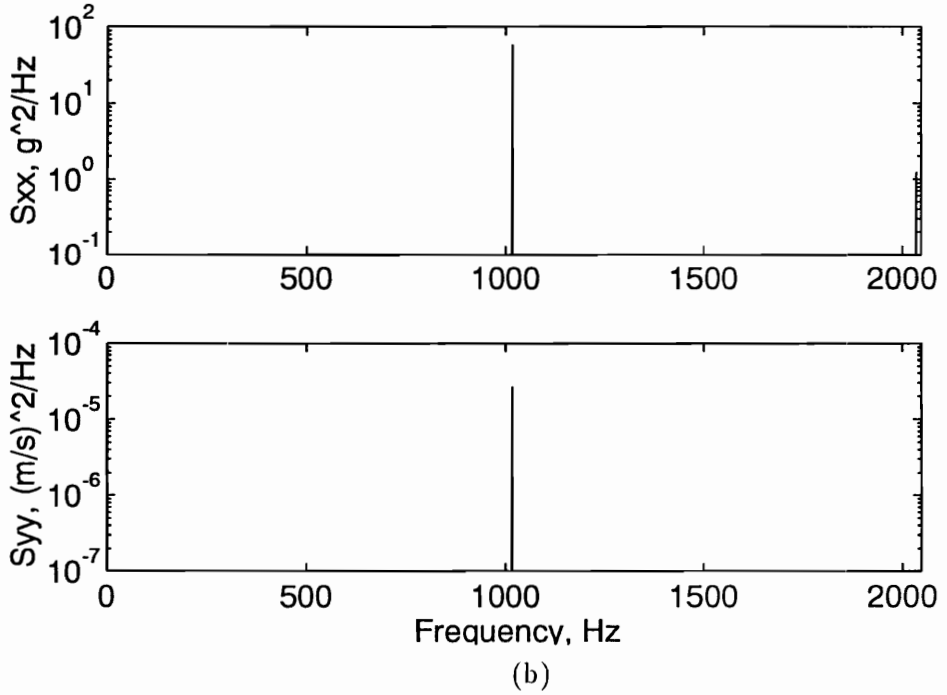

(b)

Figure 3.6: The excitation and response conditions at the location marked A on the force-response plot: (a) time traces and (b) power spectra.

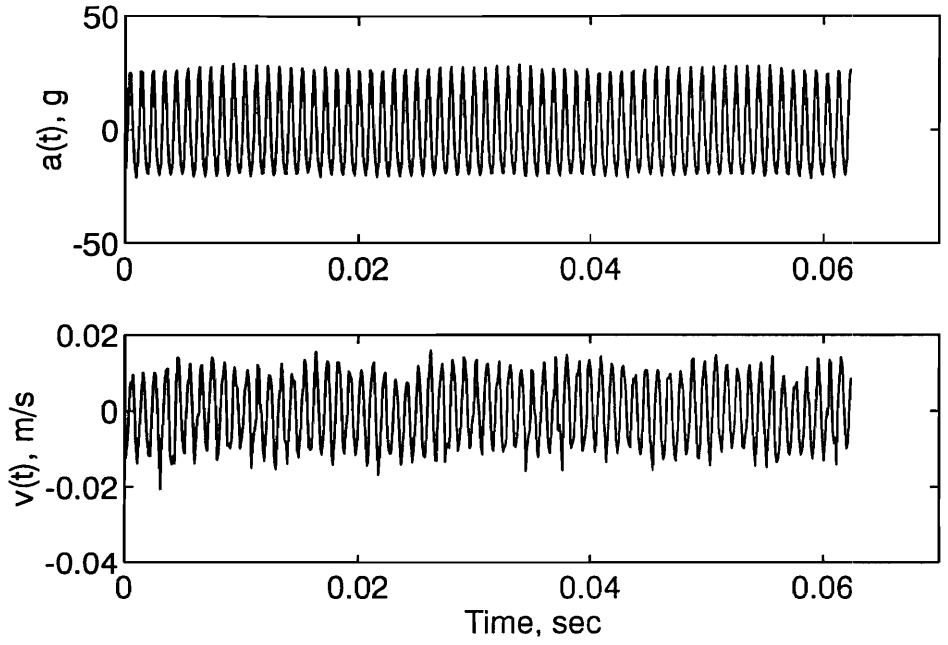

(a)

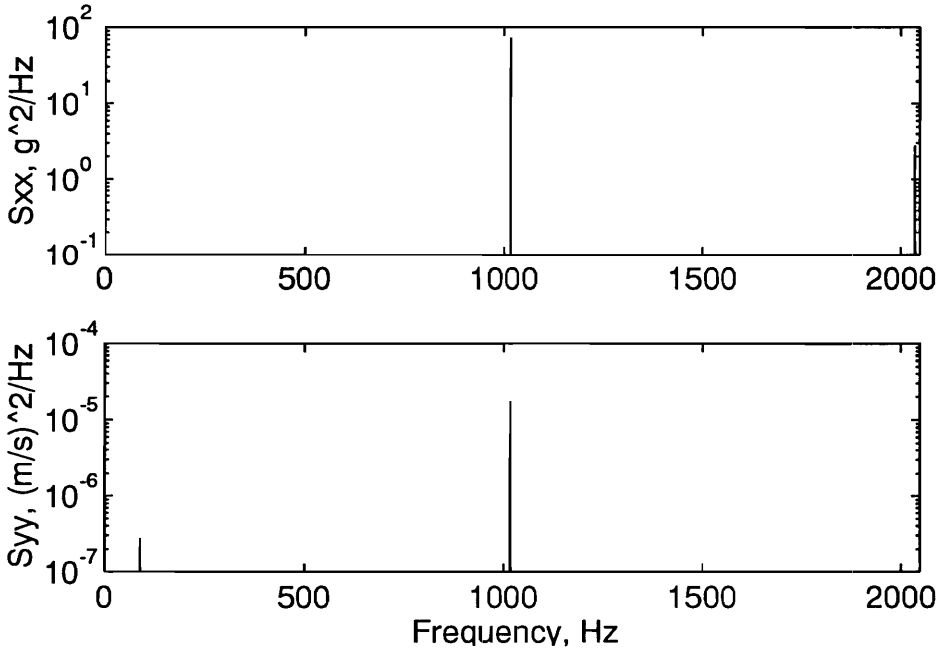

(b)

Figure 3.7: The excitation and response conditions at the location marked B on the force-response plot: (a) time traces and (b) power spectra.

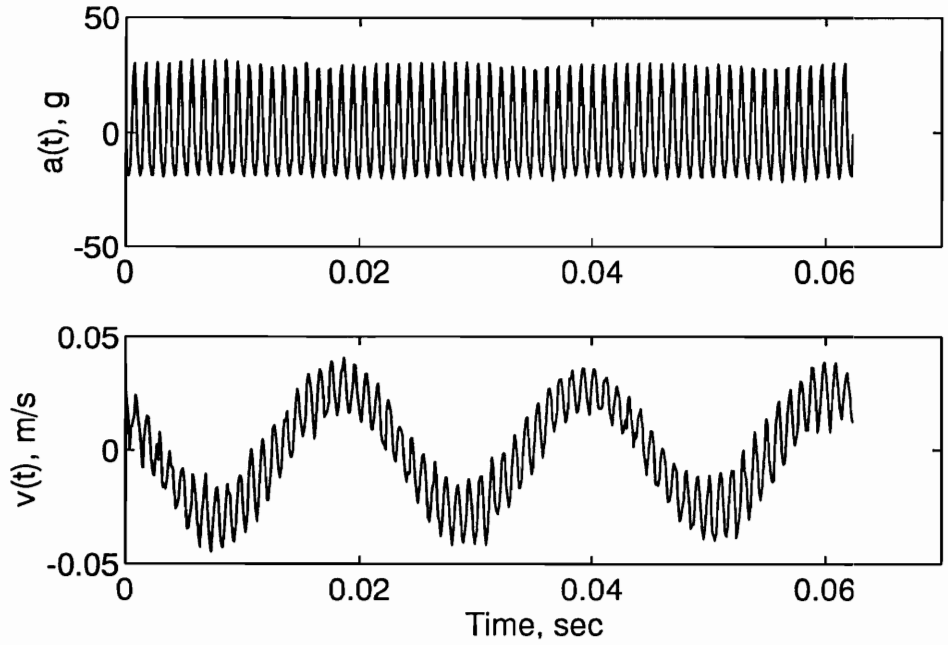

(a)

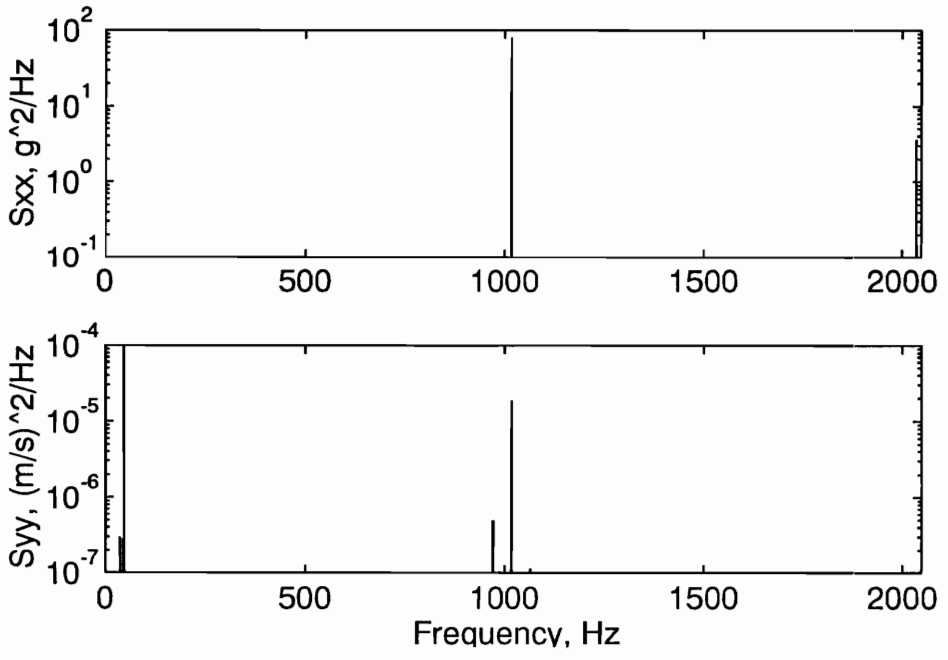

(b)

Figure 3.8: The excitation and response conditions at the location marked C on the force-response plot: (a) time traces and (b) power spectra.

from both the first and fourth modes. The time traces and power spectra of the input and response signals are shown in Fig. 3.9(a) and (b), respectively. We display 0.5 seconds worth of the time history to show that the low-frequency mode (first bending mode) activated due to its interaction with the high-frequency mode (third torsional mode) is also highly modulated. This is also suggested by the cluster of side bands around ω_1. The spacing between the side bands and ω_1 is approximately 6 Hz, which is not associated with any of the natural frequencies of the plate. We also note that the activation of the first mode had affected the input excitation condition, as shown in the trace of the excitation shown in part (a). However, this effect is not apparent in the power spectrum S_{xx} of the input acceleration shown in part (b).

The response at ω_4 disappears at approximately $A_e = 18.20\ g$, reappears at $A_e = 21.16\ g$, and remains until $A_e = 21.45\ g$. During this time, the amplitude of the first mode seems to oscillate about 0.017 m/s, increase at $A_e = 18.75\ g$, and finally drop at $A_e = 21.16\ g$ to approximately 0.01 m/s. On the reverse-amplitude sweep, the amplitude of the first mode decreased close to zero at $A_e = 21.06\ g$ and jumped up again at $A_e = 18.66\ g$, where it started to rise. The amplitude of the first mode rapidly decreased and finally settled down to zero at $A_e = 15.80\ g$. The amplitude of the fourth mode also settled down to zero at $A_e = 15.20\ g$.

We have characterized two simultaneously occurring nonlinear mechanisms: (i) a two-to-one internal resonance and (ii) an energy transfer between high-frequency and low-frequency modes using force-response curves, time traces, and power spectra. From the amplitude-response patterns shown in Fig. 3.5, there seems to be some correlation between fluctuations of the amplitude and phase of the first mode and the activation of the fourth mode.

3.4 *Closure*

We have shown through experiment an energy transfer from a high-frequency to a low-frequency mode in a base excited composite plate. Our observations and characterizations

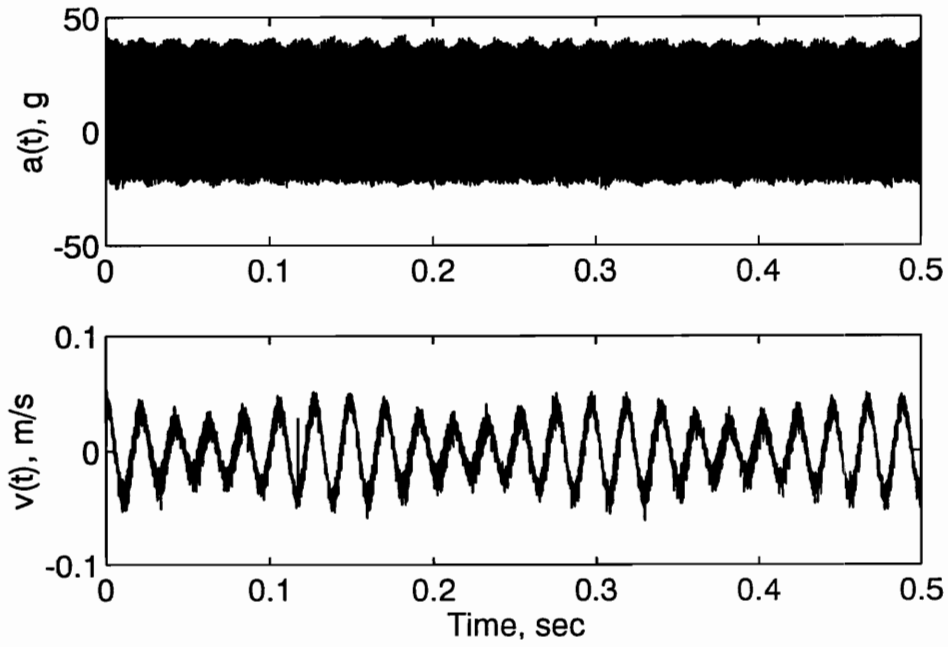

(a)

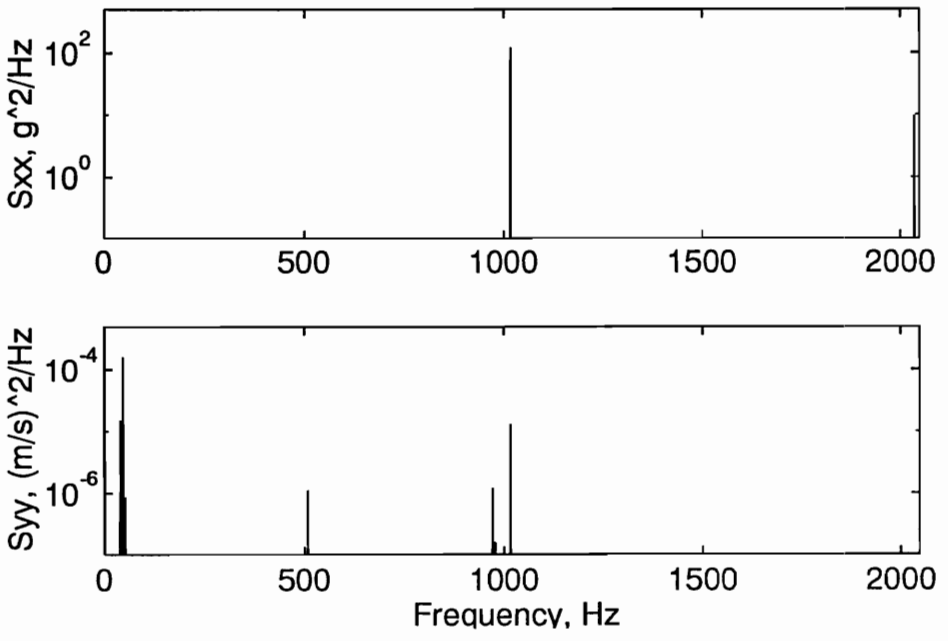

(b)

Figure 3.9: The excitation and response conditions at the location marked D on the force-response plot: (a) time traces and (b) power spectra.

of such a phenomenon in a stiff cantilever composite plate agree with those made in flexible beam and frame structures. Hence, we conclude that this type of interaction is possible for all range of structural stiffness and configurations whenever there exist modes whose natural frequencies are much lower than the natural frequencies of the directly excited modes. In addition, we found that multiple modal interactions can occur concurrently. These interactions involve energy transfer between a high-frequency and a low-frequency mode and a two-to-one internal resonance.

Chapter 4

Nonlinear Combination Resonances

4.1 *Introduction*

The complicated dynamic behavior of weakly nonlinear systems has been the focus of recent research efforts. A large number of these investigations involves a special frequency relationship between two or more linear natural frequencies and/or a special relationship between the natural frequencies and the excitation frequencies, where the steady-state response of the system may contain large contributions from several modes. Interaction among the modes (i.e., modal interactions) can lead to surprisingly large-amplitude responses in modes that are predicted by linear analyses to have no response. The possible types of modal interactions depend on the natural frequencies of and the type of nonlinearities present in the system.

Modes with commensurate or nearly commensurate natural frequencies ω_i may interact via internal or autoparametric resonances. In systems having cubic nonlinearities, internal resonances may occur if $\omega_n \approx \omega_m$, $\omega_n \approx 3\omega_m$, $\omega_n \approx |\pm 2\omega_m \pm \omega_k|$, or $\omega_n \approx |\pm\omega_m \pm \omega_k \pm \omega_l|$. In systems with quadratic nonlinearities, additional resonances may occur if $\omega_n \approx 2\omega_m$ and $\omega_n \approx \omega_m + \omega_k$. Analyses of nonlinear oscillators with internal resonances have been successfully investigated using perturbation methods (e.g., Nayfeh, 1973, 1981; Nayfeh and Mook, 1979; Crespo da Silva, 1980; Bajaj and Johnson, 1990). These analyses have been experimentally validated (e.g., Nayfeh and Balachandran, 1989). The perturbation results are in good agreement with the experimental results. Therefore, the activation of a low-frequency mode with an excitation frequency near that of a high-frequency mode through an internal resonance is well documented.

Other types of nonlinear modal interactions are possible for a multidegree-of-freedom system subjected to a simple-harmonic excitation. For a system with cubic nonlinearities, if the excitation frequency $\Omega \approx 2|\pm\omega_m \pm \omega_k|$, $\Omega \approx |\pm 2\omega_m \pm \omega_k|$, $\Omega \approx \frac{1}{2}(\omega_m \pm \omega_k)$, or $\Omega \approx |\pm\omega_m \pm \omega_k \pm \omega_l|$, then a combination resonance may occur. Additional combination resonances may occur in systems with quadratic nonlinearities if $\Omega \approx |\pm\omega_m \pm \omega_k|$. Dugundji and Mukhopadhyay (1973) investigated the response of a cantilever beam to a transverse excitation whose frequency is close to the sum of the first bending and first torsional modes. They observed a large contribution from the low-frequency first bending mode besides the one at the excitation frequency and the one from the first torsional mode. Thus, a high-frequency excitation can produce a large-amplitude response in a low-frequency mode. Similar modal interactions were observed for other parametrically excited systems via combination resonance. Interested readers are referred to Nayfeh and Mook (1979) and Schmidt and Tondl (1986) for comprehensive treatments of this class of problems and additional references.

The nonlinear free and forced vibrations of composite plates have been extensively studied by many investigators. The most comprehensive review of geometrically nonlinear laminated composite plates can be found in the book by Chia (1980). Other reviews on the nonlinear vibration of plates have been conducted by Sathyamoorthy (1983), Nayfeh and Mook (1979), and Nayfeh (1990). Analytical investigations of multimode nonlinear vibrations of rectangular angle-ply and cross-ply plates were investigated by Chia and Prabhakara (1978). Reddy and Chao (1981, 1982) and Reddy (1982) used a finite-element method to study the nonlinear vibrations of laminated plates with all clamped and all simply supported edges. Nonlinear vibrations of an imperfect laminated plate were investigated by Kapania and Yang (1987) using the finite-element method.

There were several investigations of the effects of harmonic excitations on the nonlinear vibrations of composite plates. Bennett (1971) investigated the nonlinear vibrations of simply supported angle-ply laminated plates and Huang (1973) studied finite-amplitude vibrations of an orthotropic plate with an isotropic core. Additional surveys on the non-

linear vibrations of composite plates under harmonic excitations were conducted by Bert (1982). Gary et al. (1984) studied large-amplitude vibrations and random responses of symmetrically laminated rectangular plates. Wentz et al. (1988) studied large-amplitude forced vibrations of laminated composite rectangular plates by a finite-element method. Eslami and Kandil (1989) used the method of multiple scales to study the nonlinear response of an orthotropic panel to a harmonic excitation. They considered the cases of primary, subharmonic, and superharmonic resonances. Nayfeh et al. (1989) considered the case of two-to-one internal resonance for an antisymmetric cross-ply laminate subjected to a harmonic load.

In this paper, we present an experimental investigation into combination resonances in the responses of two cantilever six–layer symmetric laminated composite plates to a harmonic transverse excitation. The plates under study have the layups $(90/30/-30/-30/30/90)_s$ and $(-75/75/75/-75/75/-75)_s$. We refer to the first laminate as the *quasi-isotropic* plate, and refer to the second laminate as the ± 75 plate. We activated the external combination resonance $\Omega \approx \omega_2+\omega_7$ in the quasi-isotropic plate and the external combination resonance $\Omega \approx \frac{1}{2}(\omega_2+\omega_5)$ and the internal combination resonance $\Omega \approx \frac{1}{2}(\omega_2+\omega_{13}) \approx \omega_8$ in the ± 75 plate. The dynamics of the plates were characterized using time histories, power spectra, pseudo-state portraits, Poincaré maps, and force-response and frequency-response curves.

4.2 *Linear Natural Frequencies and Mode Shapes*

Two six-layer symmetric laminated composite plates were manufactured at the Virginia Tech Center for Composite Materials and Structures, Fabrication Laboratory. The stacking sequence for the quasi-isotropic plate is $(90/30/-30/-30/30/90)_s$ and that for the ± 75 plate is $(-75/75/75/-75/75/-75)_s$. As a first part of this study, we identified the natural frequencies and mode shapes of both plates using a finite-element analysis (FEA) and an experimental-modal analysis (EMA).

Table 4.1: Physical dimensions and material properties of the tested plates.

Properties	Mean Value
Thickness (h)	**quasi-isotropic**: 0.138 in., **±75**: 0.139 in.
Width (a)	**quasi-isotropic**: 6.870 in., **±75**: 6.859 in.
Length (b)	**quasi-isotropic**: 11.50 in., **±75**: 11.51 in.
E_{11}	$22.14 \times 10^6\ lbf/in^2$
E_{22}	$1.281 \times 10^6\ lbf/in^2$
E_{33}	$1.165 \times 10^6\ lbf/in^2$
G_{12}	$0.765 \times 10^6\ lbf/in^2$
G_{23}	$0.668 \times 10^6\ lbf/in^2$
G_{13}	$0.765 \times 10^6\ lbf/in^2$
ν_{12}	0.297
ν_{23}	0.485
ν_{13}	0.297
ρ	$1.460 \times 10^{-4}\ lbf\,s^2/in^4$

4.2.1 Finite-element analysis

For the finite-element analysis, we used the commercially available software ABAQUS. We used the material properties obtained experimentally by Anderson (1993) using uniaxial and symmetric cross-ply plates. These test plates were made from the same material and using the same cure cycle as the plates used in this paper. The measured dimensions and material properties are listed in Table 4.1. In the analysis, we assumed that each layer is orthotropic and that the thickness of each layer is equal to the overall thickness of the plate divided by the number of layers. Therefore, for the quasi-isotropic plate, the thickness of each layer is (0.138/12) in. = 0.012 in.

The plates were subdivided into 30 by 20 elements in the length and width directions, respectively. The eight noded quadrilateral thick shell element (S8R) and reduced integration scheme were used in the analysis. This element approximates the Mindlin-type element, which accounts for first-order shear deformations through the thickness and rotary inertia effects. The first 12 natural frequencies obtained for both plates are listed in Table 4.2 along with those estimated with the experimental modal analysis. The corresponding mode

Table 4.2: Comparison of the natural frequencies obtained with a finite-element analysis (FEA) with those obtained with the experimental modal analysis (EMA).

Mode number	Quasi-isotropic		±75	
	FEA [Hz]	EMA [Hz] (MDF)	FEA [Hz]	EMA [Hz] (MDF)
1	41.636	42.792 (4.9e-2)	61.320	58.920 (0.1e-2)
2	151.60	145.75 (0.2e-2)	138.11	132.52 (0.6e-2)
3	258.38	275.11 (0.5e-2)	359.04	342.78 (0.2e-2)
4	503.11	489.68 (1.1e-2)	406.49	410.16 (2.6e-2)
5	712.41	734.66 (0.4e-2)	513.59	492.53 (0.7e-2)
6	813.48	798.03 (0.3e-2)	846.95	826.88 (0.3e-2)
7	999.26	1001.4 (0.2e-2)	891.53	910.18 (0.3e-2)
8	1161.5	1110.4 (0.4e-2)	1064.4	1036.9 (1.6e-2)
9	1426.5	1507.1 (0.6e-2)	1190.0	1135.7 (0.7e-2)
10	1639.2	N.A. (N.A.)	1374.5	1370.7 (0.7e-2)
11	1690.6	1679.8 (0.4e-2)	1559.2	1503.3 (1.6e-2)
12	1745.5	1733.9 (0.3e-2)	1678.7	1715.6 (0.7e-2)

shapes obtained with the FEA are displayed in Fig. 3.3 for the quasi-isotropic plate and in Fig. 4.1 for the ±75 plate.

4.2.2 Experimental-modal analysis

A schematic of the experimental-modal analysis (EMA) setup is shown in Fig. 3.1. The plates were vertically clamped at the base and fixed to the floor. We imported an impulse force to the plate using an instrumented hammer and measured the plate response using a laser vibrometer. The spatial discretization of the plate is discussed in Section 3.2.2. The modal parameter estimation procedure is also discussed in Section 3.2.2. The resulting modal parameters are listed in Table 4.2 and the corresponding mode shapes for the quasi-isotropic and ±75 plates are shown in Figs 3.4 and 4.2, respectively.

4.2.3 Results

It follows from Table 4.2 that the FEA and EMA estimated natural frequencies for the quasi-isotropic plate are in good agreement. The largest percentage difference is in the estimated value of the second natural frequency rather than the 10th, 11th, or 12th natural frequencies. This difference is approximately 6%, which is within the bounds of the experimental uncertainties and theoretical simplifications in the finite-element method.

Comparing Figs 3.3 and 3.4, we conclude that the shapes of the first nine modes estimated with the FEA and EMA correlate very well. However, the tenth mode estimated with the FEA is the first in-plane stretching mode. This mode was not estimated with the EMA because the excitation and measurement directions were only capable of exciting and detecting out-of-plane modes. Moreover, there is a switch in the order of the 11th and 12th mode shapes predicted with the FEA when compared with those predicted with the EMA. This switching may be due to the inability of the used FEM to model higher-order shear deformations through the thickness. The higher-order shear deformations are important for the higher-order modes, as found by Hadian and Nayfeh (1993) in their study of the free vibration and buckling of shear-deformable cross-ply laminated plates.

To test the consistency of the mode shapes predicted with the EMA using the polyreference method, we took the same set of transfer functions and repeated the parameter estimation procedure using the direct parameter method. The direct parameter estimation technique is a multidegree-of-freedom frequency-domain curve-fitting technique. The largest difference in the estimates of the natural frequencies of the quasi-isotropic plate obtained with the two methods is for the first bending mode; it is approximately 4.2%. The mode shapes estimated with both methods are qualitatively the same. Similarly, to test the consistency of the mode shapes predicted with the FEA, we perturbed all three dimensions, material properties, and lay-up angles in sequence and in some cases in combinations. We did not find any mode switching or skipping. Thus, using a first-order shear-deformation element along with rotary inertia effects and using the material properties measured by

Anderson (1993), we conclude that the mode shapes estimated with this method are also consistent.

The natural frequencies and mode shapes for the ± 75 plate obtained with the FEA and EMA are in good agreement. The largest difference in the estimates of the natural frequencies is approximately 5%. It follows from Figs 4.1 and 4.2 that all twelve mode shapes obtained with the FEA and EMA are qualitatively in good agreement.

4.3 *External Combination resonance in the response of the quasi-isotropic plate*

In this experiment, we observed the activation of a combination resonance of the additive type in an externally excited cantilever quasi-isotropic composite plate. The plate response was characterized by using force-response curves, time traces, power spectra, pseudo-state portraits, and Poincaré maps. We documented how the plate response changed from a single-frequency periodic motion to a two-period quasiperiodic motion as the excitation amplitude was increased. Moreover, we observed a high-amplitude low-frequency response to a low-amplitude high-frequency excitation in a stiff graphite-epoxy composite cantilever plate.

To investigate the nonlinear behaviors of the plates, we changed the experimental setup to that displayed in Fig. 3.2. We base excited the plates using a 2000-lb shaker. The input was monitored using an accelerometer mounted on the base of the clamp, and the plate response was monitored using a laser vibrometer. The accelerometer signal was fed to a charge amplifier and the vibrometer signal was fed to a signal tracker. In this way, we always monitored the frequency contents of the input and output. The acceleration level was obtained from the autospectrum of the accelerometer signal and the amplitude of the response was obtained from the autospectrum of the vibrometer signal. A computer with an A/D card was also used to acquire time-domain data for additional spectral and time-domain analyses and data presentations.

The control parameters in these series of experiments were the excitation amplitude

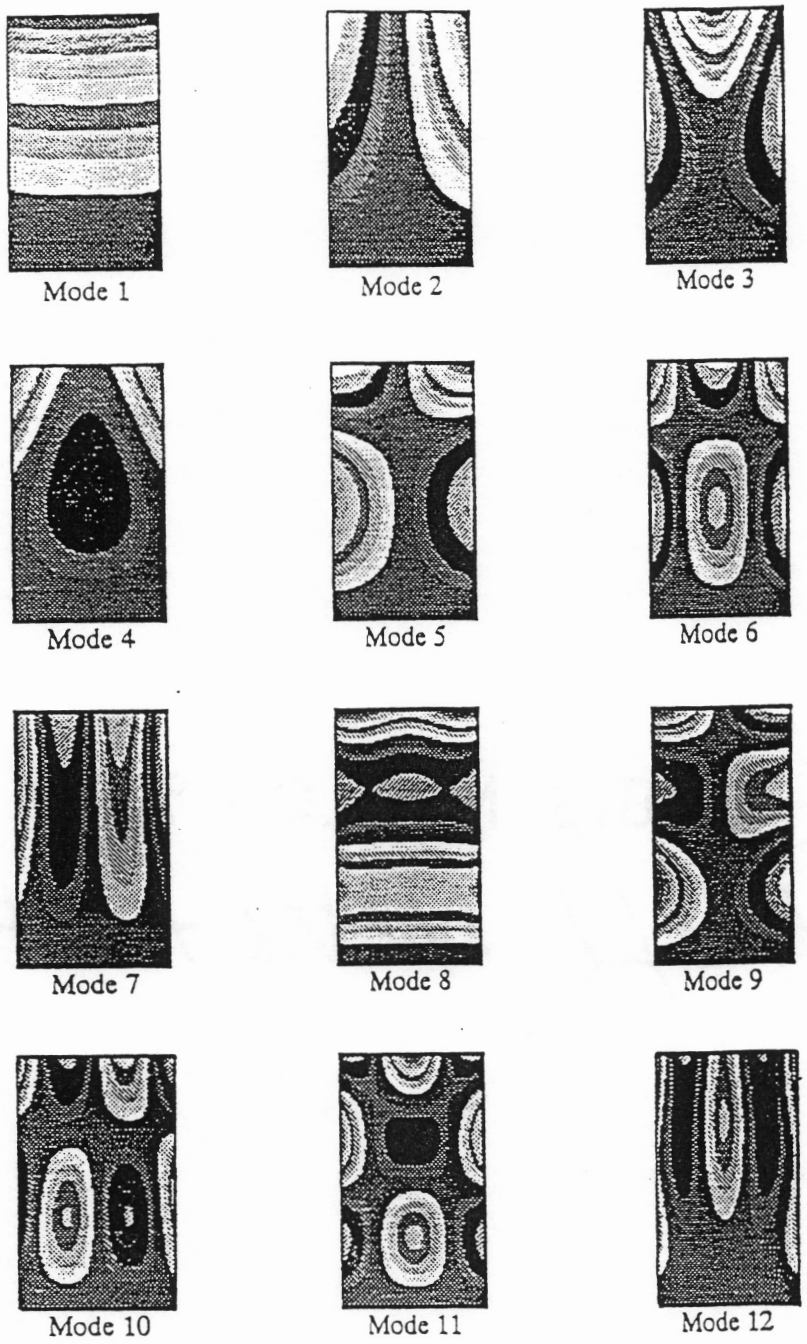

Figure 4.1: The first 12 mode shapes obtained by using the finite-element analysis (FEA) for the ± 75 plate.

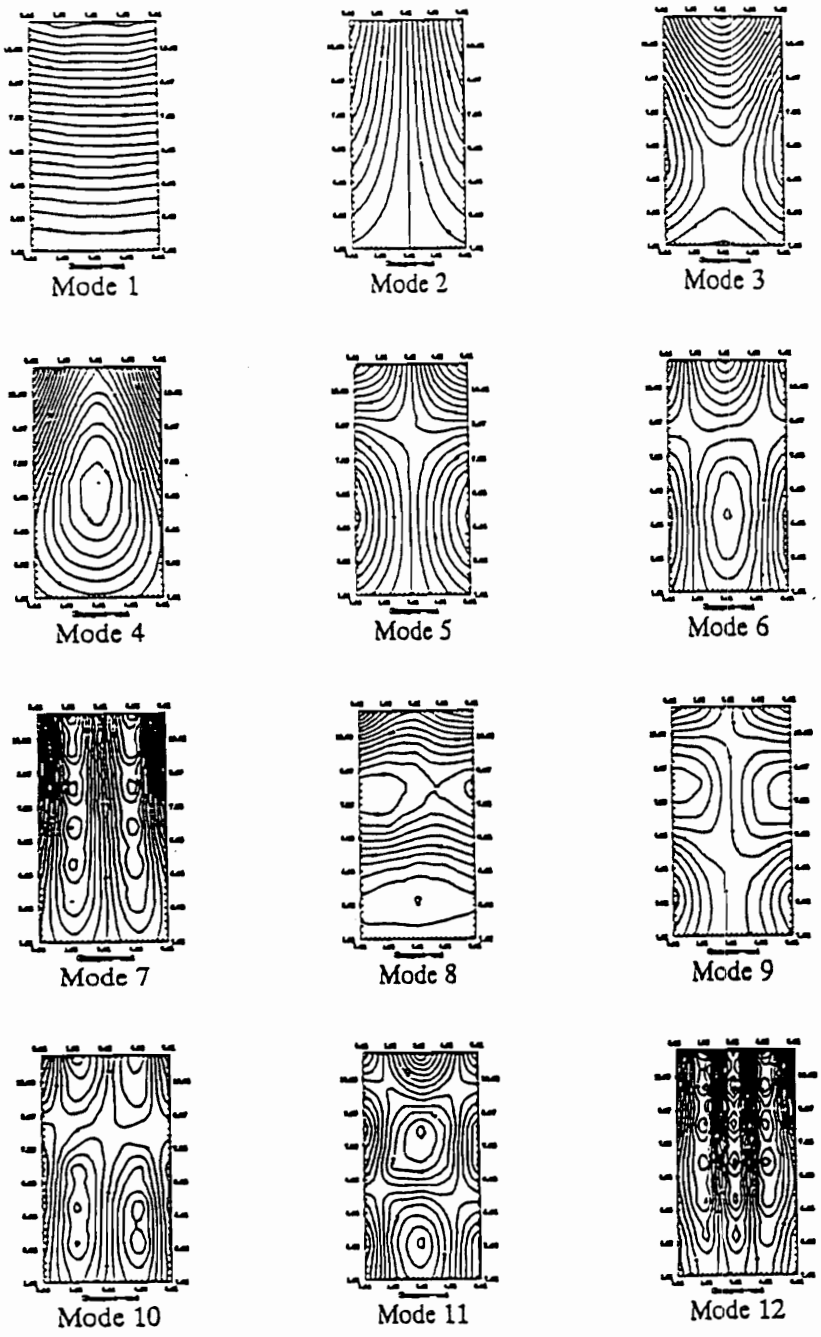

Figure 4.2: The first 12 mode shapes obtained with the experimental modal analysis (EMA) for the ± 75 plate.

and frequency. For the quasi-isotropic plate, we fixed the excitation frequency at f_e = 1133.79 Hz $\approx \omega_2 + \omega_7$ and slowly varied the excitation amplitude up and down from F = 6.8 g to F = 16.9 g. At each increment of the excitation amplitude, we waited until the transients had settled down by observing the input and output signals on an oscilloscope and a spectral analyzer. The analyzer was set to display the dynamic range of 60 dB from the highest signal level. We assumed that any signals below the 60 dB range were insignificant. After the transients had settled down, we obtained the autospectra of the input and output signals using the analyzer. We used 50 averages for each measurement. The resulting force-response curves are shown in Fig. 4.3. The solid symbols and lines represent data obtained during the forward sweep, and the hollow symbols and dashed lines represent data obtained during the reverse sweep. We denote the plate response at the excitation frequency f_e with the symbol ○, the response at the first torsional frequency (second mode, ω_2) with the symbol □, and the response at the third torsional frequency (seventh mode, ω_7) with the symbol △.

In the forward sweep, the response consisted of a motion at the excitation frequency with an amplitude a_e until F reached 8.00 g. As F was increased past 8.00 g approximately, the second and seventh modes were activated but with small amplitudes a_2 and a_7. As F was increased further, a_2 and a_7 increased slowly until F exceeded approximately 13.66 g, where a_2 and a_7 jumped to large values. As F was increased further, a_2 and a_7 increased slowly. The forward sweep was terminated at $F \equiv 17.00\ g$. During the forward sweep, a_e increased approximately linearly with increasing F.

In the reverse sweep, a_e, a_2, and a_7 traced approximately the force-response curves obtained in the forward sweep. However, as F was decreased below approximately 12.27 g, a_2 and a_7 jumped down to zero, whereas a_e followed the force-response curve obtained in the forward sweep. We note that the critical value of F for the jump-down motion is smaller than the critical value of F for the jump-up motion. Consequently, there are two stable motions in the interval $12.27\ g < F < 13.66\ g$. Except for the slow increase in a_2 and a_7 in the forward sweep in the interval $8.00\ g < F < 13.66\ g$, the force-response curves in Fig. 4.3

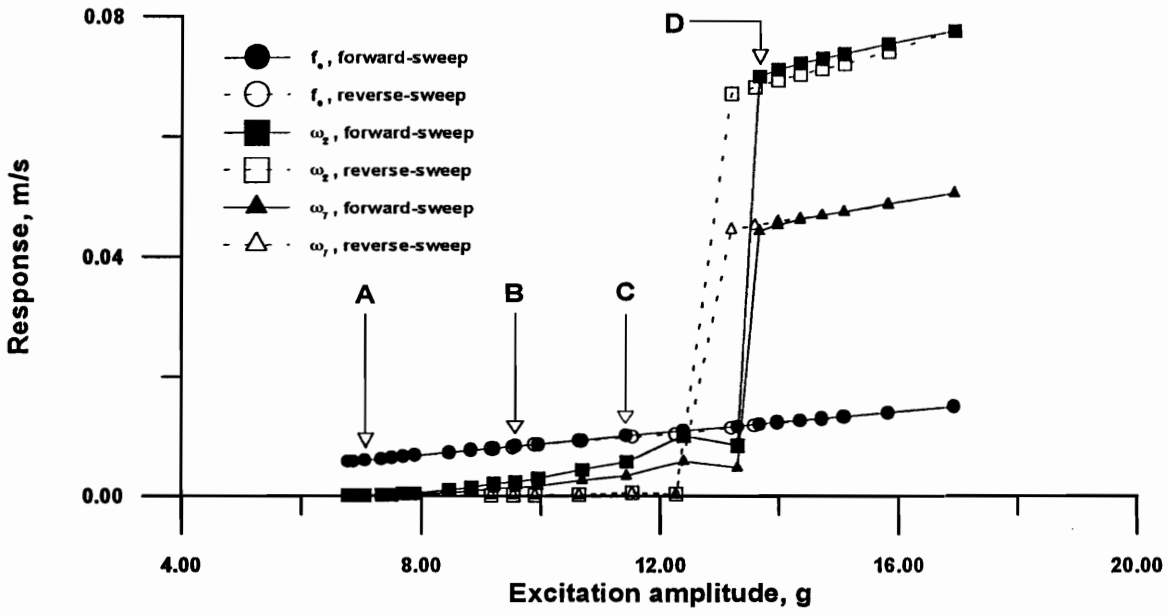

Figure 4.3: Force-response curves for the quasi-isotropic plate when $f_e = 1133.8$ Hz.

are qualitatively similar to those found analytically by Nayfeh (1983) in the response of a bowed structure to a combination resonance of the additive type by using the method of multiple scales.

To characterize the different responses, we collected the accelerometer and vibrometer signals for four excitation levels using an A/D card installed in a computer. We acquired four seconds of time-domain data using the sampling frequency $f_s = 8192$ Hz. For the Poincaré maps, we acquired additional data using the excitation frequency f_e as the clock frequency. These data were used to generate (a) time histories, (b) power spectra, (c) pseudo-state portraits, and (d) Poincaré maps. The time-domain data were collected for the four locations marked by the letters A, B, C, and D on the force-response curves in Fig. 4.3. These locations correspond to the excitation amplitudes $F = 7.05$, 8.83, 11.44, and 13.66 g, respectively.

Pseudo-state portraits were reconstructed by using the method of delays (see Moon,

1987; Nayfeh and Balachandran, 1994). Thus, we plot the velocity signal $v(t)$ from the vibrometer against $v(t+T)$, where the time delay $T = n/f_s = n\,dt$, $n = 1, 2, \ldots, N$, N is number of data points, and $dt = 1/f_s$. We chose the time delay to be half the time corresponding to the first zero crossing of the autocorrelogram of $v(t)$. Thus, we let $T = 2\,dt$.

The data corresponding to point A on the force-response curves are displayed in Fig. 4.4. Parts (a) and (b) in Fig. 4.4 represent the time history and the power spectrum of the input signal and parts (c) and (d) represent the time history and power spectrum of the plate response. Part (b) clearly shows that the input consists of a single frequency. The power spectra in parts (b) and (d) show that the output is mainly at the excitation frequency and hence the response is a simple-harmonic motion. The pseudo-state portrait in part (e) shows a closed curve with slight scatter due to noise, indicating a periodic response. Moreover, the Poincaré map in part (f) shows a single point with slight scatter due to noise, confirming that the response is periodic with the frequency f_e.

As the excitation amplitude was increased from that corresponding to position A to that corresponding to position B on the force-response curves, we obtained the response displayed in Fig. 4.5. The time trace and power spectrum of the excitation, shown in parts (a) and (b), are qualitatively similar to those in Fig. 4.4. However, the time trace and spectrum of the response shown in parts (c) and (d) indicate that the motion consists of more than one frequency. The power spectrum in part (d) contains peaks at 1133.8 Hz, corresponding to the input, and at approximately 144 Hz and 990 Hz, corresponding to the first and third torsional modes, respectively, suggesting that the response may be periodic with large period or two-period quasiperiodic. For two-period quasiperiodic motions, the Poincaré map should be a closed curve and the pseudo-state portrait should not close on itself. However, because the magnitudes of the peaks at 144 Hz and 990 Hz are small compared with the peak at the excitation frequency and because of the presence of noise, the Poincaré map in part (f) is a large cluster of points and the pseudo-state portrait in part (e) appears not to be a closed curve. Hence, we cannot ascertain whether the motion is periodic or quasiperiodic.

Increasing the excitation amplitude further to $F = 11.44\ g$, corresponding to the position marked C on the force-response curves, we found that the amplitudes of the first and third torsional modes were larger than those occurring at the position B. The power spectrum of the excitation shown in Fig. 4.6(b) consists of a single peak and hence we conclude that the feedback from the plate to the shaker was below 60 dB. It is clear from the power spectrum of the response shown in Fig. 4.6(d) that the amplitudes of the first and third torsional modes are much larger than those shown in Fig. 4.5(d) and hence their contribution to the total response is much larger than that in Fig. 4.5. Again, the motion may be periodic with a large period or two-period quasiperiodic. Most likely the response is quasiperiodic because the Poincaré map shown in Fig. 4.6(f) is a closed though smeared curve due to noise. Moreover, the data points in the pseudo-state portrait shown in Fig. 4.6(e) are more spread than those in Fig. 4.5(e) and the portrait appears not to form a closed curve.

It is clear from Fig. 4.3 that, increasing the excitation amplitude beyond $F \approx 13.66\ g$, produced a jump of the amplitudes of the first and third torsional modes to large values. The characteristics of the excitation and response are shown in Fig. 4.7. Again, the power spectrum of the excitation shown in Fig. 4.7(b) consists of a single peak, indicating that any feedback from the plate to the shaker was negligible. The time trace and power spectrum of the response (Figs 4.7(c) and (d)) clearly show that the plate motion was dominated by the first torsional mode. It is also clear from Fig. 4.7(d) that the contributions of the first and third torsional modes to the plate response were much larger than the contribution at the excitation frequency. Because the Poincaré map (Fig. 4.7(f)) is a closed curve, the plate motion was two-period quasiperiodic. The pseudo-state portrait (Fig. 4.7(e)) indicates that the motion was a two-torus.

4.4 Combination external resonance in the response of the ±75 plate

In this experiment, we activated the combination resonance $f_e \approx \frac{1}{2}(\omega_2 + \omega_5)$ in the ±75 cantilever plate. We used frequency-response curves to characterize the dynamics of

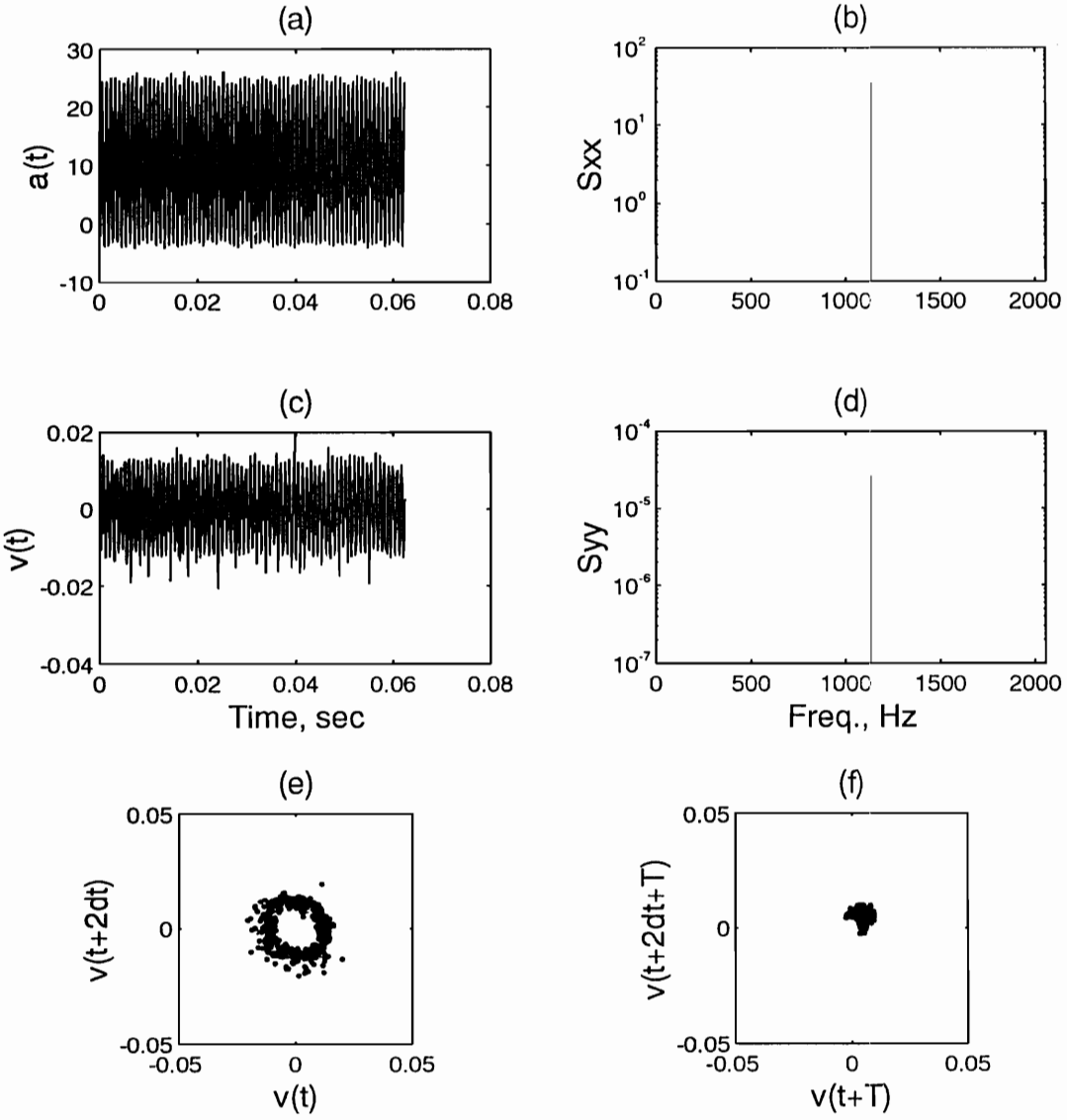

Figure 4.4: The excitation and response conditions at the location marked A on the force-response curve: (a) input time trace, (b) input power spectrum, (c) response time trace, (d) response power spectrum, (e) pseudo-state portrait, and (f) Poincaré map.

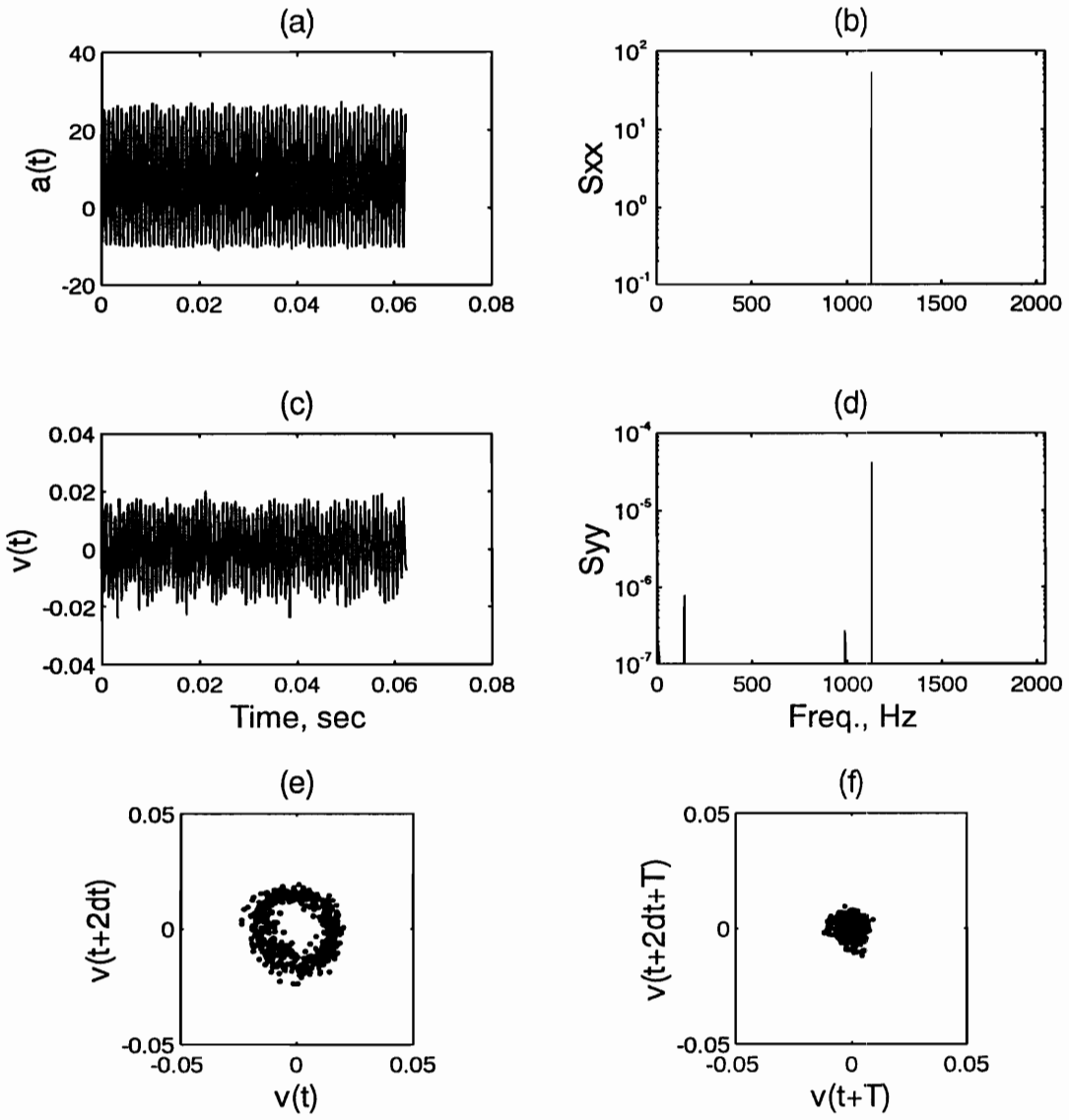

Figure 4.5: The excitation and response conditions at the location marked B on the force-response curve: (a) input time trace, (b) input power spectrum, (c) response time trace, (d) response power spectrum, (e) pseudo-state portrait, and (f) Poincaré map.

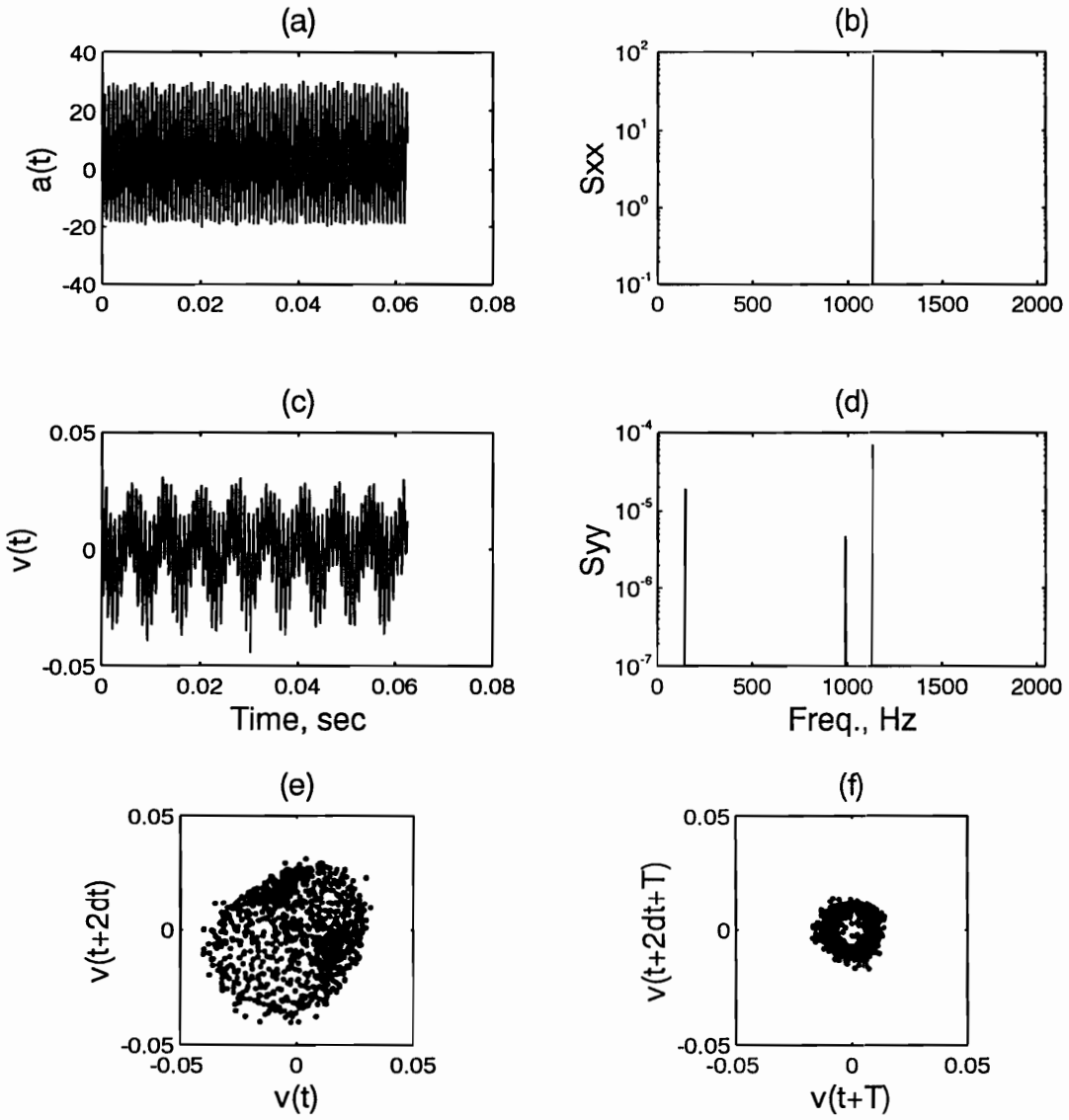

Figure 4.6: The excitation and response conditions at the location marked C on the force-response curve: (a) input time trace, (b) input power spectrum, (c) response time trace, (d) response power spectrum, (e) pseudo-state portrait, and (f) Poincaré map.

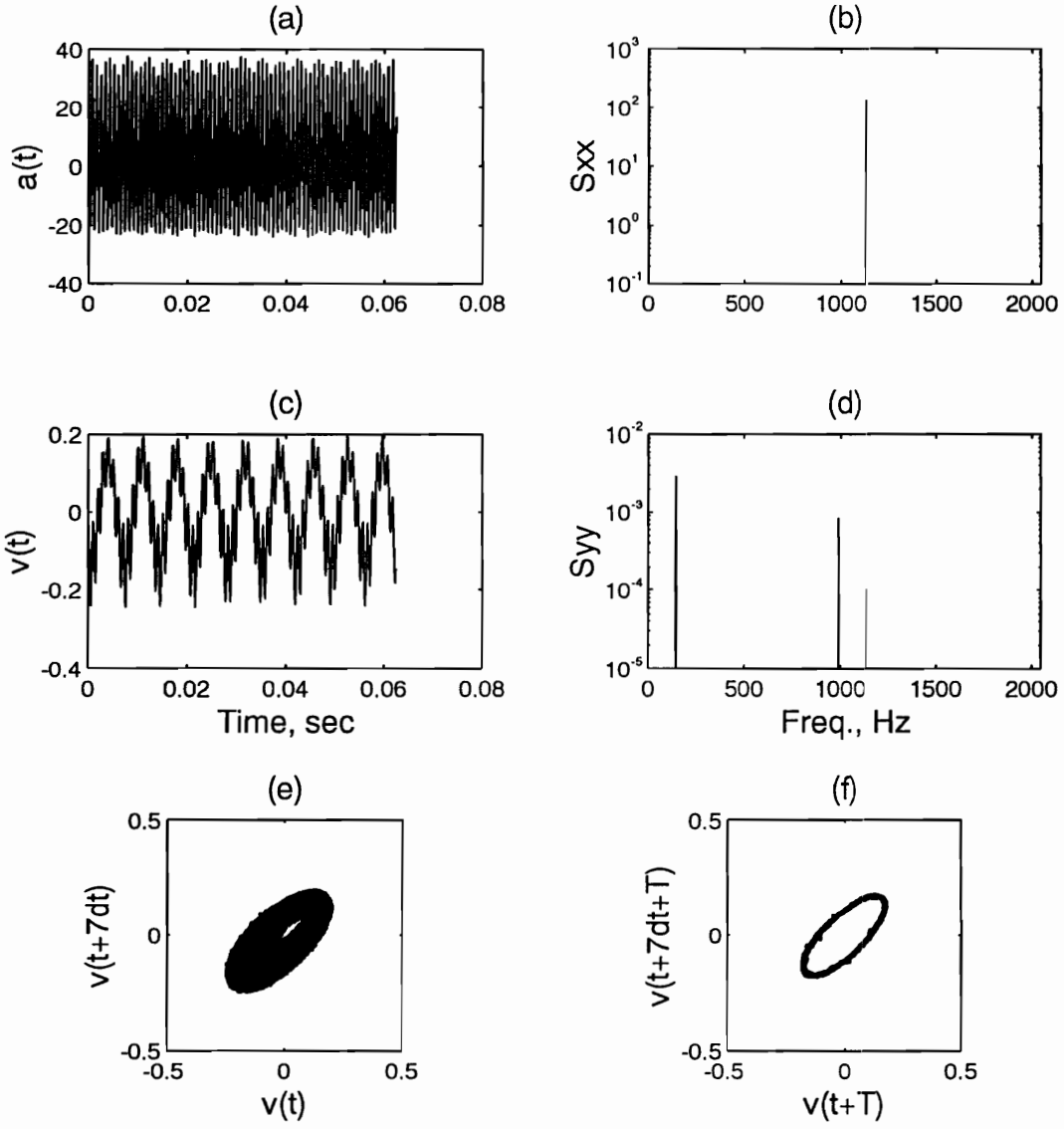

Figure 4.7: The excitation and response conditions at the location marked D on the force-response curve: (a) input time trace, (b) input power spectrum, (c) response time trace, (d) response power spectrum, (e) pseudo-state portrait, and (f) Poincaré map.

the plate. Time-domain data digitized using an A/D card in the computer were used to generate time traces, power spectra, pseudo-state portraits, and Poincaré maps. They were used to identify changes in the plate response during the reverse sweep.

The excitation amplitude was fixed at $F = 12.42\ g$ and the excitation frequency f_e was varied slowly over the frequency range 304.50 Hz to 309.25 Hz. During the forward and reverse incremental sweeps, we manually adjusted the excitation amplitude to keep it constant at each excitation frequency. We monitored the excitation frequency and determined the excitation amplitude by averaging the power spectrum of the accelerometer signal obtained with the signal analyzer. The results of the sweeps are displayed in Fig. 4.8. The plate response at the excitation frequency is represented by the symbol o. It is clear from the frequency-response curves that there were errors associated with keeping the excitation amplitude constant. The plate response at the first torsional frequency (ω_2) is represented by the symbol □ and the response at the second torsional frequency (ω_5) is represented by the symbol △. The solid symbols represent data collected during the forward sweep, and the hollow symbols represent data collected during the reverse sweep.

The frequency-response curves in Fig. 4.8 show that the response at the directly excited frequency did not change much in both the forward and reverse sweeps and that the responses at the first and second torsional frequencies had undergone many changes. In the forward sweep, the plate response consisted of a simple-harmonic motion until f_e increased past $f_e = 305.25$ Hz, where the first (second) and second (fifth) torsional modes were activated, but with small amplitudes. It seems that the amplitudes a_2 and a_5 of the second and fifth modes had undergone a pitchfork bifurcation at $f_e \approx 305.25$ Hz. As f_e was increased, a_2 and a_5 slowly increased and peaked at $f_e = 307.25$ Hz. As f_e was increased further, a_2 and a_5 decreased with a steeper slope to zero at $f_e = 308.25$ Hz. Thus, the frequency-response curve is weighted more to the right. Starting the reverse sweep at $f_e = 309.25$ Hz, we found that the plate response consisted of a simple-harmonic motion with a_2 and a_5 being equal to zero until f_e was decreased below 308.50 Hz, where the second and fifth modes were activated but with small amplitudes. As f_e was slowly decreased, a_2 and a_5

traced approximately the frequency-response curves obtained in the forward sweep.

To identify the changes in the plate response in the reverse sweep, we collected the accelerometer and vibrometer signals at the three locations marked A′, B′, and C′ on the frequency-response curve in Fig. 4.8. These locations correspond to the excitation frequencies f_e = 308.25, 308.00, and 307.25 Hz, respectively. We acquired 4 seconds of data using the sampling frequency f_s = 4096.0 Hz. For the Poincaré maps, we acquired additional data sets using the excitation frequency as the clock frequency. A pseudo-state space was reconstructed by using the time delay $4\,dt$, which corresponds to half the time corresponding to the first zero crossing of the autocorrelation function of the plate response.

Characteristics of the excitation and plate response at f_e = 304.50 Hz, corresponding to point A′ on the frequency-response curve in Fig. 4.8, are shown in Fig. 4.9. The power spectrum of the excitation in Fig. 4.9(b) consists of a single peak, indicating that the feedback from the plate to the shaker was negligible. The plate response was periodic as evident from the single-peak power spectrum, the closed curve pseudo-state portrait, and the single dot Poincaré map.

Characteristics of the excitation and plate response at the position marked B′ on the frequency-response curve of Fig. 4.8 are shown in Fig. 4.10. Again, the single-peak power spectrum of the excitation in part (b) indicates that the input was harmonic and the feedback from the plate to the shaker was negligible. The characteristics of the plate response in Fig. 4.10(c)-(f) indicate that the motion was two-period quasiperiodic. The time trace in Fig. 4.10(c) consists of two frequencies and the power spectrum in Fig. 4.10(d) has three peaks at 130.50 Hz, 308.00 Hz, and 485.50 Hz. Because f_e = 308.00 Hz = $\frac{1}{2}(130.50 + 485.50)$ Hz $\approx \frac{1}{2}(\omega_2 + \omega_5)$, the plate motion consisted of two frequencies, suggesting a two-period quasiperiodic motion or a periodic motion with large period. The pseudo-state portrait in Fig. 4.10(e) appears to be a complicated closed curve, indicating a periodic motion with a large period. However, the Poincaré map in Fig. 4.10(f) is a closed curve and hence the motion was two-period quasiperiodic.

Characteristics of the excitation and the plate response at f_e = 307.25 Hz, corresponding

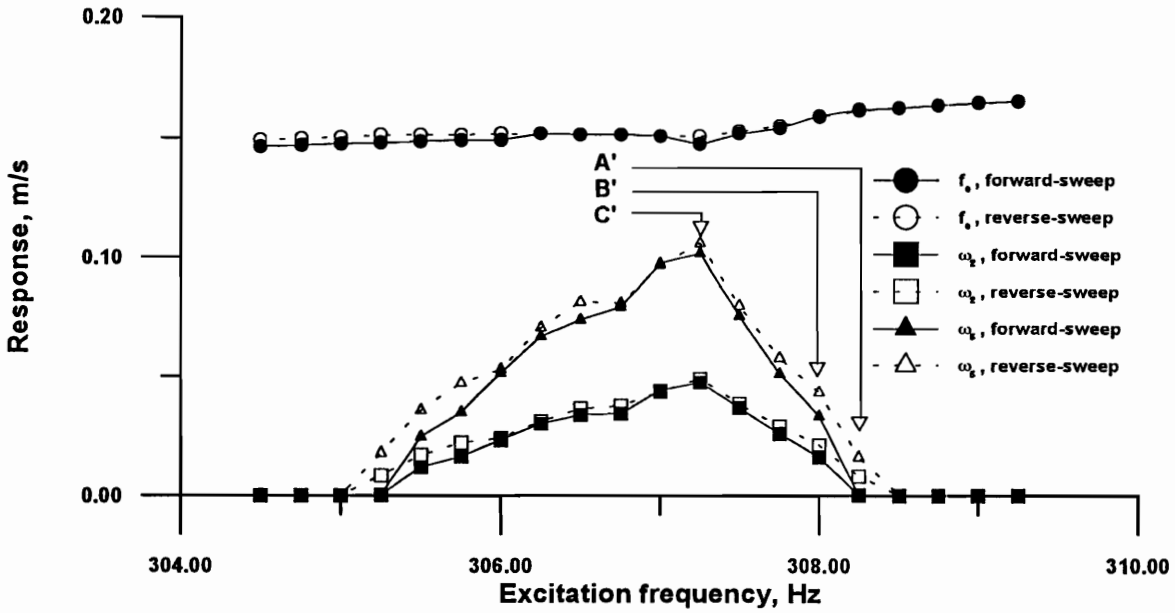

Figure 4.8: Frequency-response curves for the ±75 plate when $F = 12.42\ g$ and $f_e \approx \frac{1}{2}(\omega_2 + \omega_5)$.

to the position marked C′ on the frequency-response curve, are shown in Fig. 4.11. Again, the single-peak power spectrum of the excitation indicates that the feedback from the plate to the shaker was negligible. The time trace in Fig. 4.11(c) and the power spectrum in Fig. 4.11(d) suggest that the response consisted of two independent frequencies and that it might have been periodic with large period or two-period quasiperiodic. The pseudo-state portrait in Fig. 4.11(e) and its enlargement in Fig. 4.12 suggest that the plate motion was a two-torus. This is confirmed by the closed curve in the Poincaré map in Fig. 4.11(f).

4.5 Combination internal resonance in the response of the ±75 plate

In this experiment, we activated the combination internal resonance $f_e \approx \omega_8 \approx \frac{1}{2}(\omega_2 + \omega_{13})$ in the ±75. We used force-response curves to characterize the plate dynamics. To identify the changes in the response during the forward sweep, we acquired the accelerom-

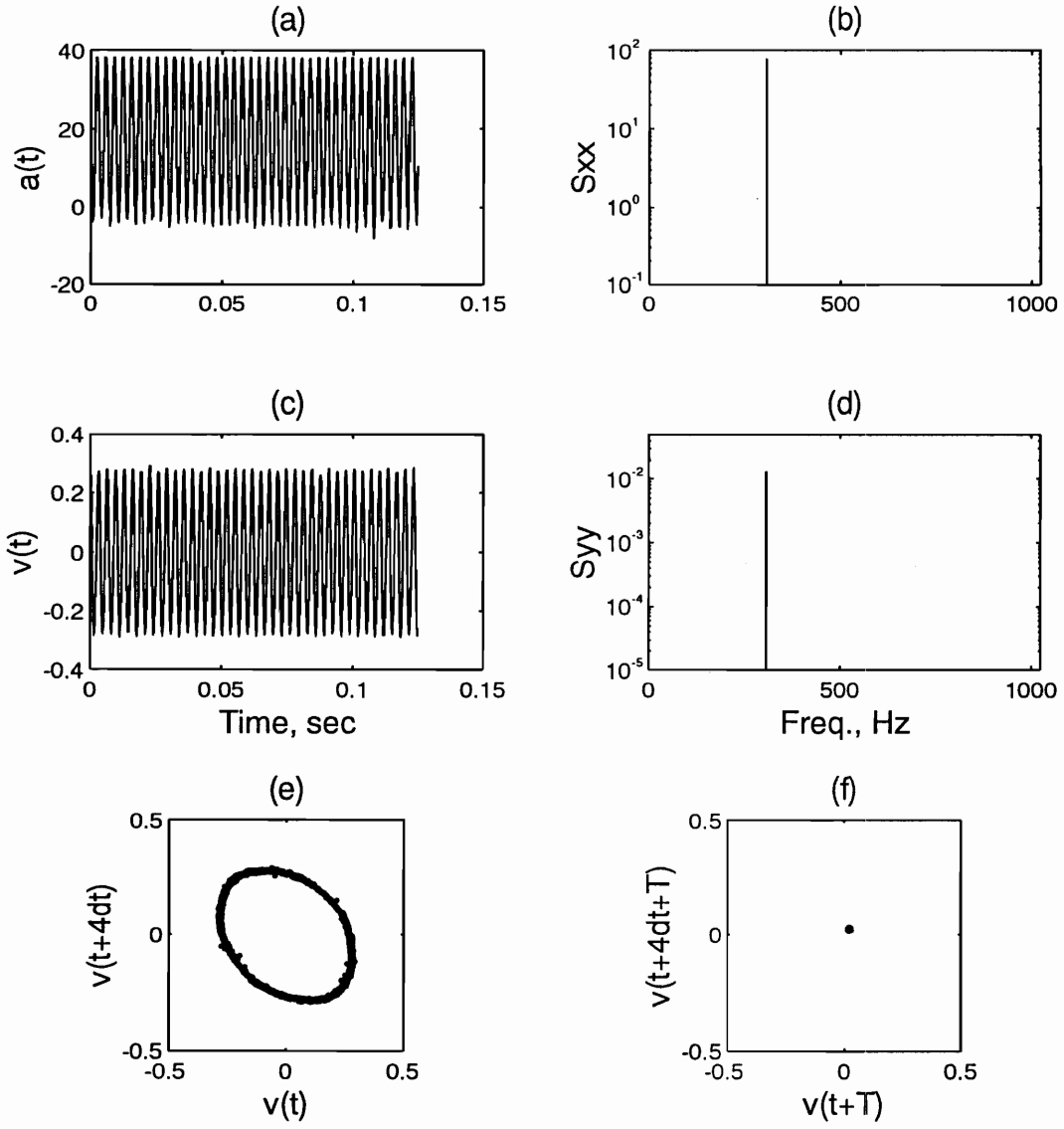

Figure 4.9: The excitation and response conditions at the location marked A′ on the frequency-response curve: (a) input time trace, (b) input power spectrum, (c) response time trace, (d) response power spectrum, (e) pseudo-state portrait, and (f) Poincaré map.

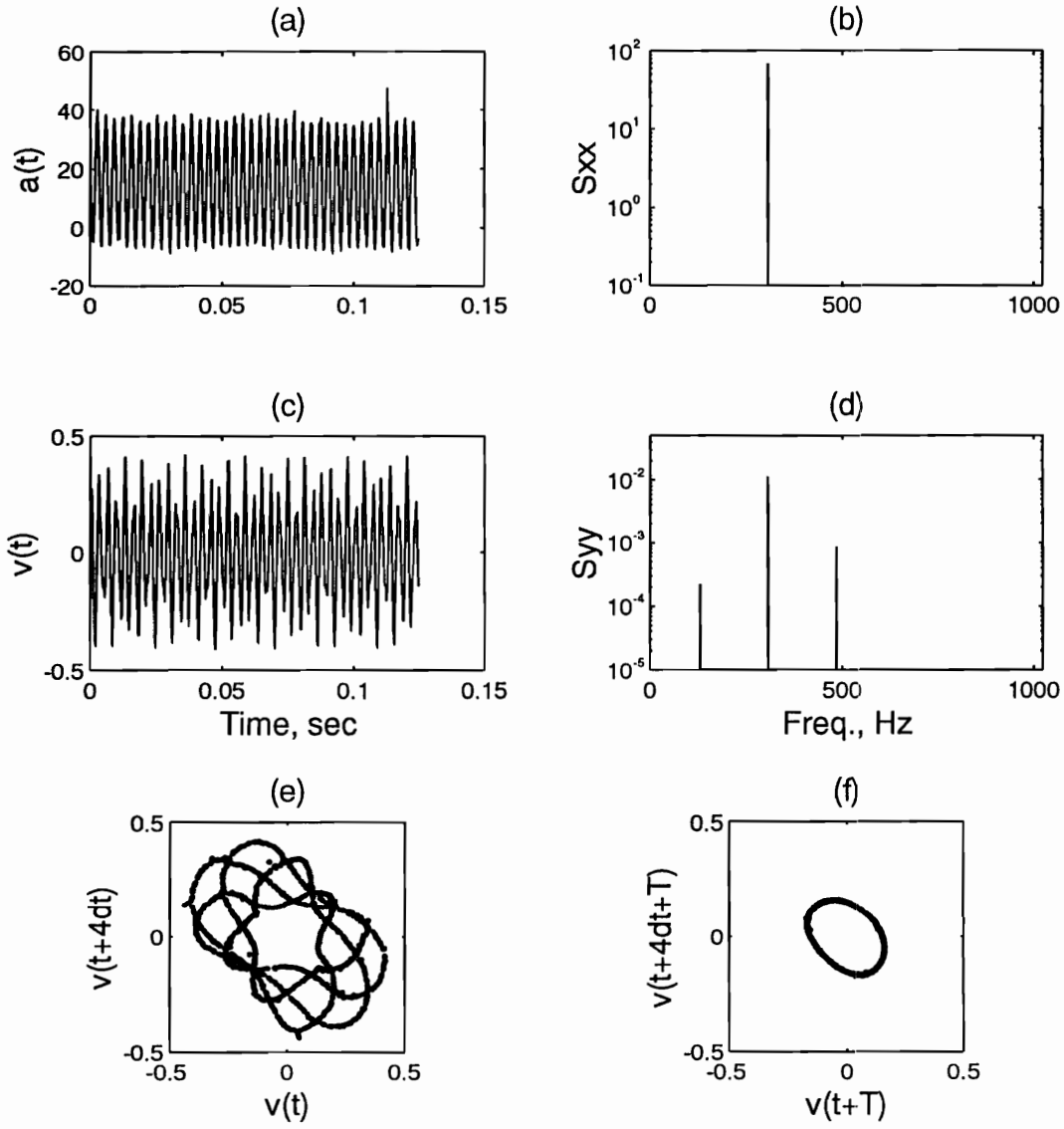

Figure 4.10: The excitation and response conditions at the location marked B′ on the frequency-response curve: (a) input time trace, (b) input power spectrum, (c) response time trace, (d) response power spectrum, (e) pseudo-state portrait, and (f) Poincaré map.

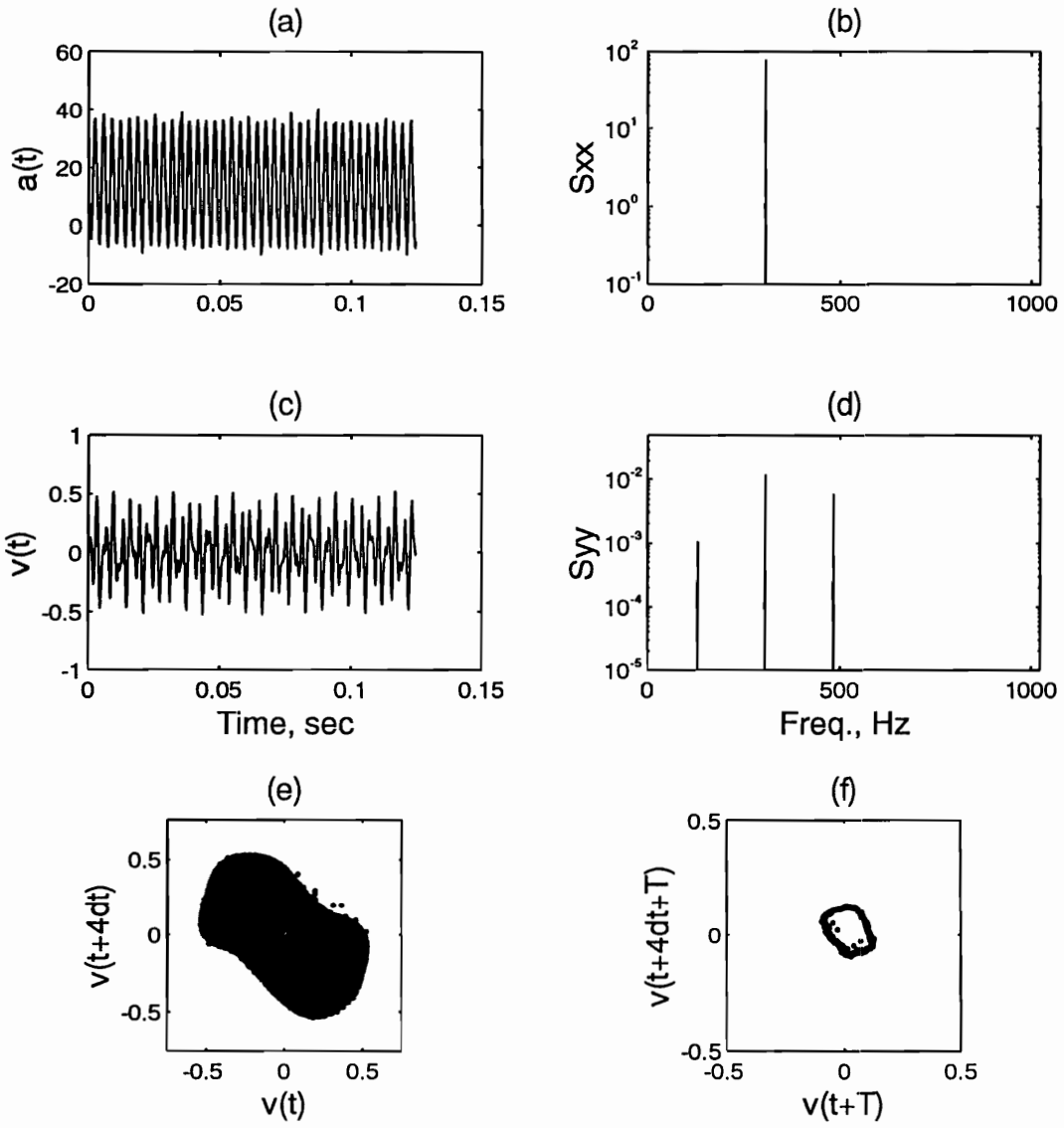

Figure 4.11: The excitation and response conditions at the location marked C′ on the frequency-response curve: (a) input time trace, (b) input power spectrum, (c) response time trace, (d) response power spectrum, (e) pseudo-state portrait, and (f) Poincaré map.

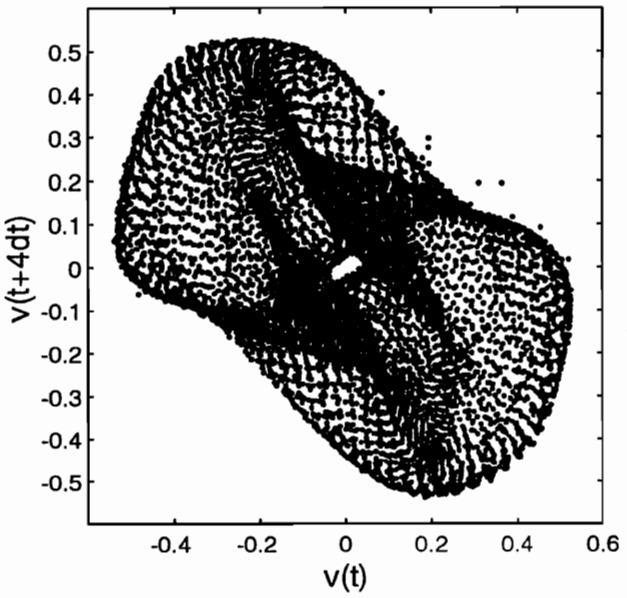

Figure 4.12: The pseudo-state portrait at the location marked C′ on the frequency-response curve characterizing a combination resonance in the response of the ±75 plate.

eter and vibrometer signals at three frequencies and used them to generate time traces, power spectra, pseudo-state portraits, and Poincaré maps. We found that a low-amplitude high-frequency excitation can produce a high-amplitude low-frequency (motion) through a combination internal resonance.

The plate was base excited at $f_e = 1048.2\,\text{Hz} \approx \omega_8 \approx \frac{1}{2}(\omega_2 + \omega_{13})$ and the excitation amplitude was used as the control parameter. Thus, we fixed the excitation frequency and incrementally swept the excitation amplitude forward and backward over the range $F = 13.57\ g$ to $17.98\ g$. We acquired four seconds of time-domain data with the sampling frequency 8192 Hz at the three locations marked by A″, B″, and C″ on the force-response curves. They correspond to the forcing amplitudes $15.12\ g, 15.33\ g$, and $17.98\ g$, respectively. For Poincaré maps, we collected additional data sets using the input frequency 1048.2 Hz as the clock frequency. At the positions A″ and B″, we constructed pseudo-state portraits using the time delay $T = 2\,dt$, which represents a half way point from the first zero crossing of the autocorrelation function of the response data. However, for the position C″, the time delay was chosen as $T = 5\,dt$, which represents the first minimum of the autocorrelation function of the response data (see Nayfeh and Balachandran, 1994). This change in the choice of the time delay is due to the fact that the response at point C″ was dominated by the low-frequency (first torsional) mode.

The force-response curves are displayed in Fig. 4.13. The symbol ○ represents the response at the excitation frequency, the symbol □ represents the response at the first torsional (ω_2) frequency, and the △ represents the response at the fourth bending (ω_{13}) frequency. The fourth bending mode (13th mode) is not included in Table 4.2 or in Figs 4.1 and 4.2. Due to the limitation of the frequency resolution of the signal analyzer, we were able to resolve only up to the 12th mode. However, we identified the frequency and mode shape of the 13th mode with the finite-element analysis. The solid symbols represent data collected during the forward sweep, and the hollow symbols represent data collected during the reverse sweep.

The force-response curves obtained from this experiment are qualitatively different from

those shown in Fig. 4.3 for the quasi-isotropic plate. The force-response curves in Fig. 4.13 are single-valued. The amplitudes of the first torsion and fourth bending modes started to increase at $F = 15.33\ g$ and reached their maxima at $F = 17.98\ g$. We reversed the sweep direction at this excitation level. Initially, the amplitude of the first torsional mode during the reverse sweep was close to that obtained during the forward sweep until $F = 16.62\ g$. Below this value, the amplitude of the first torsional mode started to deviate from that obtained in the forward sweep. We suspect this was the result of transients. The amplitude of the first torsional mode dropped to zero at $F = 14.84\ g$.

The input and response at the position marked A″ on the force-response curves are displayed in Fig. 4.14. Parts (a) and (b) show that the excitation consisted of a single frequency and hence we conclude that the feedback from the plate to the shaker was negligible. The time trace and power spectrum of the response in parts (c) and (d) indicate that the response was a simple-harmonic motion. The pseudo-state portrait displayed in part (e) is a closed curve and the Poincaré map is a single point, confirming the period-one nature of the motion.

Increasing the excitation amplitude to that corresponding to point B″ resulted in a change in the response from a period-one periodic motion to a two-period quasiperiodic motion, as shown in Fig. 4.15. The power spectrum of the input in part (b) indicates that the input was harmonic and that the feedback from the plate to the shaker was again negligible. The time trace of the response in part (c) shows that the total response consisted of at least two frequencies - one was high and the other was low. The power spectrum of the response clearly shows two peaks corresponding to high and low frequencies. The pseudo-state plane in part (d) indicates that the motion might have been periodic with a large period or a two-torus. The closed curve in the Poincaré map in part (d) identifies the motion to be definitely two-period quasiperiodic.

Increasing the excitation amplitude to that corresponding to the position marked C″ produced a motion that was dominated by the low-frequency (first torsional) mode and had a small contribution from the high-frequency (fourth bending) mode. Characteristics of

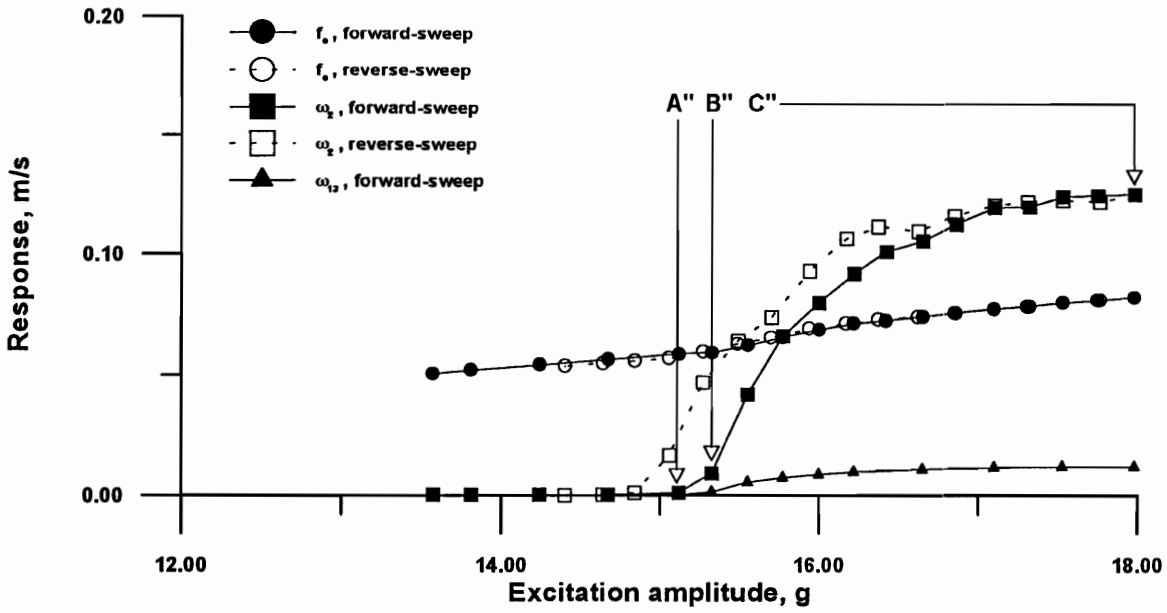

Figure 4.13: Force-response curves for the ±75 plate when $f_e = 1048.2\,\text{Hz} \approx \omega_8 \approx \frac{1}{2}(\omega_2 + \omega_{13})$.

the shaker acceleration and the plate response are displayed in Fig. 4.16. Again, the single peak in the power spectrum of the input indicates that the input was harmonic and that the feedback from the plate to the shaker was negligible. Both of the time trace and power spectrum in parts (c) and (d) show that the response was dominated by the low-frequency mode and contained two independent frequencies. However, they do not help to determine whether the motion was periodic with a large period or quasiperiodic. The pseudo-state plane in part (e) suggests that it was quasiperiodic and the closed loop Poincaré map in part (f) conclusively identifies it to be quasiperiodic in nature.

4.6 *Closure*

We experimentally identified and characterized nonlinear combination resonances in stiff cantilever graphite-epoxy composite plates. We found that a low-amplitude high-frequency

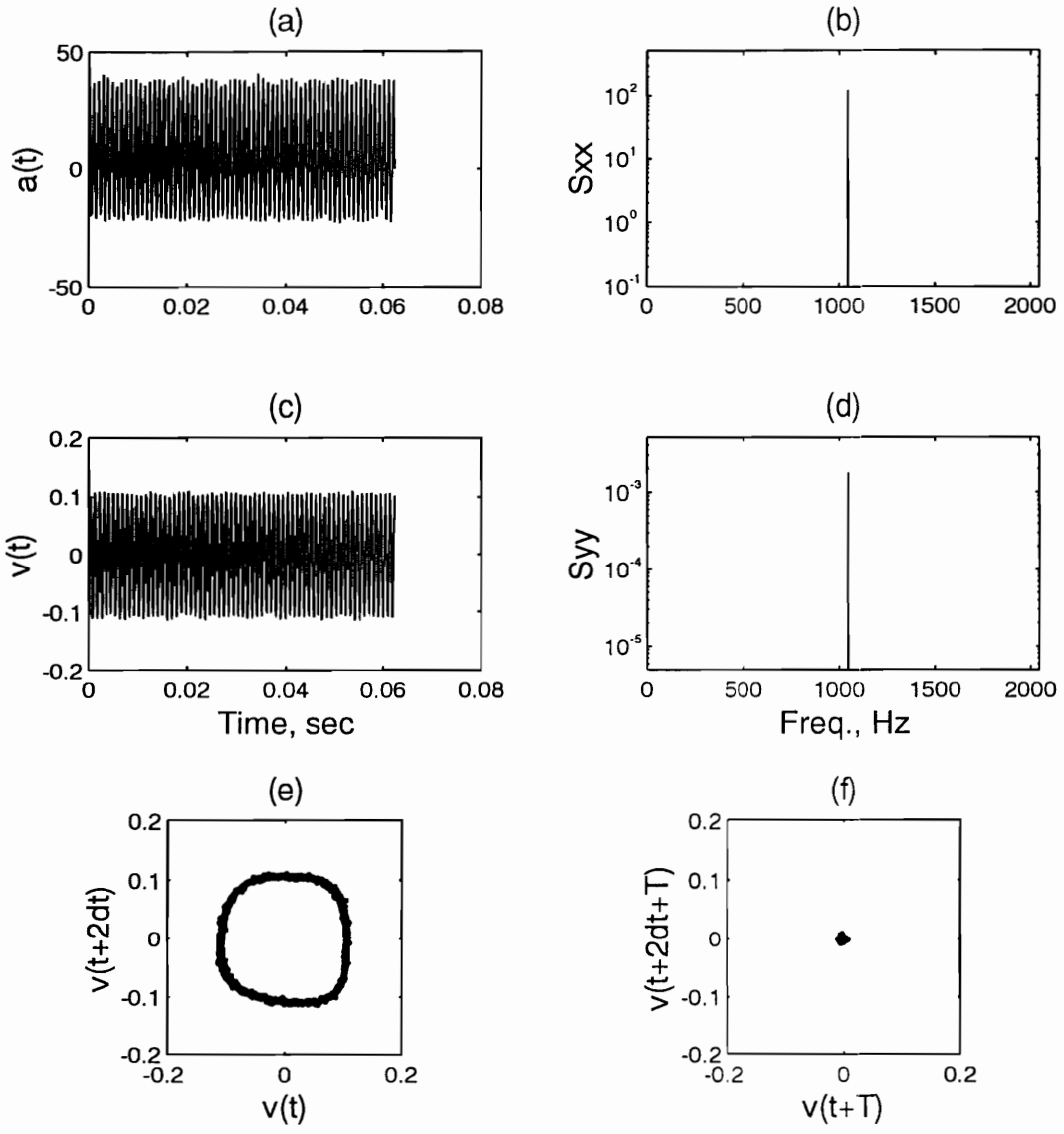

Figure 4.14: The excitation and response conditions at the location marked A″ on the force-response curves characterizing a combination internal resonance in the ±75 plate: (a) input time trace, (b) input power spectrum, (c) response time trace, (d) response power spectrum, (e) pseudo-state portrait, and (f) Poincaré map.

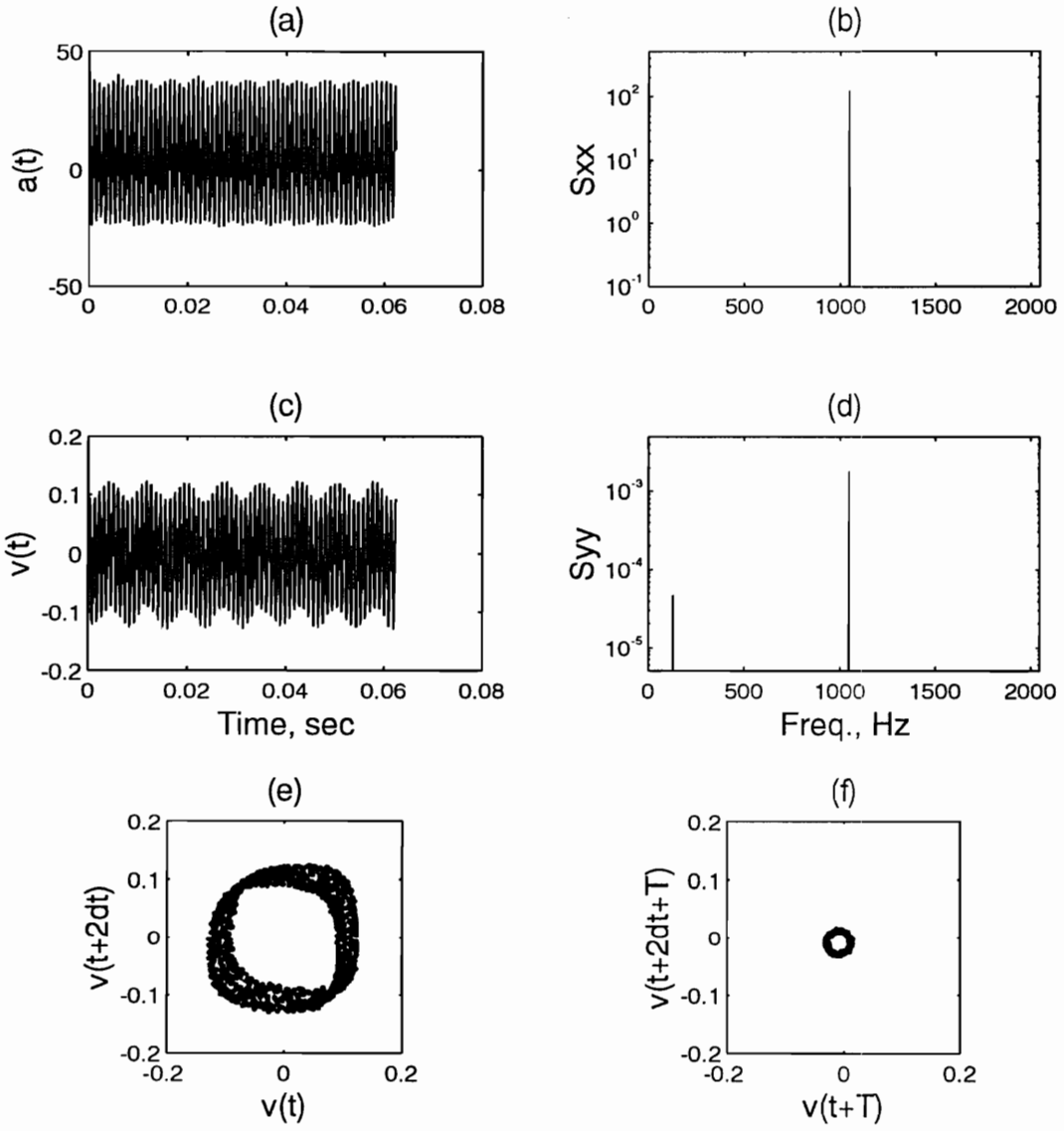

Figure 4.15: The excitation and response conditions at the location marked B″ on the force-response plot characterizing a combination internal resonance in the ±75 plate: (a) input time trace, (b) input power spectrum, (c) response time trace. (d) response power spectrum, (e) pseudo-state portrait, and (f) Poincaré map.

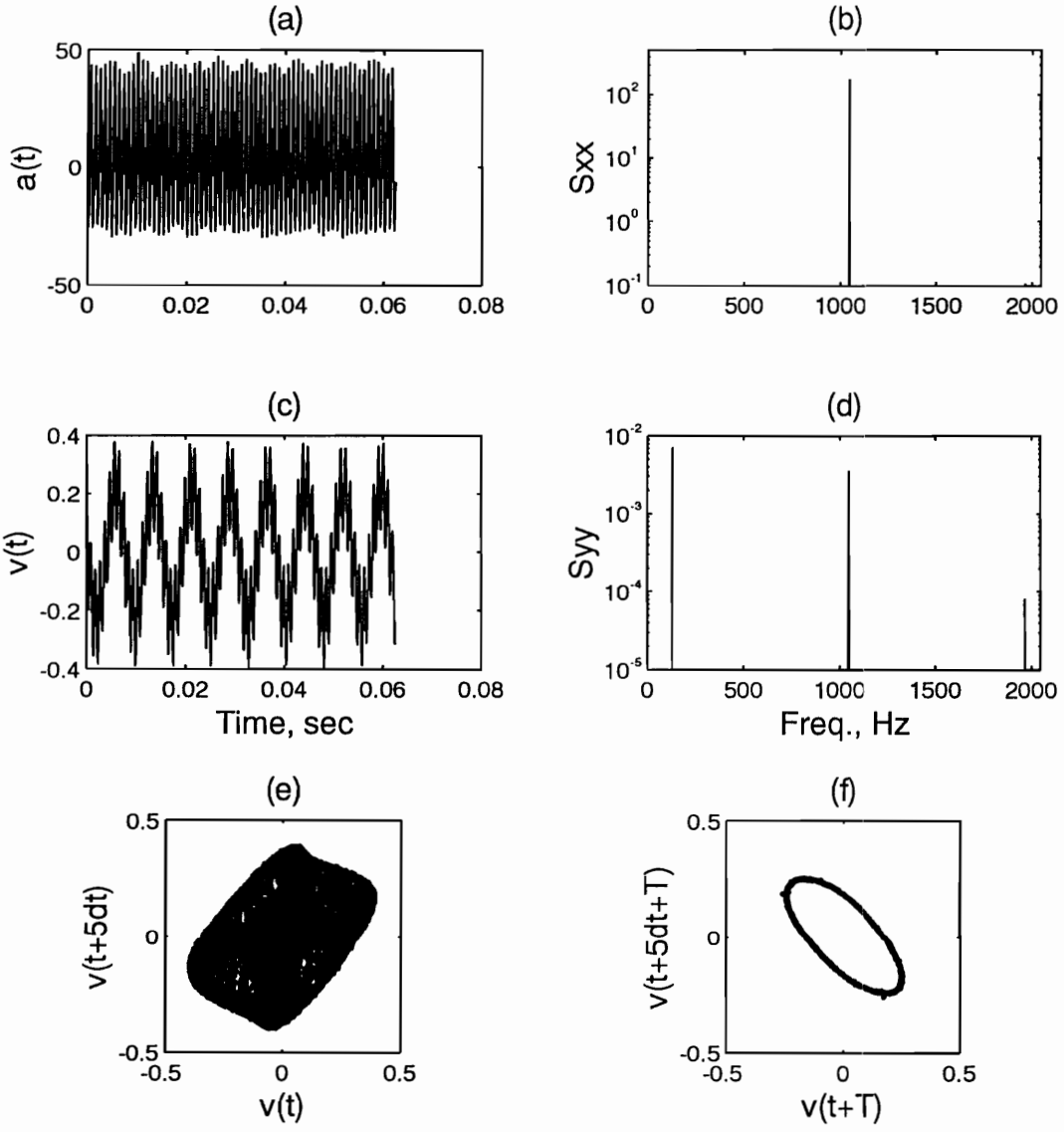

Figure 4.16: The excitation and response conditions at the location marked C″ on the force-response plot characterizing a combination internal resonance in the ±75 plate: (a) input time trace, (b) input power spectrum, (c) response time trace, (d) response power spectrum, (e) pseudo-state portrait, and (f) Poincaré map.

excitation can produce a large-amplitude low-frequency motion.

We activated the combination resonance $f_e = 1133.8\,\text{Hz} \approx \omega_2 + \omega_7$ in a quasi-isotropic composite plate. We fixed the excitation frequency and used the excitation amplitude to generate force-response curves. We collected time-domain data for four different excitation levels and used them to generate time traces, power spectra, pseudo-state portraits, and Poincaré maps. We observed that as the forcing amplitude exceeded a threshold value, a period-one harmonic motion evolved into a two-period quasiperiodic motion. In that process, we observed that a low-amplitude high-frequency excitation produced a high-amplitude low-frequency (first torsional) motion through a combination resonance of the additive type.

We activated the external combination resonance $f_e = 310.37\,\text{Hz} \approx \frac{1}{2}(\omega_2 + \omega_5)$ and the internal combination resonance $f_e = 1048.2\,\text{Hz} \approx \omega_8 \approx \frac{1}{2}(\omega_2 + \omega_{13})$ in a plate with the layup $(-75/75/75/-75/75,-75)_s$. For the external combination resonance, we fixed the excitation level and used the excitation frequency to generate frequency-response curves. Moreover, we collected time-domain data at three different frequencies and generated time traces, power spectra, pseudo-state portraits, and Poincaré maps. We found that, as the excitation frequency exceeded a threshold value, the plate response changed from a period-one harmonic motion to a two-period quasiperiodic motion consisting of low and high frequencies. As the excitation frequency was increased further, the response was dominated by the low-frequency mode.

For the internal combination resonance, we fixed the excitation frequency and slowly varied the excitation amplitude to generate force-response curves. Moreover, we collected time-domain data for three excitation amplitudes and used them to generate time traces, power spectra, pseudo-state portraits, and Poincaré maps. Increasing the excitation amplitude, we found that the response continuously evolved from a period-one harmonic motion to a two-period quasiperiodic motion. Increasing the excitation level further produced a response that was dominated by the low-frequency mode.

Chapter 5

MODAL ANALYSIS OF NONCLASSICALLY SUPPORTED PLATE

5.1 *Introduction*

It is a common practice among the noise and vibration engineers to estimate the dynamics of a structure by first determining the structure's natural frequencies and mode shapes. They are usually obtained with modal analyses. These analyses assume that the structure's total response can be represented as the superposition of individual modal responses. Typically, one can perform the modal superposition in the time or frequency domain. In the time domain, the modal responses are evaluated as a function of time and then combined to yield the total response history of the structure. In the frequency domain, the modal maxima of the structure are obtained from the response spectrum. Therefore, selecting a particular damping model, one can determine the maximum response of the structure by approximately combining the model maxima. The literature review on the damping models is discussed in Section 1.1.3.

In an experimental-modal analysis, one chooses between a proportional and a nonproportional damping model. The proportional damping model assumes the damping matrix to be a linear combination of the mass and stiffness matrices. This assumption results in the normal modes. This model is widely available in commercial modal and finite-element-analyses packages.

A comprehensive literature search on nonproportional damping was conducted by Bellos and Inman (1989). Lang (1989) illustrated the similarities and differences between the normal and complex modes through an example. He showed the physical connection between

the complex mode shapes and frequencies. Lang's method is similar to the approach of Veletsos and Ventura (1986), which they based on relating the corresponding displacements for nonclassically damped multi-degree-of-freedom systems. They modeled such systems as a linear combination of displacements and relative velocities of a series of single-degree-of-freedom systems subjected to similar excitations. Özgüven (1981) compared the results for a two-degree-of-freedom system using the uncoupled mode superposition method with his single-mode method. The former ignores the off-diagonal elements of the transformed damping matrix. Özgüven (1981) decoupled the equations of motion of nonproportionally damped systems at an undamped natural frequency. Therefore, the total response was approximated by the modal response that belongs to the mode of excitation. Suarez and Singh (1987a) proposed a method for determining the exact complex eigenproperties of a nonclassically damped structure supporting a single-degree-of-freedom oscillator. They obtained the eigenvalues as the solution of a simple nonlinear equation with real coefficients. They concluded that this method can be used effectively to obtain the exact eigenproperties for very light as well as very heavy equipment supported on structures. Suarez and Singh (1987b) also investigated the use of a perturbation method to obtain the complex eigenproperties of such damped structures. They considered the dynamic response of equipment supported on structures subjected to earthquake induced ground motions.

Recently, the idea of complex eigenproperties has been used in the automotive industry where the dynamics of a locally supported structure is evaluated as a function of the global excitation and the damping. The complex mode shapes are being experimentally quantified using a holographic interferometry technique at the Ford Research Computer Aided Holometry Laboratory.

In this chapter, we present the results of an experimental modal analysis (EMA) of a nonclassically supported plate with and without a constrained-layer damping (CLD) patch attached on its upper-left hand corner. The natural frequencies and mode shapes are compared to ascertain the effect of the patch and to evaluate the performance of the EMA for systems with high damping. We also use the modal damping factors to determine the

effect of the patch on particular modes.

5.2 *Methodology*

In this chapter, we discuss two experimental conditions. The first condition is a nonclassically supported plate without a damping patch attached. The second condition is an extension of the first where a damping patch was attached to the plate's surface. This damping patch is called a constrained-layer damping patch because it consists of three layers: an aluminum foil, a viscoelastic material, and an adhesive material.

The plate under study was made of aluminum and its dimensions are listed in Table 5.1. Nonclassical clamping conditions were created by cutting a 60% groove with respect to the plate thickness around the perimeter of a nearly square plate. The effective groove-to-groove dimensions are also listed in Table 5.1. Note that there was a 2 inch offset from the outside edge-to-edge plate dimension to the inside groove-to-groove dimension. To create this clamping condition, we used a 0.5 inches thick aluminum face plate that covers most of the 2 inch offset between the edge and groove side dimensions. There is just enough space between the edge and groove sides to simulate the no-displacement and some rotation-degree-of-freedom conditions at the grooved edges. A schematic of the geometry layout and the excitation and measurement point locations for the experiment without the damping patch is displayed in Fig. 5.1. This figure shows that the plate surface was divided into a 7 by 7 grid distribution. The excitation point was fixed at the grid point 19Z for the experiment without the damping patch. The origin of the reference coordinate was placed at the lower left-hand corner of the grooved edge. A schematic of the overall experimental setup and section drawing of the test fixture is displayed in Fig. 5.2.

The constrained-layer damping material was provided by Ford Motor Company. The damping sheet thickness was 0.040 inches. The sheet consisted of a 5 mil thick high-strength acrylic pressure sensitive adhesive and it was faced with a 5 mil aluminum constraining layer. The dimensions of the sheet were 4" x 4". The total mass of the damping sheet

Table 5.1: Physical dimensions of the plate

Outside dimensions:	14.869 x 14.874 x 0.039 inches
Inside (grooved) dimensions:	12.869 x 12.874 x 0.039 inches

was 0.058 lb. The constrained-layer damping patch was attached to the plate surface in the second experiment. The lower left corner of the damping patch started approximately at (1.44", 7.43") and the upper right corner ended approximately at (5.44", 11.43") with respect to the reference coordinate system. A schematic of the geometry layout for the modal analysis with the damping patch is displayed in Fig. 5.3. In this setup, we moved the location of the excitation point from 19Z to 52Z, which was not symmetric with respect to the diagonal of the plate. We added seven additional grid points to the existing geometry file to accommodate the shift in the excitation location. The additional grid points were numbered from 50Z to 56Z, and they are displayed in Fig. 5.3.

The face and test plates were clamped to support blocks by two sets of bolt screw patterns. The first set was located close to the grooved edges to clamp both the face and test plates to the support blocks. The torque on the first set of screws was set at 12 ft-lbs. The second set of screws was designed to provide enough torque to support the first set of screws and at the same time not to impose additional moments. The torque on the second set of screws was set at 6 ft-lbs.

During the initial phase of our investigation, we attempted to estimate the frequency-response functions using an instrumented impact hammer to provide the input and a laser vibrometer to measure the plate response. However, due to the high damping caused by the grooved edges, we were unable to excite many modes of interest. Therefore, we used a mono-excitation and a multiple-response method to generate the frequency-response functions necessary to conduct the experimental-modal analysis.

The plate was excited using a 2-lb modal shaker. The shaker was placed inside the support blocks surrounding the perimeter of the plate. A schematic of the setup is displayed

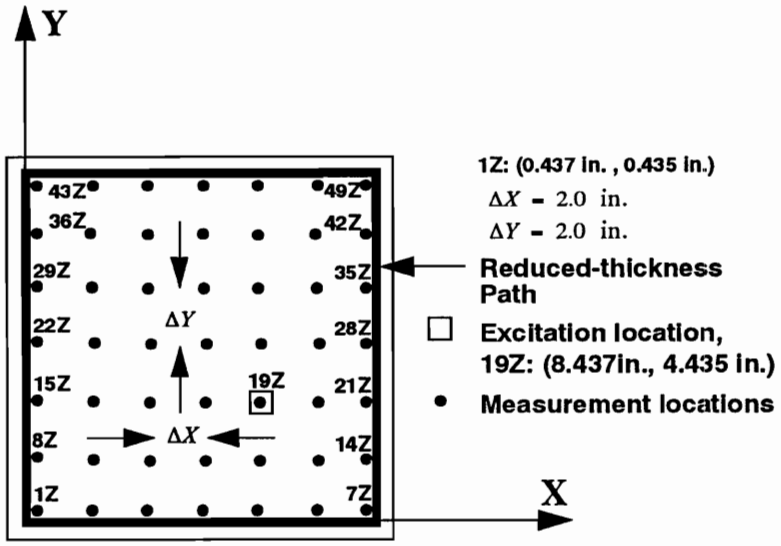

Figure 5.1: A schematic of the nonclassically supported plate without the damping patch and the grid point distribution for the experimental-modal analysis.

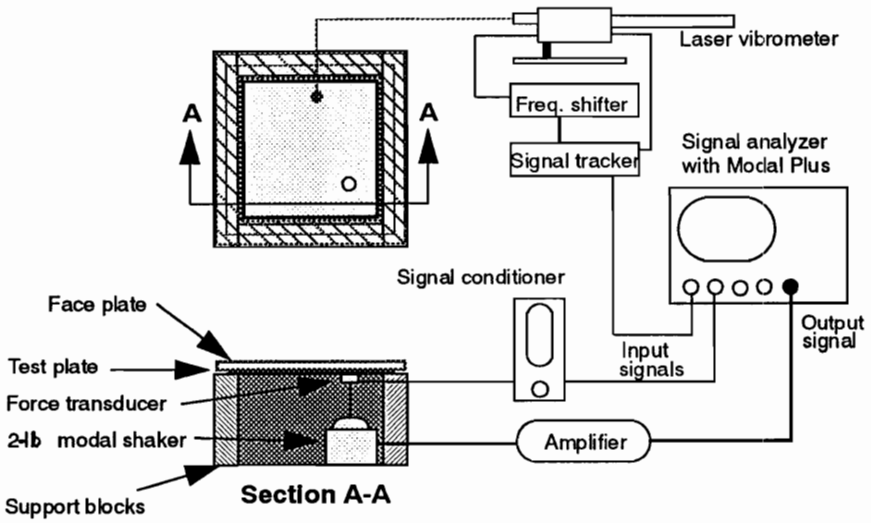

Figure 5.2: A schematic of the experimental setup and section drawing of the test fixture.

in a section drawing in Fig. 5.2. A force transducer was glued to the plate surface using an epoxy compound and a stinger was attached to the modal shaker. Hence, we were able to monitor the excitation condition. The plate responses at the grid points marked on the plate surface were measured using a laser vibrometer. The use of a nonintrusive sensor was important for these experiments because the structure under investigation was light and flexible.

The signals from the force transducer and laser vibrometer were sampled using a computer-aided test system. We used the frequency bandwidth 0 to 256 Hz and 512 lines of resolution. The input for the modal shaker was controlled by the computer-aided test. We selected the input signal to be a random burst with the frequency bandwidth 0 to 256 Hz. The duration of the excitation was set to synchronize with the data acquisition process and each random burst was passed through a Hanning window. The transfer functions estimated from the spectrum analyzer were used in the modal analysis. We used the modal-plus soft-

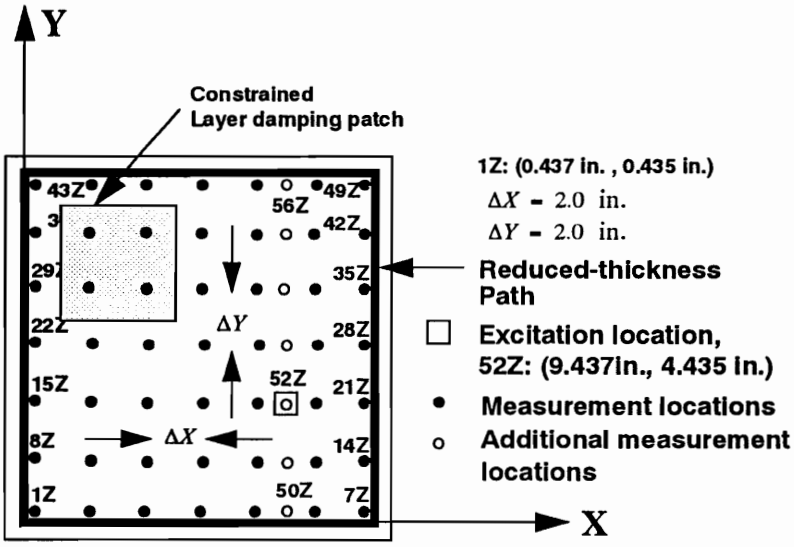

Figure 5.3: A schematic of the nonclassically supported plate with the damping patch and the grid point distribution for the experimental-modal analysis.

ware resident in the computer-aided test. An example of the frequency-response function at the excitation point is shown in Fig. 5.4. Usually, modal analysis softwares contain many curve fitting techniques for estimating the natural frequencies and mode shapes. In this experiment, we tried two curve fitting techniques: (i) the direct parameter method and (ii) the polyreference method. Both methods are applicable to multi-degree-of-freedom systems but the direct parameter method operates in the frequency domain while the polyreference method operates in the time domain. We found that, for highly damped systems such as our plate, results from the direct parameter method gave inconsistent damping values. Therefore, we decided to use results from the polyreference method. The residue generation procedure in the modal-plus software was set to assume complex numbers. This allowed the mode shapes to be complex, thereby allowing the phase to change from point to point on the surface of the plate. For the second experiment, the natural frequencies and mode shapes of the plate were estimated using a similar procedure. The estimated natural frequencies for both plate conditions are listed in Table 5.2.

5.3 *Results*

The estimated complex mode shapes are displayed in three columns. The first column represents the commonly known normal modes, the second column represents the imaginary modes, and the third column represents the phase relationships on the plate surface. If the complex mode shape vector is expressed as

$$\Phi = \phi_r + i\phi_i,$$

then the normal mode is the imaginary component ϕ_i and the imaginary mode is the real component ϕ_r. The phase relationship on the plate surface is represented by

$$\Theta = \text{atan}(\phi_i/\phi_r).$$

The units on the mode shape plots are normalized to the driving-point measurements, and the phase plots have the unit of radians. The complex mode shapes for the plate without

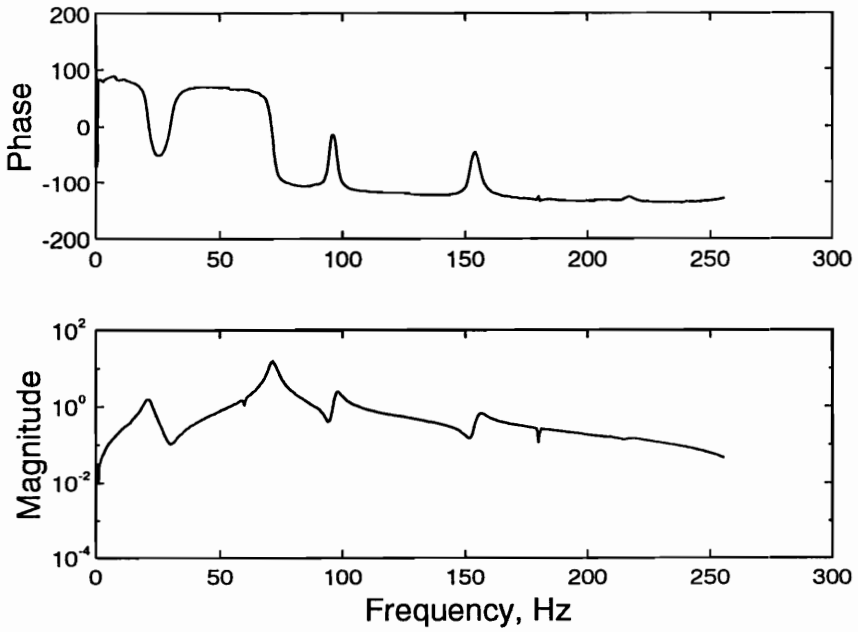

Figure 5.4: A frequency-response function at the excitation point.

the CLD patch are displayed in Figs 5.5 through 5.7, and the mode shapes for the plate with the CLD patch are displayed in Figs 5.8 through 5.10.

The first mode shape in Fig. 5.5 (without CLD) shows the pumping motion on the imaginary mode, but the normal mode shape is slightly skewed and unsymmetric. The normal mode is an order of magnitude smaller than that of the imaginary mode. Therefore, the first mode shape of the plate from the first experiment without the CLD patch is dominated by the imaginary mode. However, in the second experiment with the CLD patch, the mode shape is dominated by the normal mode, as shown in Fig. 5.8. The imaginary mode of the plate from the second experiment with the CLD patch is slightly skewed relative to the normal mode. The nodal line is at a different location. However, the dominant modes from both experimental configurations, with and without the CLD patch, are similar to each other. The natural frequency increased from 21.32 Hz to 22.586 Hz due to the CLD patch. This 5.94% increase in the natural frequency suggests that adding the

Table 5.2: Estimated modal parameters with and without the constrained-layer damping patch.

Root	Frequency			Modal damping factor		
	plate	plate w/ CLD	% diff.	plate	plate w/ CLD	% diff.
1	21.32	22.59	5.94	0.085	0.092	7.85
2	71.67	83.18	16.1	0.021	0.026	26.8
3	89.67	93.45	4.22	0.019	0.048	150
4	97.57	107.00	9.67	0.016	0.045	187
5	155.28	161.67	4.12	0.014	0.064	360
6	208.97	204.15	-2.31	0.012	0.032	176
7	216.46	220.74	1.98	0.013	0.020	58.4

CLD patch had increased the stiffness of the plate. We also find that the modal damping factor had increased by 7.85%.

The second mode is slightly different from the first mode. For the first case without the CLD patch, the normal and imaginary modes are very similar. Both mode shapes have a nodal-band going through the left side of the mode shape, as displayed in Fig. 5.5. We define a nodal-band as a region near the nodal line where the phase distribution on either side of the nodal line is not 180 degrees apart. The third columns of Figs 5.5 and 5.8 show the nodal-band areas. These regions are also known as the "nodal-galloping" regions. However, for the case with the CLD patch, the normal mode dominates the response. Therefore, although the imaginary mode displayed in the second row and second column of Fig. 5.8 contains a zero-displacement line, the phase changes across the plate surface do not contain any nodal-galloping region. The phase distribution on this mode is wide spread across the plate surface, and it is similar to that of the first mode. The second natural frequency had increased by 16.1% and the modal damping factor also increased by 26.8% with the addition of the CLD patch, as seen from Table 5.2. These changes suggest that the second mode was more affected by the change in the local stiffness caused by the addition of the CLD patch on the upper-left hand corner. The larger increase in the modal damping factor for this mode compared with that of the first mode led us to assume that with the CLD

patch the distinction between the two modes comes form the imaginary mode although the normal mode shapes of these two modes appear to be similar. We see that near the CLD patch there is more curvature in the second imaginary mode than in the first imaginary mode.

The third mode of the plate without the CLD patch has a nodal-region running diagonally from the top-left corner to the mid-right edge of the plate. The fourth mode is approximately 90 degrees out-of-phase with the third mode, as seen in Fig. 5.6. The nodal region of the fourth mode starts from the mid-right edge of the plate and runs to the left-bottom edge of the plate. The difference between the frequencies of the third (89.67 Hz) and fourth (97.57 Hz) modes is only 7.9 Hz, as evident in Table 5.2. The repeated or nearly repeated frequencies with the corresponding mode shapes being 90 degrees out-of-phase in structural vibration were mainly observed in lightly damped symmetric structures. It is interesting to observe such a phenomenon in a highly damped system in which the modal damping factors are 1.9% and 1.6% for the third and fourth modes, respectively. However, because of the large damping originating from the nonclassical support around the grooved edges, the nodal regions for both modes do not expand from one corner to the opposite corner, as evident from Fig. 5.6. For each of these modes, the normal and imaginary modes have similar shapes.

For the case of the plate with the patch, the third and fourth natural frequencies are 93.45 Hz and 107.00 Hz, respectively. The difference between them is 13.55 Hz, and they differ by 4.22% and 9.67% from those for the plate without the patch. The modal damping factors increased from 1.9% to 4.8% (150% change) for the third mode, and from 1.6% to 4.5% (187% change) for the fourth mode.

The patch resulted in a rotation of the nodal region of the third mode as displayed in Fig. 5.9. The largest difference between the normal and imaginary modes is in the number of nodal regions present in each mode. The imaginary mode has two diagonal nodal regions whereas the normal mode has one. However, the phase distribution across the plate face appears to resemble more that of the normal mode. This is because the deformation due

the normal mode dominates that of the imaginary mode. We note that the nodal region of the normal mode passes through the maximum deflection area of the imaginary mode. Similarly, the location of the maximum deflection of the normal mode passes through the two nodal regions of the imaginary mode. The phase map also displays the effect of the patch; that is, the nodal region passes parallel to the attached right side and curves in the negative x-direction after it passes the edge of the patch. These are shown in Fig. 5.9.

The normal and imaginary modes of the fourth mode with the patch are also different, as displayed in Fig. 5.9. The nodal region of the fourth normal mode is oriented in the same direction as that of the third mode without the patch. The phase distribution is relatively straight across the surface. However, the shape of the fourth imaginary mode does not match any recognizable mode shape. The phase map is similar to that of the normal mode shape.

In summary, the third and fourth mode shapes with the patch show that the normal and imaginary mode shapes do not have to be similar. We note that they could be different by an order of magnitude from the higher mode shapes. However, the phase map reflects the phase distribution of the dominant mode shape. The third and fourth mode shapes with the patch are not similar to the corresponding mode shapes without the patch. The large increase in the modal damping factors for both the third and fourth modes are due to the location of the patch with respect to the curvatures of these mode shapes.

The fifth mode for both plate configurations with and without the patch is a two-by-two symmetric mode shape, as displayed in Figs 5.7 and 5.10. In the case without the patch, the normal mode shape is slightly skewed, but the imaginary mode seems to be equally spaced. The phase map for this mode is similar in appearance to that of the normal mode shape. The normal mode with the patch is slightly skewed but maintains a two-by-two mode shape. The imaginary mode shape is smaller in magnitude and more skewed from the two-by-two mode shape. Therefore, the phase map shows the phase variations around the nodal regions having the normal mode shape. The difference between the fifth natural frequencies with (161.67 Hz) and without (155.28 Hz) the patch is 4.12%. However, the

modal damping factor was changed from 1.4% to 6.4%, an increase of 360%. This change in the modal damping factor was the largest increase for this test with the patch, and it is due to the location of the patch at the anti-node of the mode shape.

The sequence of the sixth and seventh mode shapes are similar to those of the third and fourth modes. The sixth mode has two nodal regions in the y-direction, and the seventh mode has two nodal regions in the x-direction. The difference in the natural frequency is 7.49 Hz (208.97 Hz to 216.46 Hz) without the patch and 16.59 Hz (204.15 Hz to 220.74 Hz) with the patch. The modal damping factor changed from 1.2% to 3.2% (176% change) for the sixth mode and from 1.3% to 2.0% (58.4% change) for the seventh mode. The normal mode dominates both mode shapes. The phase map for these modes indicates such mode shapes. The phase distributions for the plate with the patch, displayed in Fig. 5.10, show that the nodal regions seem to be bundled together and run straight across the patch face. The phase distributions for the plate configuration without the patch, displayed in Fig. 5.7, show that the nodal region seems to be more widespread and to have more curvature near the area where the patch would have been positioned. The sixth mode shape with the patch seems to pull the nodal region more toward the left plate edge. Similarly, the seventh mode shape with the patch seems to pull the nodal region more toward the top plate edge.

5.4 *Closure*

We have shown through experimental modal analysis the difference between the normal and imaginary modes of a highly damped nearly square aluminum plate. The phase distribution map exhibits the classical "nodal-galloping" region on the plate surface. The normal modes were qualitatively similar to the imaginary mode shapes.

We investigated the effect of adding a constrained-layer damping material on one corner of the plate. The natural frequencies of all seven modes increased when compared to the case without the constrained-layer damping patch. This suggests that the overall stiffness of the structure was increased by local positioning of the damping patch. The normal mode

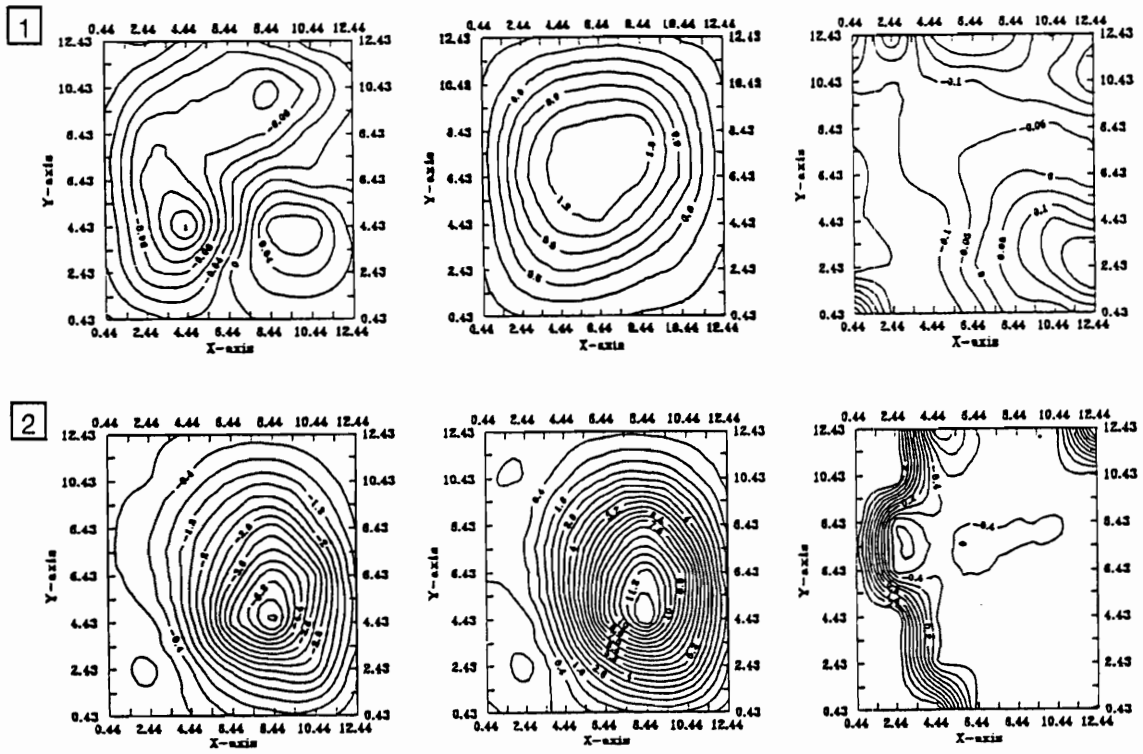

Figure 5.5: Mode shape numbers one and two of the nonclassically supported plate without the damping patch: (1st column) normal mode, (2nd column) imaginary mode, and (3rd column) phase in radians.

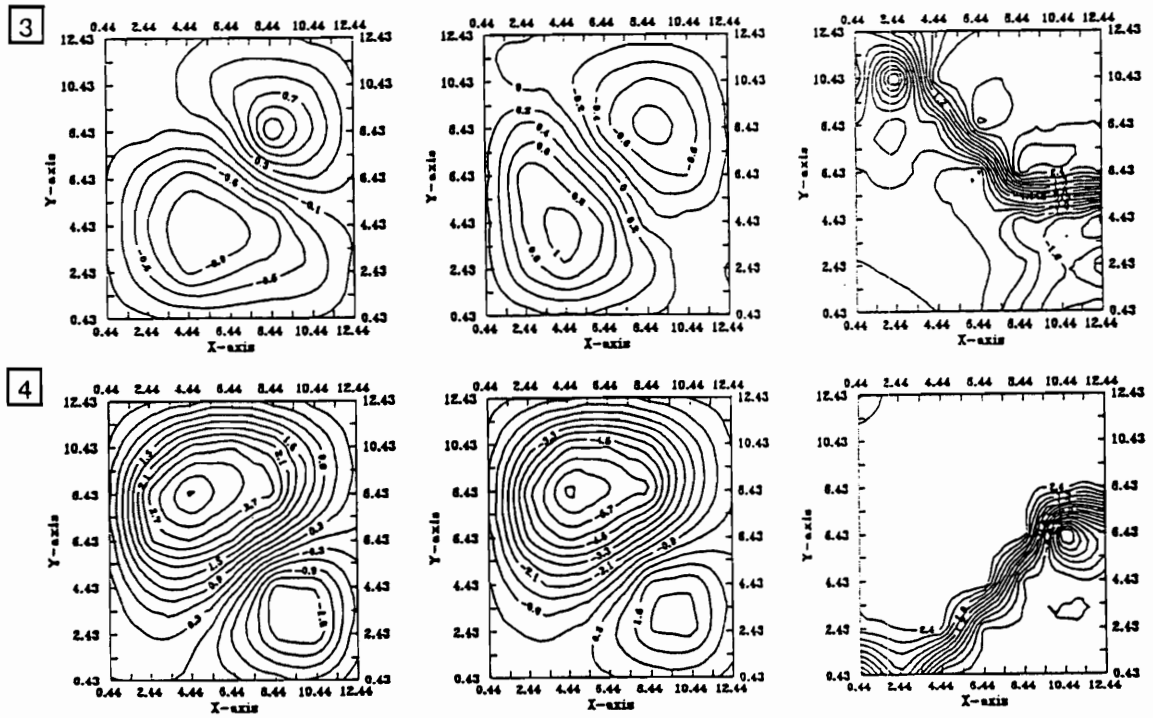

Figure 5.6: Mode shape numbers three and four of the nonclassically supported plate without the damping patch: (1st column) normal mode, (2nd column) imaginary mode, and (3rd column) phase in radians.

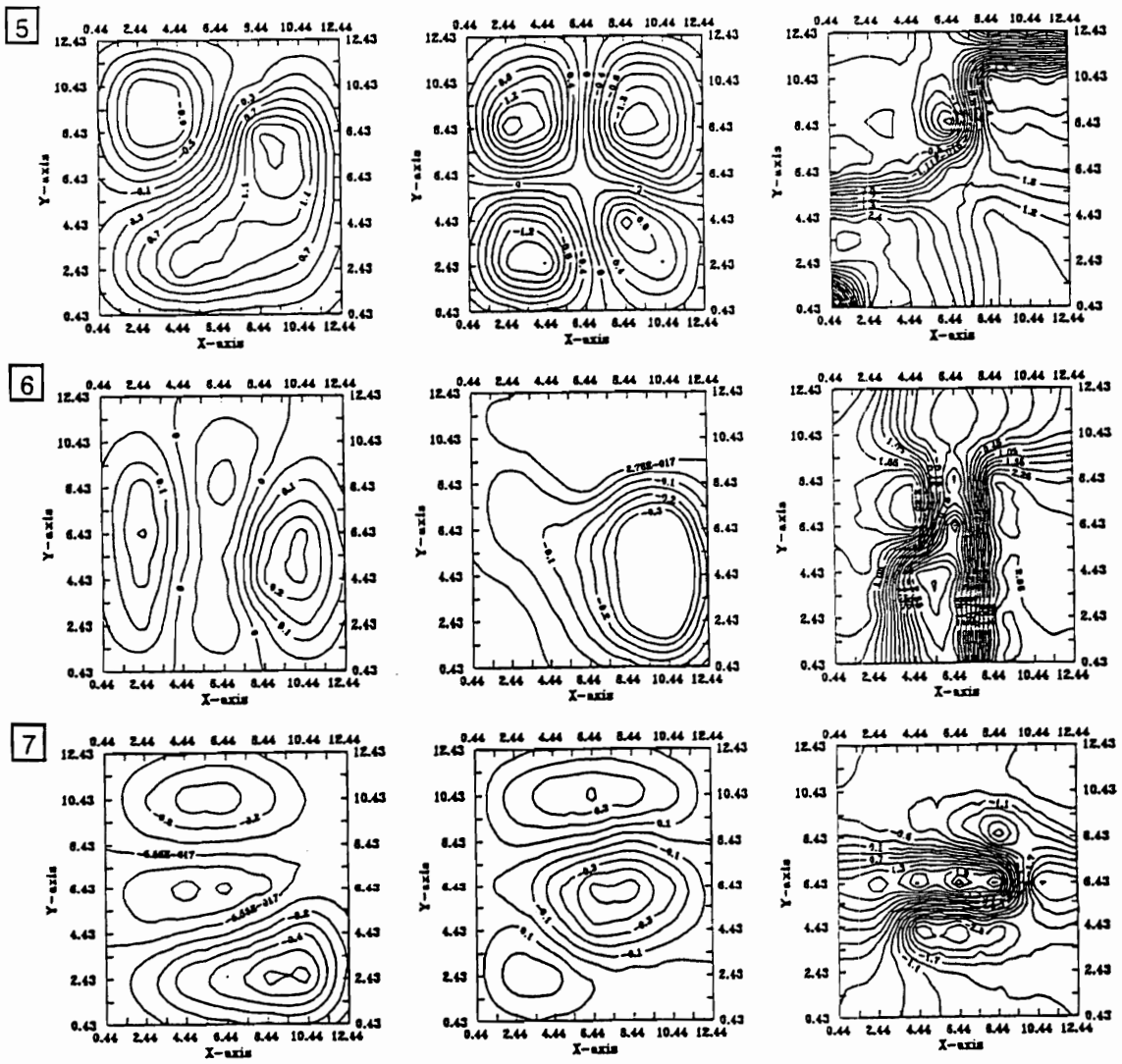

Figure 5.7: Mode shape numbers five, six, and seven of the nonclassically supported plate without the damping patch: (1st column) normal mode, (2nd column) imaginary mode, and (3rd column) phase in radians.

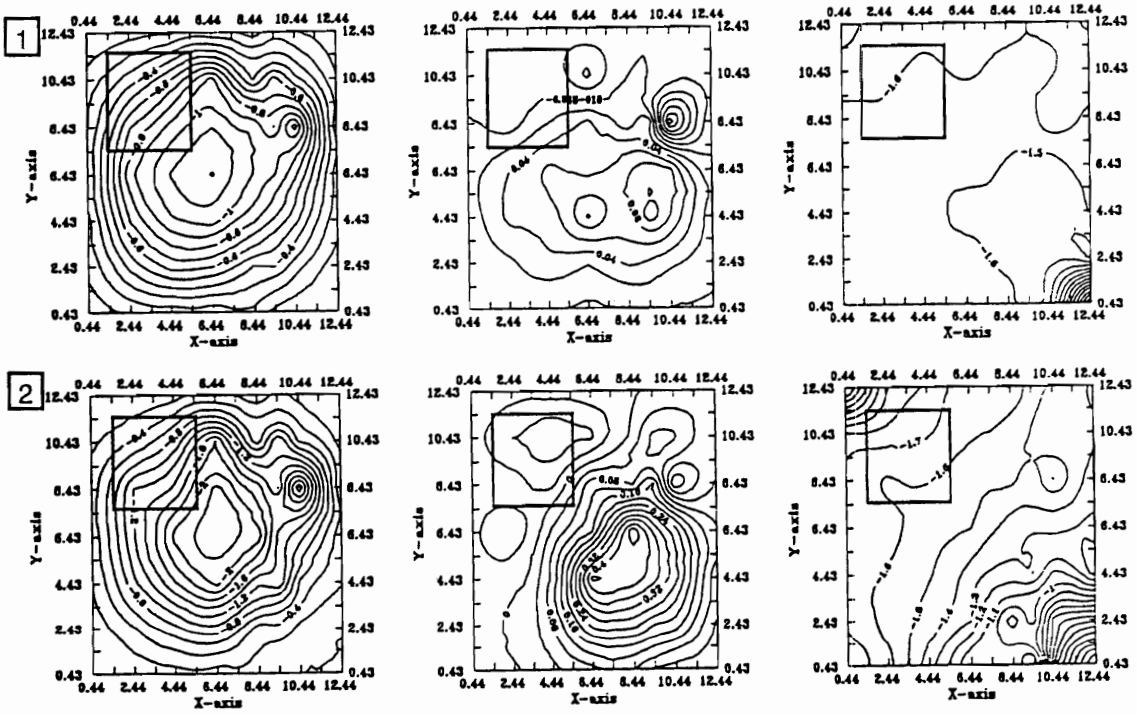

Figure 5.8: Mode shape numbers one and two of the nonclassically supported plate with the constrained-layer damping patch attached on the top left corner: (1st column) normal mode, (2nd column) imaginary mode, and (3rd column) phase in radians.

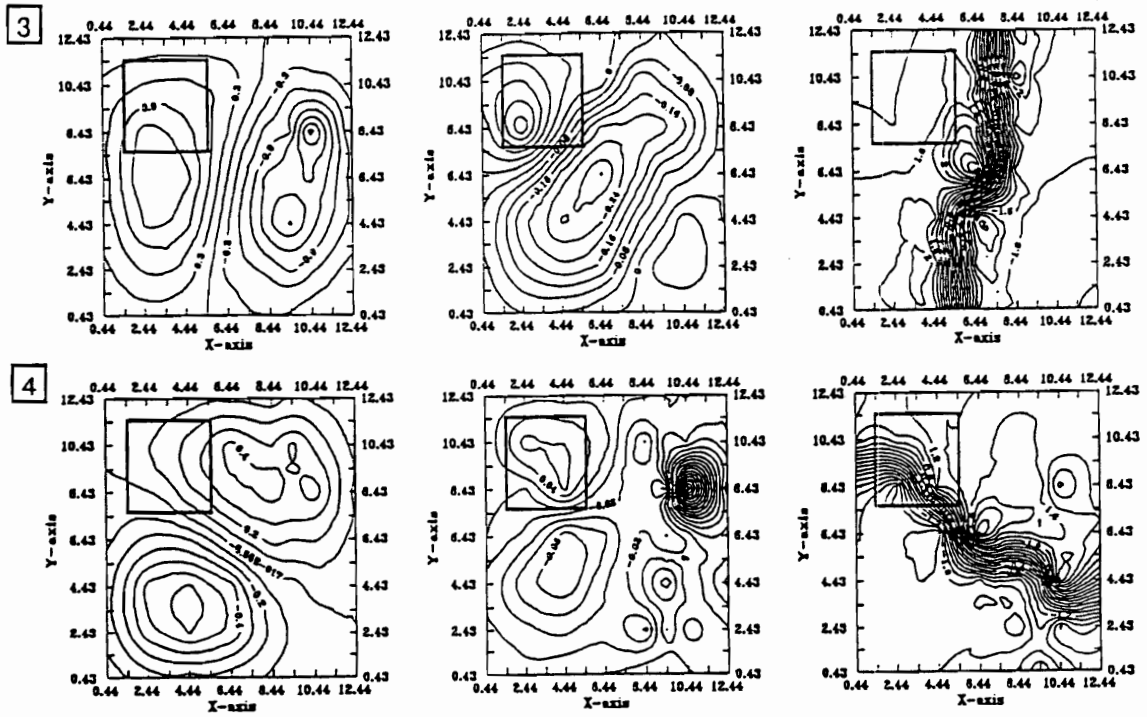

Figure 5.9: Mode shape numbers three and four of the nonclassically supported plate with the constrained-layer damping patch attached on the top left corner: (1st column) normal mode, (2nd column) imaginary mode, and (3rd column) phase in radians.

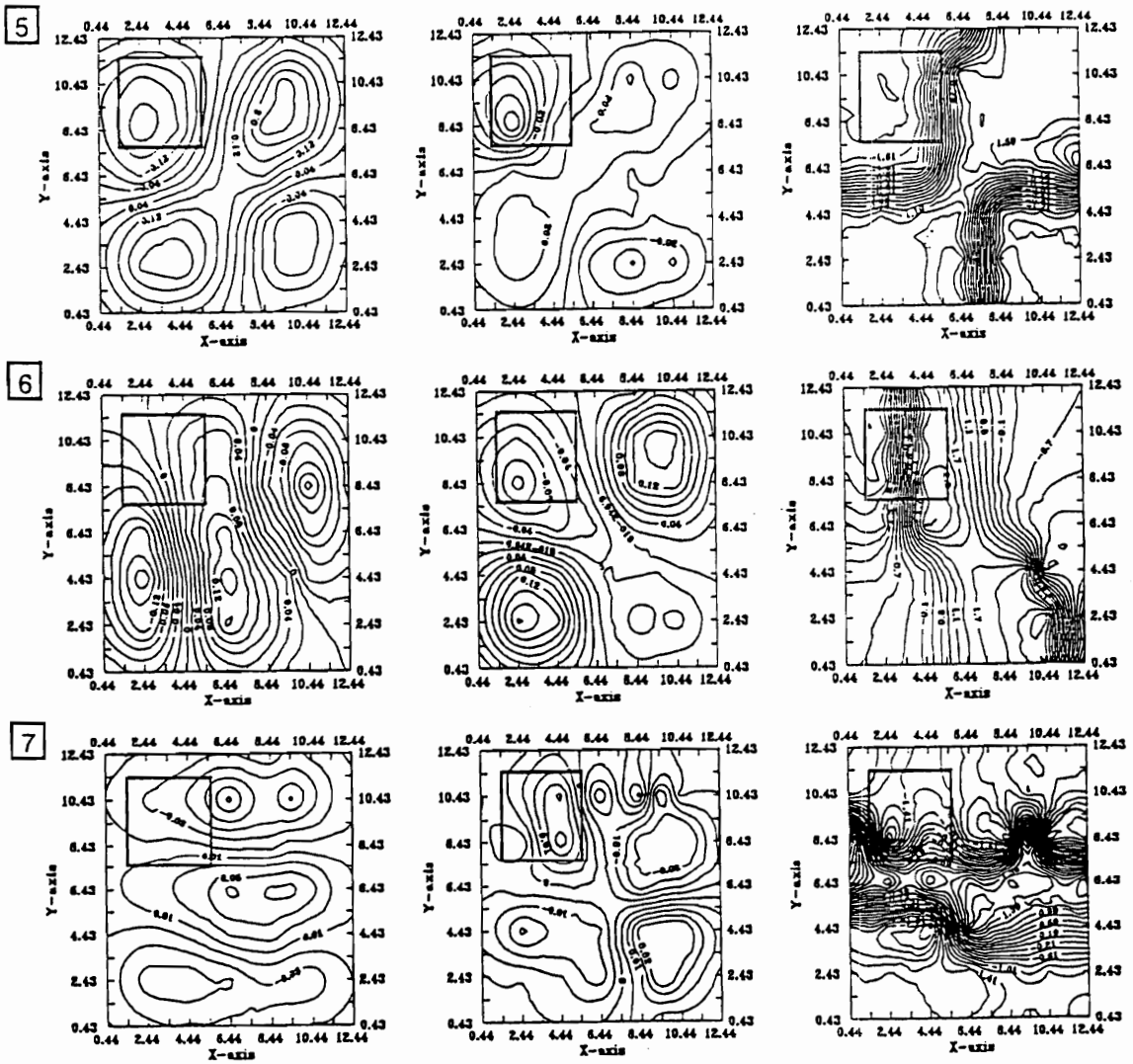

Figure 5.10: Mode shape numbers five, six, and seven of the nonclassically supported plate with the constrained-layer damping patch attached on the top left corner: (1st column) normal mode, (2nd column) imaginary mode, and (3rd column) phase in radians.

shapes were not similar to the imaginary mode shapes. The nodal galloping region appears to avoid the damping patch. However, upon crossing the damping patch, it deforms linearly without any curvature.

Using the complex mode shapes of the plate, we presented the effect of phase variations on the plate surface. The difference between the normal and imaginary modes constitutes the contribution of our investigation. We verified from our tests that, for a highly damped system, the mode shapes must be defined in both the time and spatial domain. We also demonstrated the tremendous increase in the modal damping factors for modes having their anti-nodes near the location of the constrained-layer damping patch.

Chapter 6

DISCUSSION AND CONCLUSIONS

6.1 Discussion of the Current Work

In this dissertation, we investigated nonlinear modal interactions in the response of stiff cantilever plates. We observed classical internal and combination resonances, a combination internal resonance, and more significantly a modal interaction between widely spaced modes. The experimental studies compiled in this dissertation illustrate the complexity of the plate dynamics. Moreover, the results presented in Chapter 3 corroborate the theoretical findings of Nayfeh and Nayfeh (1993) that high- to low-frequency modal interactions can occur in structures with widely spaced frequencies.

We activated the first torsional mode through a two-to-one internal resonance by exciting a cantilever metallic plate near the frequency of its second bending mode. The two-to-one internal resonance was activated by the quadratic nonlinearity arising from the coupling of twisting and bending motions. This mechanism may explain the torsional instability observed by Cole (1990) in his experiments on the influence of spoilers on the flutter of wings in a wind-tunnel.

In the experiments with $(90/30/-30/-30/30/90)_s$ laminated composite plate, we observed a modal interaction that is not the result of an internal resonance or combination parametric or external resonances. The experimental results show an interaction between a high-frequency (seventh) mode and a low-frequency (first) mode whose frequencies are approximately in the ratio of 23 to 1. This interaction is similar to those observed in flexible beams (Anderson et al, 1992; Nayfeh and Nayfeh, 1994) and a frame structure (Popovic et al., 1994). In addition, we observed simultaneous modal interactions: a two-to-one internal

resonance between the directly excited seventh (third torsional) mode and the fourth (second torsional) mode and an interaction between two widely spaced modes (the seventh and first modes).

In the experiments with the $(90/30/-30/-30/30/90)_s$ and $(-75/75/75/-75/75/-75)_s$ laminated composite plates, we observed combination and combination internal resonances. For the $(90/30/-30/-30/30/90)_s$ plate, we activated the combination resonance $f_e = 1133.79\,\text{Hz} \approx \omega_2 + \omega_7$. We observed a harmonic response evolving into a two-period quasi-periodic motion. For some excitation parameters, the low-frequency second (first torsional) mode activated through the combination resonance dominated the plate response.

For the $(-75/75/75/-75/75/-75)_s$ plate, we observed both combination external and combination internal resonances. As a result of the activation of the combination resonance $f_e = 310.37\,\text{Hz} \approx \frac{1}{2}(\omega_2 + \omega_5)$, a harmonic motion jumped-up into a two-period quasi-periodic motion as the excitation amplitude was slowly increased. Moreover, we activated the combination internal resonance $f_e = 1048.22\,\text{Hz} \approx \omega_8 \approx \frac{1}{2}(\omega_2 + \omega_{13})$ as the excitation amplitude increased above a threshold. For certain excitation parameters, we found that the low-frequency second (first torsional) mode dominated the two-period quasi-periodic plate response.

Lastly, we studied the complex mode shapes of a highly damped nearly square aluminum plate. We observed that the imaginary component of the complex eigenvector represents the normal mode shape and the real component represents the imaginary mode shape. The phase distribution map exhibits the classical "nodal-galloping" region on the plate surface. However, we found that the normal mode shapes were qualitatively similar to the imaginary mode shapes. We also studied the effect of placing a constrained-layer damping (CLD) patch on the natural frequencies and complex mode shapes of the plate. The application of the patch increased the first seven natural frequencies and their modal damping factors. The increase in the modal damping factor of the fifth mode was the largest (360%). The noticeable differences were in the normal and imaginary mode shapes, which were qualitatively different. The phase map indicates that the normal mode shapes dominate the

imaginary mode shapes. We conclude that structures with high damping exhibit nodal galloping. We found that adding the constrained-layer damping patch produced the largest difference between the normal and imaginary modes.

6.2 Suggestions for Future Work

There are many aspects of modal interactions between widely spaced modes that are not fully understood. The present effort demonstrates that interaction between widely spaced modes could occur in stiff as well as flexible structures. Moreover, the present experimental study demonstrates some of the complexities in the plate dynamics. The work by Anderson et al. (1992), Nayfeh and Nayfeh (1994), and Popovic et al. (1994) on flexible structures and the present work on a stiff structure demonstrate that modal interactions can occur in systems with widely spaced frequencies. However, an investigation needs to be conducted to provide necessary and sufficient conditions for the activation of this mechanism and the attendant transfer of energy from high- to low-frequency modes.

Nayfeh (1993) developed a theory for the excitation of the low-frequency mode when the high-frequency mode is excited by a primary resonance in a two-degree-of-freedom system. His work needs to be extended to provide analytical criteria for the energy transfer between widely spaced modes in multi-degree-of-freedom system. Moreover, by exciting the seventh mode with a primary resonance, we simultaneously activated the low-frequency (first) mode and the fourth mode whose frequency is half that of the seventh mode. Thus, an analytical study needs to be conducted to determine the conditions under which internal resonances and the interaction between widely spaced modes could occur simultaneously. Most importantly, there needs to be an investigation to see if multi-modal interactions during the energy transfer between widely spaced modes reduces the amount of energy that can be transferred to the lower mode(s).

Currently, there is a research effort at Ford Motor Company to utilize computer-aided holometry to characterize and visualize velocity propagation in a flexible panel-type struc-

ture and investigate the effect of surface attached constrained-layer damping patchs. Since the goal of such an investigation is to aid in the assessment of the sound quality in automobiles, a study needs to be conducted to minimize the sound radiation from a given structure by varying the profile of the constrained-layer damping patch.

REFERENCES

Anderson, T. J., 1993, "Nonlinear Vibrations of Metallic and Composite Structures," *PhD Dissertation, Department of Engineering Science and Mechanics, Virginia Polytechnic Institute and State University*, Blacksburg, Virginia.

Anderson, T. J., Balachandran, B., and Nayfeh, A. H., 1992, "Observations of Nonlinear Interactions in a Flexible Cantilever Beam," AIAA Paper No. 92-2332, *Proceedings of the 33rd AIAA Structures, Structural Dynamics, and Materials Conference*, Dallas, TX.

Bajaj, A. K. and Johnson, J. M., 1990, "Asymptotic Techniques and Complex Dynamics in Weakly Non-Linear Forced Mechanical Systems," *International Journal of Non-Linear Mechanics*, Vol. 25, pp. 211–226.

Balachandran, B. and Nayfeh, A. H., 1990, "Nonlinear Oscillations of a Harmonically Excited Composite Structure", *Composite Structures*, Vol. 16, pp. 323–339.

Balachandran, B., Nayfeh, A. H., Smith, S. W., and Pappa, R. S., 1992, "On Identification of Structures with Internal Resonances", *30th Aerospace Sciences Meeting*, Reno, Nevada.

Bellos, J. and Inman, D. J., 1989, "A Survey on Nonproportional Damping," *The Shock and Vibration Digest*, Vol. 21, No. 10, pp. 7–12.

Banks, H. T. and Inman, D. J., 1991, "On Damping Mechanisms in Beams", *Journal of Applied Mechanics*, Vol. 58, pp. 716–723.

Bendat, J. S. and Piersol, A. G., 1986, *Random Data: Analysis and Measurement Procedures*, Wiley, New York.

Bennett, J. A., 1971, "Nonlinear Vibration of Simply Supported Angle-Ply Laminated Plates," *AIAA Journal*, Vol. 9, pp. 1977–2003.

Bert, C. W., 1973, "Material Damping: An Introduction Review of Mathematical Mod-

els, Measures and Experimental Techniques", *Journal of Sound and Vibration*, Vol. 29, No. 2, pp. 129–153.

Bert, C. W., 1982, "Research on Dynamics of Composite and Sandwich Plates," *Shock and Vibration Digest*, Vol. 14, pp. 17–34.

Bert, C. W., 1985, "Research on Dynamic Behavior of Composite and Sandwitch Plates", *Shock and Vibration Digest*, Vol. 17, pp. 3–15.

Bert, C. W. and Mayberry, B. L., 1969, "Free Vibrations on Unsymmetrically Laminated Anisotropic Plates", *Journal of Composite Materials*, Vol. 3, pp. 282–293.

Bhimaraddi, A. and Stevens, L. K., 1984, "Higher-order theory for free vibration of orthotropic, homegeneous, and laminated rectangular plates", *Journal of Applied Mechanics*, Vol. 51, pp. 195–198.

Brown, G. M., Allen, T. E., Chen, S. -E., and Moeller, M., 1992a, "Sound Pressure Computed from CAH Measured Shape and Vibration Amplitude/Phase", *Ford Motor Company Research Laboratory Report*, No. SR-92-57.

Brown, G. M., Allen, T. E., Chen, S. -E., and Moeller, M., 1992b, "Stepped Strobe Phase CAH Technique for Measuring Vibration Amplitude and Phase", *Proceedings of the SPIE*, Vol. 1755, pp. 53–60.

Burton, T. D., and Kolowith, M., 1988, "Nonlinear Resonances and Chaotic Motion in a Flexible Parametrically Excited Beam," *Proceedings of the Second Conference on Nonlinear Vibrations, Stability, and Dynamics of Structures and Mechanisms*, Blacksburg, VA.

Chang, S. I., Bajaj, A. K., and Krousgrill, C. M., 1993, "Non-Linear Vibrations and Chaos in Harmonically Excited Rectangular Plates with One-to-One Internal Resonance," *Nonlinear Dynamics*, Vol. 4, pp. 433–460.

Chia, C. Y., 1980, *Nonlinear Analysis of Plates*, McGraw-Hill, New York.

Chia, C. Y. and Prabhakara, M. K., 1978, "A General Mode Approach to Nonlinear Flexural Vibrations of Laminated Rectangular Plates," *ASME Journal of Applied Mechanics*, Vol. 45, pp. 623–628.

Clary, R. R., 1972, "Vibration Characteristics of Unidirectional Filamentary Composite

Panels", *Composite Materials: Testing and Design*, pp. 415–438.

Cole, S. R., 1990, "Effects of Spoiler Surfaces on the Aeroelastic Behavior of A Low-Aspect-Ratio Rectangular Wing," *AIAA Paper No. 90-0981.*

Crandall, S. H., 1970, "The Role of Damping in Vibration Theory", *Journal of Sound and Vibration*, Vol. 11, No. 1, pp. 3–18.

Crandall, S. H., 1977, "Structural Response Patterns due to Wide-Band Random Excitation", *Stochastic Problems in Dynamics*, Ed., Clarkson, B. L., Pitman, London, pp. 366–389.

Crandall, S. H. and Kulvets, A., 1977, "Source Correlation Effects on Structural Response", *Application of Statistics*, Ed. Krishnaiah, P. R., North-Holland, pp. 163–182.

Crandall, S. H. and Zhu, W. -Q., 1983, "Wide-Band Random Vibration of Circular Plates", *Random Vibrations and Reliability*, Proceedings of the IUTAM Symposium", Akademie-Verlag, Berlin, pp. 231–243.

Crawley, E. F., 1979, "The Natural Modes of Graphite/Epoxy Cantilever Plates and Shells", *Journal of Composite Materials*, Vol. 13, pp. 195–205.

Crespo da Silva, M. R. M., 1980, "On the whirling of a Base Excited Cantilever Beam," *Journal of the Acoustical Society of America*, Vol. 67, pp. 707–740.

Cusumano, J. P. and Moon, F. C., 1989, "Low Dimensional Behavior in Chaotic Nonplanar Motions of a Forced Elastic Rod: Experiment and Theory," in *Nonlinear Dynamics in Engineering Systems,* W. Schiehlen, ed., Springer-Verlag, Berlin, pp. 55-66.

Dowell, E. H. and Kubota, Y., 1985, "Asymptotic Modal Analysis and Statistical Energy Analysis of Dynamical Systems", *Journal of Applied Mechanics*, Vol. 52, pp. 949–957.

Dugundji, J. and Mukhopadhyay, V., 1973, "Lateral Bending-Torsion Vibrations of a Thin Beam Under Parametric Excitation," ASME *Journal of Applied Mechanics*, Vol. 44, pp. 693–698.

Eslami, H. and Kandil, O. A., 1988, "Nonlinear Forced Vibration of Orthotropic Plates Using the Method of Multiple Scales," *AIAA Journal*, Vol. 27, pp. 955–960.

Gary, C. E., Decha-Umphai, K., and Mei, C., 1984, "Large Deflection, Large Ampli-

tude Vibration and Random Response of Symmetrically Laminated Rectangular Plates," *AIAA/ASME/ASCE/AHS 25th Structures, Structural Dynamics and Materials Conference*, Palm Springs, CA.

Haddow, A. G., and Hasan, S. M., 1988, "Nonlinear Oscillations of a Flexible Cantilever: Experimental Results," *Proceedings of the Second Conference on Nonlinear Vibrations, Stability, and Dynamics of Structures and Mechanisms*, Blacksburg, VA.

Hadian, J. and Nayfeh, A. H., 1993, "Free Vibration and Buckling of Shear-Deformable Cross-Ply Laminated Plates Using the State-Space Concept," *Computers & Structures*, Vol. 48, No. 4, pp. 677-693.

Huang, C. L., 1973, "Finite Amplitude Vibration of an Orthotropic Plate with an Isotropic Core," *International Journal of Non-Linear Mechanics*, Vol. 8, pp. 445–457.

Kapania, R. K. and Yang, T. Y., 1987, "Buckling, Postbuckling, and Nonlinear Vibrations of Imperfect Plates," *AIAA Journal*, Vol. 25, pp. 1338–1346.

Kubota, Y. and Dowell, E. H., 1986, "Experimental Investigation of Asymptotic Modal Analysis for a Rectangular Plate", *Journal of Sound and Vibration*, Vol. 106, No. 2, pp. 203–216.

Lang, G. F., 1989, "Demystifying Complex Modes," *Sound and Vibration*, pp. 36–40.

Leissa, A. W., 1981, "Advances in Vibrations, Buckling, and Postbuckling Studies on Composite Plates", *Composite Structures*, Ed. Marshall, T. H., Applied Science Publishers, London, pp. 312–334.

Librescu, L. and Reddy, J. N., 1989, "A Few Remarks Concerning Several Refined Theories of Anisotropic Composite Laminated Plates", *International Journal of Engineering Science*, Vol. 27, pp. 515–527.

Lyons, R. H., 1975, *Statistical Energy Analysis of Dynamical Systems: Theory and Applications*, The MIT Press, Cambridge, Massachusetts.

Mayberry, B. L. and Bert, C. W., 1968, "Experimental Investigation of Nonlinear Vibrations of Laminated Anisotropic Panels", *The Shock and Vibration Bulletin*, No. 39, pp. 191–199.

REFERENCES

Moon, F. C., 1987, *Chaotic Vibrations: An Introduction for Applied Scientists and Engineers*, Wiley-Interscience, New York.

Nayfeh, A. H., 1973, *Perturbation Methods*, Wiley-Interscience, New York.

Nayfeh, A. H., 1981, *Introduction to Perturbation Techniques*, Wiley-Interscience, New York.

Nayfeh, A. H., 1983, "Combination Resonances in the Non-Linear Response of Bowed Structures to a Harmonic Excitation," *Journal of Sound and Vibration*, Vol. 90, No. 4, pp. 457–470.

Nayfeh, A. H., 1984, "Quenching of a Primary Resonance by a Combination Resonance of the Additive or Difference Type", *Journal of Sound and Vibrations*, Vol. 97, No. 1, pp. 65–73.

Nayfeh, A. H. and Balachandran, B., 1989, "Modal Interactions in Dynamical and Structural Systems", *Applied Mechanics Review*, Vol. 42, pp. 175–201.

Nayfeh, A. H. and Balachandran, B., 1990, "Experimental Investigation of Resonantly Forced Oscillations of a Two-Degree-Of-Freedom Structure", *International Journal of Non-Linear Mechanics*, Vol. 25, No. 2/3, pp. 199–209.

Nayfeh, A. H. and Balachandran, B., 1994, *Applied Nonlinear Dynamics*, Wiley, New York, in press.

Nayfeh, A. H., El-Zein, M. S., and Nayfeh, J. F., 1989, "Nonlinear Oscillations of Composite Plates Using Perturbation Techniques," *Proceedings of the American Society for Composites, 4th Technical Conference on Composite Material Systems*, October 3-5, VPI&SU, Blacksburg, Virginia, Technomic Publishing, Lancaster, PA.

Nayfeh, A. H. and Mook, D. T., 1979, *Nonlinear Oscillations*, Wiley-Interscience, New York.

Nayfeh, J. F., 1990, *Nonlinear Dynamics of Composite Plates and Other Physical Systems*, PhD Dissertation, Department of Engineering Science and Mechanics, Virginia Polytechnic Institute and State University, Blacksburg, Virginia.

Nayfeh, S. A., 1993, *Nonlinear Dynamics of Systems Involving Widely Spaced Frequen-*

cies, M.S. Thesis, Department of Engineering Science and Mechanics, Virginia Polytechnic Institute and State University, Blacksburg, Virginia.

Nayfeh, S. A. and Nayfeh, A. H., 1993, "Nonlinear Interaction between Two Widely Spaced Modes–External Excitation," *International Journal of Bifurcation and Chaos*, Vol. 3, No. 2, pp. 417–427.

Nayfeh, S. A. and Nayfeh, A. H., 1994, "Energy Transfer From High- to Low-Frequency Modes in a Flexible Structure via Modulation," ASME *Journal of Vibration and Acoustics*, Vol. 116, pp. 203–207.

Oh, K. and Pryputniewicz, R. J., 1990, "Application of Electro-Optic Holography in the Study of Cantilever Plate Vibrations With Concentrated Masses," *Proceedings of the 25th Anniversary Edition of Hologram Interferometry*, November 5–8, Baltimore, Maryland, Society of Experimental Mechanics, Inc.

Özgüven, H. N., 1981, "Modal Analysis of Non-Proportionally Damped Mechanical Structures," presented at the American Society of Mechanical Engineers *Design Engineering Technical Conference*, Hartford, Connecticut, September 20-23.

Pai, P. F. and Nayfeh, A. H., 1990, "Non-Linear Non-Planar Oscillations of a Cantilever Beam Under Lateral Base Excitations", *International Journal of Non-Linear Mechanics*, Vol. 5, pp. 455–474.

Pai, P. F. and Nayfeh, A. H., 1991a, "A Nonlinear Composite Plate Theory", *Nonlinear Dynamics*, Vol. 2, pp. 445–477.

Pai, P. F. and Nayfeh, A. H., 1991b, "Three-Dimensional Nonlinear Vibrations of Composite Beams – II. Chordwise Excitations", *Nonlinear Dynamics*, Vol. 2, pp. 137–156.

Pai, P. F. and Nayfeh, A. H., 1991c, "Three-Dimensional Nonlinear Vibrations of Composite Beams – I. Flapwise Excitations", *Nonlinear Dynamics*, Vol. 2, pp. 1–34.

Pai, P. F. and Nayfeh, A. H., 1991d, "Three-Dimensional Nonlinear Vibrations of Composite Beams – III. Chordwise Excitations," *Nonlinear Dynamics*, Vol. 2, pp. 137–156.

Popovic, P., Nayfeh, A. H., Oh, K., and Nayfeh, S. A., 1994, "Experimental Investigation of High-Frequency to Low-Frequency Modal Interactions in a Three-Beam Frame

Structure," *Nonlinear and Stochastic Dynamics*, 1994 International Mechanical Engineering Congress and Exposition, The American Society of Mechanical Engineers, Chicago, IL, Nov. 6-11, 1994.

Pryputniewicz, R. J., 1985, "Time-average Holography in Vibration Analysis," *Optical Engineering*, Vol 24. pp. 843–850.

Reddy, J. N., 1982, "Large Amplitude Flexural Vibrations of Layered Composite Plates with Cutouts," *Journal of Sound and Vibrations*, Vol. 83, pp. 1–10.

Reddy, J. N., 1984a, "A Refined Nonlinear Theory of Plates with Transverse Shear Deformation", *International Journal of Solids and Structures*, Vol. 20, pp. 881–896.

Reddy, J. N., 1984b, "A Simple Higher-order Theory for Laminated Composite Plates", *Journal of Applied Mechanics*, Vol. 45, pp. 745–752.

Reddy, J. N., 1985, "A Review of the Literature on Finite-Element Modeling of Laminated Composite Plates and Shells", *Shock and Vibration Digest*, Vol. 17, pp. 3–8.

Reddy, J. N. and Chao, W. C., 1981, "Large Deflection and Large-Amplitude Free Vibrations of Laminated Composite-Material Plates," *Composite Structures*, Vol. 13, pp. 341–347.

Reddy, J. N. and Chao, W. C., 1982, "Nonlinear Oscillations of Laminated Anisotropic Rectangular Plates," *Journal of Applied Mechanics*, Vol. 49. pp. 396–402.

Sathyamoorthy, M., 1983, "Nonlinear Vibration of Plates – A Review," *Shock and Vibration Digest*, Vol. 15, pp. 3–16.

Schmidt, G. and Tondl, A., 1986, *Non-Linear Vibrations*, Akademie-Verlag, Berlin.

Suarez, L. E. and Singh, M. P., 1987a, "Perturbed Complex Eigenproperties of Classically Damped Primary Structure and Equipment Systems," *Journal of Sound and Vibration*, Vol. 116, No. 2, pp. 199–219.

Suarez, L. E. and Singh, M. P., 1987b, "Eigenproperties of Nonclassically Damped Primary Structure and Oscillator Systems," *Journal of Applied Mechanics*, Vol. 54, pp. 668–673.

Tuer, K. L., Duquette, A. P., and Golnaraghi, M. F., 1991, "Regulation of Flexible

REFERENCES

Structures Via Internal Resonance", *Proceedings of the Eighth VPI&SU Symposium on Dynamics and Control of Large Structures*, Blacksburg, Virginia.

User Manual for Modal Analysis 9.0, 1985, *SDRC I-DEAS, Level 2.5*, General Electric CAE International.

Yamaki, N. and Chiba, M., 1983, "Nonlinear Vibrations of a Clamped Rectangular Plate with Initial Deflection and Initial Edge Displacement–Part I: Theory", *Thin-Walled Structures*, Vol. 1, pp. 3–29.

Yamaki, N., Otomo, K., and Chiba, M., 1983, "Nonlinear Vibrations of a Clamped Rectangular Plate with Initial Deflection and Initial Edge Displacement–Part II: Experiment". *Thin-Walled Structures*, Vol. 1, pp. 101–119.

Yang, X. L. and Sethna, P. R., 1992, "Non-Linear Phenomena in Forced Vibrations of a Nearly Square Plate: Antisymmetric Case", *Journal of Sound and Vibrations*, Vol. 155. pp. 413–441.

Veletsos, A. S. and Ventura, C. E., 1986, "Modal Analysis of Non-Classically Damped Linear Systems," *Earthquake Engineering and Structural Dynamics*, Vol. 14, pp. 217–243.

Vest, C. M., 1979, *Holographic Interferometry*, Wiley, New York.

Wentz, K. R., Mei, C., and Chiang, C. K., 1988, "Large Amplitude Forced Vibration Response of Laminated Composite Rectangular Plates by a Finite Element Method," *Composite Structures*, I. H. Marshal, Ed., Elsevier Applied Science Publishers, pp. 703–716.

Whitney, J. M., 1987, *Structural Analysis of Laminated Anisotropic Plates*, Technomic. Lancaster, PA.

VITA

The author was born to Jung Ja and Sei Yun Oh on December 21, 1966. He moved at the age of six from Korea to Jakarta, Indonesia. He finished his high school at the Jakarta International School in 1984. He entered the Bachelor of Science program in the Mechanical Engineering department at Worcester Polytechnic Institute (WPI), Worcester, Massachusetts. He finished his B.S. program in 1988 under the academic advise of Dr. Hartley Grandin and the Major Qualifying Project advise of Dr. Mohammad Noori.

He entered the Master of Science program in the Mechanical Engineering department at WPI. He worked as a Teaching and Research Assistant in the Center of Holographic Studies and Laser Technology (CHSLT) under the supervision of Dr. Pryputniewicz. In the middle of the program, he married Petrina Lynn Birky. In the middle of struggle to complete the program, they were blessed with a baby girl named Alythea Hyun-Sook Oh. He finished his M.S. degree in 1990 under the committe members: Drs M. Noori, R. Cohn, and K. Stetson, and chaired by Dr. Pryputniewicz.

In 1990, he entered the Doctorate program in Engineering Mechanics in the Engineering Science and Mechanics Department at Virginia Polytechnic Institute and State University, Blacksburg, Virginia. He worked as a Research Assistant in the Nonlinear Vibrations Laboratory under the supervision of Dr. Nayfeh. Towards the end of the program, he accepted a permanent position as a Technical Manager in the Belt Systems Technology with the Gates Rubber Company. His first assignment is to lead the automatic tensioner technology transfer from Gates Canada, Inc. to Gates Korea Co., Ltd. He completed the Doctorate program requirements in December 1994 under the committee members: Drs Mook, Hyer, Hendriks, and Burns, and chaired by Dr. Nayfeh. He will be moving to Taegu, Korea with his family at the end of December, 1994 for four years.